UNCLASSIFIED

CENTRAL RESEARCH LIBRARY
DOCUMENT COLLECTION

ORNL-2302
Progress

MARTIN MARIETTA ENERGY SYSTEMS LIBRARIES
3 4456 0350481 1

cy 5

PHYSICS DIVISION

SEMIANNUAL PROGRESS REPORT

FOR PERIOD ENDING MARCH 10, 1957

CENTRAL RESEARCH LIBRARY
DOCUMENT COLLECTION
LIBRARY LOAN COPY
DO NOT TRANSFER TO ANOTHER PERSON
If you wish someone else to see this document, send in name with document and the library will arrange a loan.

OAK RIDGE NATIONAL LABORATORY
OPERATED BY
UNION CARBIDE NUCLEAR COMPANY
A Division of Union Carbide and Carbon Corporation
UCC
POST OFFICE BOX X · OAK RIDGE, TENNESSEE

UNCLASSIFIED

Printed in USA. Price 40 cents. Available from the

Office of Technical Services
U. S. Department of Commerce
Washington 25, D. C.

LEGAL NOTICE

This report was prepared as an account of Government sponsored work. Neither the United States, nor the Commission, nor any person acting on behalf of the Commission:

A. Makes any warranty or representation, express or implied, with respect to the accuracy, completeness, or usefulness of the information contained in this report, or that the use of any information, apparatus, method, or process disclosed in this report may not infringe privately owned rights; or

B. Assumes any liabilities with respect to the use of, or for damages resulting from the use of any information, apparatus, method, or process disclosed in this report.

As used in the above, "person acting on behalf of the Commission" includes any employee or contractor of the Commission to the extent that such employee or contractor prepares, handles or distributes, or provides access to, any information pursuant to his employment or contract with the Commission.

UNCLASSIFIED

ORNL-2302
Progress

Contract No. W-7405-eng-26

PHYSICS DIVISION

SEMIANNUAL PROGRESS REPORT

for Period Ending March 10, 1957

A. H. Snell, Director
J. L. Fowler and E. O. Wollan, Associate Directors

DATE ISSUED

JUN 3 1957

OAK RIDGE NATIONAL LABORATORY
Operated by
UNION CARBIDE NUCLEAR COMPANY
A Division of Union Carbide and Carbon Corporation
Post Office Box X
Oak Ridge, Tennessee

MARTIN MARIETTA ENERGY SYSTEMS LIBRARIES

3 4456 0350481 1

UNCLASSIFIED

ORNL-2302

INTERNAL DISTRIBUTION

1. C. E. Center
2. Biology Library
3. Health Physics Library
4–6. Central Research Library
7. Reactor Experimental Engineering Library
8–19. Laboratory Records Department
20. Laboratory Records, ORNL R.C.
21. A. M. Weinberg
22. L. B. Emlet (K-25)
23. J. P. Murray (Y-12)
24. J. A. Swartout
25. E. H. Taylor
26. E. D. Shipley
27. E. J. Murphy
28. M. L. Nelson
29. A. H. Snell
30. A. Hollaender
31. K. Z. Morgan
32. F. L. Culler
33. M. T. Kelley
34. D. Phillips
35. E. O. Wollan
36. D. W. Cardwell
37. A. S. Householder
38. L. D. Roberts
39. R. B. Briggs
40. R. N. Lyon
41. W. C. Koehler
42. E. P. Blizard
43. M. E. Rose
44. G. E. Boyd
45. W. H Sullivan
46. R. W. Stoughton
47. C. E. Winters
48. W. H. Jordan
49. E. C. Campbell
50. D. S. Billington
51. M. A. Bredig
52. R. S. Livingston
53. C. P. Keim
54. F. C. Maienschein
55. C. E. Clifford
56. R. C. Block
57. C. D. Susano
58. C. J. Borkowski
59. M. J. Skinner
60. M. K. Wilkinson
61. J. W. Cable
62. P. M. Reyling
63. G. deSaussure
64. W. M. Good
65. G. C. Williams
66. J. L. Fowler
67. R. W. Johnson
68. J. R. McNally, Jr.
69. J. L. Gabbard
70. R. A. Charpie
71. G. G. Slaughter
72. Eugene Guth
73. R. W. Peelle
74. P. R. Bell
75. G. G. Kelley
76. C. C. Harris
77. H. G. MacPherson
78. P. H. Stelson
79. J. E. Sherwood
80. W. Zobel
81. R. B. Murray
82. H. B. Willard
83. J. Schenck
84. J. H. Neiler
85. J. A. Harvey
86. C. F. Barnett
87. N. H. Lazar
88. R. R. Dickison
89. A. Simon
90. J. H. Gibbons
91. J. J. Pinajian
92. S. Bernstein
93. E. P. Wigner (consultant)
94. H. A. Bethe (consultant)
95. E. Creutz (consultant)
96. L. P. Smith (consultant)
97. R. L. Thornton (consultant)
98. R. F. Christy (consultant)
99. M. Goldhaber (consultant)
100. T. Lauritsen (consultant)
101. J. A. Wheeler (consultant)
102. N. F. Ramsey (consultant)
103. W. R. Brode (consultant)
104. ORNL – Y-12 Technical Library, Document Reference Section

EXTERNAL DISTRIBUTION

105–186. Given external distribution
187–761. Given distribution as shown in TID-4500 (13th ed.) under Physics and Mathematics category (100 copies – OTS)

Physics Division progress reports previously issued in this series are as follows:

ORNL-325 Supplement	December, January, and February, 1948-1949
ORNL-366	Period Ending June 15, 1949
ORNL-481	Period Ending September 25, 1949
ORNL-577	Period Ending December 15, 1949
ORNL-694	Period Ending March 15, 1950
ORNL-782	Period Ending June 15, 1950
ORNL-865	Period Ending September 20, 1950
ORNL-940	Period Ending December 20, 1950
ORNL-1005	Period Ending March 20, 1951
ORNL-1092	Period Ending June 20, 1951
ORNL-1164	Period Ending September 20, 1951
ORNL-1278	Period Ending December 20, 1951
ORNL-1289	Period Ending March 20, 1952
ORNL-1365	Period Ending June 20, 1952
ORNL-1415	Period Ending September 20, 1952
ORNL-1496	Period Ending December 20, 1952
ORNL-1620	Period Ending September 10, 1953
ORNL-1705	Period Ending March 10, 1954
ORNL-1798	Period Ending September 10, 1954
ORNL-1879	Period Ending March 20, 1955
ORNL-2076	Period Ending March 10, 1956
ORNL-2204	Period Ending September 10, 1956

TABLE OF CONTENTS AND SUMMARY

A HIGH-INTENSITY PROTON SYNCHROTRON
T. A. Welton 1

Extensive, but preliminary, work has led to a novel high-energy accelerator concept. This is the rapidly pulsed alternating-gradient proton synchrotron with high-energy injection from a 900-Mev AVF cyclotron. The resulting machine gives very high current for a reasonable cost.

AN INTERNAL-CONVERSION COEFFICIENT FOR THE 5p ELECTRON SHELL IN XENON
A. H. Snell and A. E. S. Green 3

The observed intensity of the singly charged ions in the charge spectrum produced by the isomeric decay of 12-day Xe^{131} is used, in conjunction with a theoretical estimate of the radiation probability of the ($5p$-$1s$) x-ray transition in the K series of xenon, to yield a value for the internal-conversion coefficient of the 163-kev gamma ray in the $5p$ shell. The value so obtained is 0.20 ± 0.03.

PHENOMENOLOGICAL NUCLEAR POTENTIALS FOR O^{17}
H. O. Cohn and J. L. Fowler 5

The s- and d-wave phase shifts for neutron scattering from oxygen, together with the single-particle bound s and d states of O^{17}, are fit reasonably well with a single static potential having a diffuse boundary and a Thomas spin-orbit energy term.

COULOMB EXCITATION OF 2^+ STATES IN EVEN-EVEN ISOTOPES OF TIN AND ZIRCONIUM
P. H. Stelson and F. K. McGowan 8

Coulomb excitation of 2^+ states in the even-even isotopes of tin and zirconium has been observed by bombarding targets of enriched tin isotopes and normal zirconium with 8-, 9-, and 10-Mev doubly ionized alpha particles accelerated by the ORNL 5.5-Mv electrostatic generator.

THE REACTIONS $Si^{28}(p,p'\gamma)Si^{28}$, $P^{31}(p,\alpha\gamma)Si^{28}$, AND $P^{31}(p,p'\gamma)P^{31}$
J. K. Bair, H. O. Cohn, and H. B. Willard 11

Preliminary data are given for the $P^{31}(p,p'\gamma)P^{31}$ and $P^{31}(p,\alpha\gamma)Si^{28}$ reactions. It is shown that the latter reaction is not the source of certain weak resonances previously assigned to the $Si^{28}(p,p'\gamma)Si^{28}$ reaction.

CROSS SECTIONS FOR (p,n) REACTIONS IN INTERMEDIATE NUCLEI
C. H. Johnson and A. Galonsky 13

Absolute (p,n) cross sections are reported for Cl^{37}, Cr^{53}, Co^{59}, Cu^{65}, Se^{77}, Se^{82}, and Nb^{93} for proton energies from threshold to 0.5 Mev above threshold. The theoretical cross section for formation of the compound nucleus is compared with the experimental results for these nuclei and for Ti^{49}, V^{51}, Mn^{55}, Ga^{71}, and As^{75}.

ENERGY LEVELS OF C^{13}
A. Galonsky, C. D. Moak, R. L. Traughber, and C. M. Jones 17

By studying the proton spectrum in the $B^{11}(He^3,p)C^{13}$ reaction, two new levels of C^{13} have been found at excitations 5.49 ± 0.08 and 6.09 ± 0.08 Mev.

MILLIMICROSECOND NEUTRON TIME-OF-FLIGHT SPECTROME' RY
J. H. Neiler, W. M. Good, and J. H. Gibbons 20

Results are given for the total neutron cross section of the separated isotopes K^{39}, K^{41}, and Rb^{87} in the kilovolt energy region. Primary neutron spectra have been obtained from the reactions $Be^9(d,n)B^{10}$ and $B^{11}(d,n)C^{12}$ for studying states in B^{10} and C^{12}, respectively.

ELASTIC SCATTERING OF NEUTRONS BY C^{12}

H. B. Willard, J. K. Bair, and H. O. Cohn 23

Elastic-scattering angular distributions of 1.45- to 4.1-Mev neutrons by C^{12} have been repeated, using a gas recoil detector. Results are in good agreement with earlier work.

PRELIMINARY FAST-NEUTRON POLARIZATION MEASUREMENT

H. O. Cohn, J. K. Bair, and H. B. Willard 24

A helium-filled cloud chamber was used as a fast-neutron polarization analyzer and was checked with neutrons from the $H^3(p,n)He^3$ reaction.

EXCITATION OF ISOMERIC STATES IN Pb AND As^{75} BY THE (n,n') REACTION

P. H. Stelson and E. C. Campbell 25

Isomeric states are observed in Pb ($T_{1/2}$ = 127 ± 10 μsec) and in As^{75} ($T_{1/2}$ = 18 ± 2 msec).

CROSS SECTION FOR THE $Be^9(n,\alpha)He^6$ REACTION

P. H. Stelson and E. C. Campbell 26

The work on the $Be^9(n,\alpha)He^6$ cross section has been completed and has been submitted to *The Physical Review.*

ACTIVATION CROSS SECTIONS WITH Sb-Be NEUTRONS

R. L. Macklin, N. H. Lazar, and W. S. Lyon 27

The neutron activation cross sections near 25 kev have been measured for about 50 nuclei. Gamma-ray scintillation spectrometers with known efficiency were used to compare the radioactivities produced by the several nuclei with I^{128}.

PROBABILITY OF THERMALIZATION OF FISSION NEUTRONS IN SMALL H_2O-U^{235} SUBCRITICAL SYSTEMS

E. C. Campbell and P. H. Stelson 29

From investigations of the kinetic behavior of small subcritical systems, the nonescape probability for a fission neutron source is obtained as a function of the size of the system. The results are compared with theory.

ORIENTATION OF ACTINIDE-GROUP NUCLEI

L. D. Roberts, J. W. T. Dabbs, and G. W. Parker 31

Uranium-233 nuclei have been aligned by electric quadrupole coupling, and the anisotropy of fission fragments from this aligned spin system has been observed. Further measurements of the magnetic susceptibility of $NpO_2Rb(NO_3)_3$ have been made.

DISSOCIATION CROSS SECTION OF H_2^+

C. F. Barnett 33

Cross sections for dissociation of H_2^+ were determined in various stopping gases in the energy range 500 kev to 2.25 Mev.

CHARGE SPECTRUM FOLLOWING THE RADIOACTIVE DECAY OF Kr^{79}

A. H. Snell and F. Pleasonton 34

A preliminary charge spectrum is shown which has a broad maximum in the range of 3 to 7 positive charges. The highest observed charge is 12. Estimated intensities are included for negatively charged and for neutral atoms. The combined spectrum yields an average charge of +4.7 ± 0.5.

MOLECULAR BREAKUP FOLLOWING RADIOACTIVE DECAY OF C^{14} IN CO_2
A. H. Snell and F. Pleasonton 36

Preliminary results indicate that the molecule remains bound as a singly charged ion, NO_2^+, in 81.4% of the decays. The distribution of other positively charged fragments is given.

ANTIFERROMAGNETIC STRUCTURES OF ANHYDROUS $[(1-x)Fe,xCo]Cl_2$ COMPOUNDS
M. K. Wilkinson, J. W. Cable, E. O. Wollan, and W. C. Koehler 37

Neutron diffraction patterns obtained on solid solutions of $FeCl_2$ and $CoCl_2$ at low temperatures indicate that the axis of magnetization in these antiferromagnetic compounds changes regularly with the sample composition.

MAGNETIC ORDERING IN HOLMIUM SESQUIOXIDE
W. C. Koehler, E. O. Wollan, M. K. Wilkinson, and J. W. Cable 39

Results of a detailed study of the magnetic-scattering properties of Ho_2O_3 as a function of temperature in the liquid-helium range and of the applied field are reported. A complex series of magnetic-ordering transformations, apparently field-induced, is described.

MAGNETIC ORDERING IN MANGANESE SESQUIOXIDE
J. W. Cable, M. K. Wilkinson, E. O. Wollan, and W. C. Koehler 43

The results of a neutron diffraction study of Mn_2O_3 are reported. Antiferromagnetic ordering is observed, the Néel temperature being 88°K. Qualitative features of the complex magnetic structure are described.

LOW-INTENSITY BACKGROUND MEASUREMENTS
P. R. Bell, R. C. Davis, and G. G. Kelley 45

Background measurements with scintillation spectrometers are being made under various conditions in order to better understand the various components in the natural background spectrum and to determine the limit for low-intensity source measurements.

THE A-8 LINEAR AMPLIFIER
G. G. Kelley 48

Several changes have been made in the A-8 linear amplifier since it was reported previously.

CONFERENCE ON NEUTRON PHYSICS BY TIME-OF-FLIGHT
Organized by W. M. Good, J. A. Harvey, and A. H. Snell 50

A conference on neutron physics by time-of-flight was sponsored by the Physics Division at Gatlinburg on November 1–2. A report of the conference has been prepared and will be published soon.

PUBLICATIONS

V. E. Pilcher, J. A. Harvey, and D. J. Hughes, "Neutron Resonance Parameters of U^{235}," *Phys. Rev.* **103**, 1342 (1956).

A. Galonsky and C. H. Johnson, "Cross Sections for the $T(d,n)He^4$ Reaction," *Phys. Rev.* **104**, 421 (1956).

E. C. Campbell and F. Nelson, "Rapid Ion Exchange Techniques for Radiochemical Separations," *J. Inorg. & Nuclear Chem.* **3**, 233 (1956).

R. L. Macklin and H. S. Pomerance, "Resonance Activation Integrals of U^{238} and Th^{232}," *J. Nuclear Energy* **2**, 243 (1956).

N. H. Lazar, R. C. Davis, and P. R. Bell, "Peak Efficiency of NaI(Tl) Crystals for Gamma Rays from 0.150 to 7.5 Mev," *IRE Trans. Nuclear Sci.* **NS3**(4), 136 (1956).

C. C. Harris and P. R. Bell, "Transmission Characteristics of Light Pipers," *IRE Trans. Nuclear Sci.* **NS3**(4), 87 (1956).

R. C. Davis, P. R. Bell, G. G. Kelley, and N. H. Lazar, "Response of Total Absorption Spectrometers to Gamma Rays," *IRE Trans. Nuclear Sci.* **NS3**(4), 82 (1956).

G. G. Kelley, P. R. Bell, R. C. Davis, and N. H. Lazar, "Intrinsic Scintillator Resolution," *IRE Trans. Nuclear Sci.* **NS3**(4), 57 (1956).

C. C. Harris, R. R. Bigelow, J. E. Francis, G. G. Kelley, and P. R. Bell, "A CsI(Tl) Crystal Surgical Scintillation Probe," *Nucleonics* **14**(11), 102 (1956).

J. K. Bair, H. O. Cohn, J. D. Kington, and H. B. Willard, "Reaction $N^{14}(p,p'\gamma)N^{14}$," *Phys. Rev.* **104**, 1595 (1956).

F. E. Senftle, T. A. Farley, and N. H. Lazar, "Half Life of Th^{232} and the Branching Ratio of Bi^{212}," *Phys. Rev.* **104**, 1629 (1956).

R. W. Lamphere, "Fission Cross Sections of the Uranium Isotopes, 233, 234, 236 and 238 for Fast Neutrons," *Phys. Rev.* **104**, 1654 (1956).

A. H. Snell, "A Survey of the Particles of Physics," *Am. Scientist* **45**, 44 (1957).

H. B. Willard, J. K. Bair, H. O. Cohn, and J. D. Kington, "Radiative Proton Capture by C^{13}," *Phys. Rev.* **105**, 202 (1957).

H. W. Newson, J. H. Gibbons, H. Marshak, R. M. Williamson, R. C. Mobley, J. R. Patterson, and P. F. Nichols, "Neutron Resonances in the kev Region: Heavier Odd Elements," *Phys. Rev.* **105**, 198 (1957).

R. B. Leachman and H. W. Schmitt, "The Cross Section for U^{238} Fission by Fission Neutrons," *J. Nuclear Energy* **4**(1), 38 (1957).

R. K. Osborn and E. D. Klema, "Analysis of Nuclear Quadrupole Moments on the Basis of a Kinematical Model," *Nuclear Physics* **2**, 454 (1956/57).

PAPERS PRESENTED AT SCIENTIFIC AND TECHNICAL MEETINGS

5th Tripartite Instrumentation Conference, Upton, New York, October 22–26, 1956

G. G. Kelley, "New Techniques in Scintillation Spectrometry and in Associated Circuitry."

Fall Meeting of American Ceramic Society, Clemson, South Carolina, November 1–3, 1956

M. K. Wilkinson (invited paper), "The Role of Neutron Diffraction in Structure Determinations."

Conference on Neutron Physics by Time-of-Flight, Gatlinburg, Tennessee, November 1–2, 1956

J. A. Harvey and R. C. Block, "Neutron Resonance Parameters of Eu^{151} and Eu^{153}."

J. H. Gibbons, "Discussion on the kev Region."

R. C. Block, "The ORNL Fast Chopper Program."

Pittsburgh Diffraction Conference, Pittsburgh, Pennsylvania, November 1956

W. C. Koehler, E. O. Wollan, M. K. Wilkinson, and J. W. Cable, "Neutron Diffraction by the Rare Earth Compounds $ErFeO_3$ and Er_2O_3."

American Physical Society Meeting, Chicago, Illinois, November 23–24, 1956

J. A. Harvey and R. C. Block, "Neutron Resonance Parameters of Eu^{151} and Eu^{153}."

H. O. Cohn, J. K. Bair, and H. B. Willard, "The 2.07-Mev Resonance in the Neutron Total Cross Section of C^{12}."

Conference on Pulse Neutron Techniques for the Investigation of Subcritical Reactors, UCRL, Livermore, California, November 29–30, 1956

E. C. Campbell and P. H. Stelson, "Reactor Parameters of Subcritical Reactor by Pulsed Neutron Techniques."

American Physical Society Meeting, New York, New York, January 30–February 2, 1956

E. C. Campbell and P. H. Stelson, "Measurement of Cross Section of $Be^9(n,\alpha)He^6$."

J. W. T. Dabbs, L. D. Roberts, and G. W. Parker, "α-Particle Anisotropy from Aligned U^{233} Nuclei."

J. L. Fowler and H. O. Cohn, "Elastic Neutron Scattering from Alpha Particle Nuclei."

A. Galonsky, C. D. Moak, R. L. Traughber, and C. M. Jones, "Energy Levels of C^{13} from $B^{11}(He^3,p)C^{13}$."

M. M. Gordon and T. A. Welton, "Acceleration of Particles Through Imperfection Resonances."

J. A. Harvey, D. J. Hughes, and V. E. Pilcher, "Distribution of Level Spacings of Heavy Nuclei."

N. H. Lazar, W. S. Lyon, and R. L. Macklin, "Neutron Activation Cross-Sections with Sb-Be Neutrons."

L. D. Roberts, J. W. T. Dabbs, and G. W. Parker, "U^{235} and U^{233} Nuclear Quadrupole Coupling in the UO_2^{++}."

A. H. Snell, F. Pleasonton, and H. E. Leming, "Radioactive Breakup of the HT Molecule."

P. H. Stelson and F. K. McGowan, "Coulomb Excitation of 2^+ States in Even-Even Isotopes of Tin and Zirconium."

T. A. Welton, "Vacuum Polarization and the π^0 Decay."

Sherwood Meeting at Berkeley, California, February 20–22, 1957

C. F. Barnett, "Charge Exchange and Dissociation of Hydrogen Ions at High Energies."

Professional Group on Nuclear Science Session, IRE National Convention, New York, New York, March 18–21, 1957

G. G. Kelley, "A New Amplifier for Pulse Spectrometry."

American Physical Society Meeting, Philadelphia, Pennsylvania, March 21–23, 1957

M. K. Wilkinson, W. C. Koehler, E. O. Wollan, and J. W. Cable, "Neutron Diffraction Study of Magnetic Ordering in Er_2O_3."

W. C. Koehler, E. O. Wollan, M. K. Wilkinson, and J. W. Cable, "Neutron Diffraction Study of Magnetic Ordering in Ho_2O_3."

ANNOUNCEMENTS

Additions to the Physics Division staff during this period were as follows: G. G. Slaughter (Neutron Velocity Selector), and H. O. Eason (Scintillation Spectrometry).

Terminations: G. P. Boicourt (Scintillation Spectrometry).

A. M. Lane (Atomic Energy Research Establishment, Harwell, England) spent the month of October working with the High Voltage Group, and also presented a series of eight lectures entitled "Nuclear Shell-Model."

W. Kofink, on loan from the Institute of Technology, Karlsruhe, Germany, for the past eight months has been located in the High Voltage Building, working on reactor theory.

PHYSICS DIVISION
SEMIANNUAL PROGRESS REPORT

A HIGH-INTENSITY PROTON SYNCHROTRON

T. A. Welton

The high-energy proton beam (β = 0.86) from the proposed ORNL 900-Mev AVF cyclotron appears to be potentially advantageous for injection into a high-energy synchrotron ring. The claimed advantages are as follows:

1. small frequency swing (~16%) required for acceleration in synchrotron,
2. low importance of space-charge effects at injection,
3. low importance of gas scattering effects at injection,
4. low importance of eddy-current and remanent field effects at injection,
5. possibility of synchronizing injector pulses with the phase equilibria in the synchrotron,
6. possibility of simultaneously using the injector as an extremely high intensity proton source for experimental purposes.

The obvious difficulties are as follows:

1. the high cost of such a cyclotron relative to a conventional injector,
2. the low phase density which characterizes cyclotron beams, again relative to the beams of conventional injectors,
3. the known difficulty of extracting cyclotron beams with reasonable efficiency,
4. the possible difficulty of designing an effective inflection scheme to operate with a beam of such high energy.

Advantage 1 can be effectively utilized by making the radio-frequency accelerating system highly resonant, with a large voltage gain per turn (~2 Mev). This, in turn, allows a pulse to be accelerated and delivered at high energy (8–12 bev) in about $\frac{1}{120}$ sec. Thus, if the magnet were pulsed at 60 cps, or if a fixed-field magnet were used, very high pulse rates could be obtained, as compared with existing machines. Note that with the low frequency swing required, it is actually realistic to expect that the required voltage gain could be obtained from simple radio-frequency equipment. In the studies which have been performed, it has been felt that the low cost associated with the pulsed machine outweighs the higher ultimate performance achievable with the fixed-field machine, but no real optimization has been attempted. Again, considerations of magnetic stored energy and the cost of the condenser bank required to store it have made an AG machine with reasonably high ν value appear most promising, particularly in view of the experience which will be obtained with a machine of this type in the next few years by the work on the Cambridge Electron Accelerator.

Advantages 2 and 3 probably serve only to guarantee that these two effects will not interfere with the formation of pulses at injection. (They do not seriously interfere in conventional machines!)

Advantage 4 makes the design of the magnet and its compensating windings considerably simpler than in conventional machines which inject at about $\frac{1}{5}$ the flux density here envisaged.

Advantage 5 makes it possible to achieve extremely precise frequency control in the synchrotron, since the beam enters automatically bunched and properly phased so that unusually low amplitudes of synchrotron oscillation result. The initial frequency standard is the cyclotron oscillator, and the bunched beam thereafter will supply a very accurate internal standard, as the magnetic field rises.

Advantage 6 will be mentioned subsequently.

As for the difficulties, the first (high cost of the injector) is felt to be amply offset by the increased performance which the injector makes possible for the synchrotron, as well as by the fact (advantage 6) that the injector is a highly useful experimental tool in its own right.

Difficulty 2 actually need not hold (see later discussion) for an AVF cyclotron; there is good reason to believe that a 900-Mev-frequency cyclotron can be constructed with a beam quality and intensity superior to those of a linear accelerator.

Difficulty 3 disappears if difficulty 2 can be overcome as indicated, since extraction of the beam of a circular machine is always predicated

on the ease with which separate turns of the orbits can be distinguished.

Difficulty 4 is serious if no attempt is made to go beyond existing techniques, but a procedure will be reported in a later paragraph which makes it plausible that multiturn injection at 900 Mev can be obtained in an AG synchrotron.

A simple explanation of how difficulty 2 is to be overcome is possible. The AVF cyclotron is similar to a conventional cyclotron in its ion source and in the fact that the radial focusing frequency is unity ($\nu_r = 1$) in its central region. It differs in the arrangement of its accelerating electrodes and in the possibility that the axial focusing frequency can be given a positive value, starting at the ion source. Magnetic-field errors (mainly with cos θ angular dependence) will disturb the radial motion in any cyclotron, by integral resonance at $\nu_r = 1$. This effect will be somewhat reduced in the AVF cyclotron because of the increase of ν_r with energy, but by reasonable shimming it can apparently be sufficiently reduced in any event. It seems unlikely that cos 2θ field errors will play a noticeable role, but shimming will suffice in case they do.

The most important resonance effect seems to be that arising from the cos 2θ electric-field component (strongly present when there are two accelerating gaps per revolution). This yields a half-integral resonance with the radial focusing motion and a consequent tendency toward exponential increase of any radial amplitude initially present. This tendency will be absent (as shown by extensive numerical calculations, and also by the general nonlinear orbit theory) if there are four or more accelerating gaps.

Normally, a cyclotron, lacking axial focusing at first, depends for its yield on the relatively rare protons emerging from the source sufficiently close to $z = 0$, with $dz/d\theta$ small enough so that the axial defocusing will nevertheless allow them to survive. To compensate for this extremely poor vertical acceptance, the radial acceptance is then made very large. The resulting beam, poorly defined radially, is then possibly made much worse by the above-mentioned exponential amplitude growth due to the dee system.

The planned 900-Mev cyclotron will have positive axial focusing at the ion source to avert the problem of low axial acceptance and will accelerate with four or more gaps to preserve the initial beam quality. It is then claimed that the output beam characteristics, determined by the ion source, rather than by the peculiarities of conventional cyclotron construction, can easily be equal or superior to the beam characteristics of a linac or electrostatic generator.

It should be noted that no resonance in the range between 0 and 900 Mev is expected to produce observable alteration of beam quality. Further, the integral resonance at 900 Mev ($\nu_r = 2$), in conjunction with high beam quality, is exactly what is needed for efficient extraction by an obvious extension of the LeCouteur scheme.

It is felt that a successful machine will depend on the development of multiturn injection techniques, in order that the small pulse size characteristic of presently planned AG machines will not more than cancel out the intensity advantage of rapid pulsing. A technique has therefore been devised, called "r-f resonant inflection," by which the theoretically available phase space in the AG synchrotron can be filled with reasonable efficiency ($\frac{1}{2}$–$\frac{2}{3}$). Note that a similar technique should be possible for any AG or CG machine.

Assume that pulses are entering the synchrotron from the cyclotron. The synchrotron magnetic field is held constant during injection (small variation is allowable) at such a value that the orbital frequency is a submultiple of the pulse frequency from the cyclotron. The synchrotron accelerating cavities are driven, during injection, at the same frequency as that of the cyclotron r-f system and at a phase such that each incoming pulse finds itself clustered around a position of phase equilibrium. Preparatory to injection, quadrupoles have been powered to move the operating point slightly to make ν_r equal to a quarter integer (the integer not being divisible by two or four!).

An injected pulse has a certain spot size at the mouth of the channel, and the channel must be separated from the accelerating region by a magnetic septum. Let the vertical spot size and divergence be such as to fill the available vertical aperture. The spot will be imaged radially after four revolutions, and in this time the radial amplitude must have been reduced by an amount equal to the radial spot size plus the septum width. This can be accomplished in an elegant way by providing one or two cavities, tuned to one-quarter of the frequency of the accelerating cavities and arranged with their electric field having a radial component ("slant gap"). These slant cavities can then systematically reduce (or later increase) the radial amplitude by the required amount. In

addition, if the angle of slant is made smaller near the desired equilibrium orbit, the form of the pulses in a radial phase plot can be molded to make possible much more efficient packing in the available aperture. Preliminary studies indicate that ten-turn injection in an aperture like that in the Cambridge Electron Accelerator should be considered quite feasible, with a resulting average output current of several microamperes of protons at 8 bev. More important, it seems that the theoretically available aperture, which must always be paid for in terms of field energy, can now be used with real efficiency.

The preliminary calculations described above are being extended, with some attempt at optimization. In addition, a promising procedure is being explored for efficient beam extraction from an AG synchrotron, using some elementary results from the recently developed nonlinear orbit theory.

AN INTERNAL-CONVERSION COEFFICIENT FOR THE 5*p* ELECTRON SHELL IN XENON

A. H. Snell A. E. S. Green[1]

An unusual opportunity to evaluate an internal-conversion coefficient for the outermost electrons of an atom is presented by the measurement[2,3] of the charge spectrum of stable Xe^{131}, following the isometric transition that constitutes the 12-day activity of Xe^{131m}. A single nuclear transition with an energy of 163 kev is involved, and it has been classified[4] as predominantly *M*4. Since there is no change in nuclear charge and no electron loss from a consequent "sudden perturbation" of the electron cortege, all ions are the result of internal conversion. We are here particularly concerned with the observation that singly charged ions are produced in 0.62% of the decays, for the singly charged ions must represent the occasions in which only the original conversion electron leaves the atom; no radiationless transitions can be involved in the reorganization of the electron shells. The situation lends itself to analysis in terms of fluorescence yields and x-ray line intensities, because at any point in the electron shells the fluorescence yield gives the probability of avoiding an immediate radiationless transition, and the relative x-ray intensities point to the relative probabilities of the next allowed steps in the radiative cascade leading to the outside of the atom. Such an analysis has been attempted,[2] and it leads broadly to the conclusion that the great majority of the ions of charge 1 result from a combination of (1) direct internal conversion in the outermost (5*p*) shell of xenon, and (2) *K*-shell conversion followed by emission of the (5*p*-1*s*) x-ray line. (We exclude the 5*s* electrons because radiationless transitions appear to be energetically possible in which a 5*s* vacancy can be filled by a 5*p* electron with the ejection of another 5*p* electron. This process would then be expected to dominate the (5*p*-5*s*) radiative transition so completely that internal conversion in the 5*s* electrons would almost certainly lead to ions of charge 2.)

In the intervening shells the fluorescence yields are so small that any internal conversion or x-ray cascade involving the creation of a vacancy in that region will, with high probability, produce a radiationless transition, with the result that the atom will be thrown into a state of higher charge. Indeed, the estimate given previously[2] indicates that only about 0.02% of the decay events lead to internal conversion in the intervening shells plus a subsequent cascade of pure x-ray transitions, leaving 0.60% to be attributed to the two main

[1] Summer research participant from Florida State University.

[2] F. Pleasonton and A. H. Snell, *Proc. Roy. Soc. (London)* (in press).

[3] A. H. Snell and F. Pleasonton, *Phys. Rev.* 102, 1419 (1956).

[4] I. Bergström *et al.*, *Arkiv Fysik* 7, 255 (1954).

processes mentioned above. We can state the situation in a simple equation:

$$(1)\quad \beta_{5p} + \beta_{1s} w_K A_{5p1s} = 0.0060 \pm 0.0008 \ ,$$

where β_{5p} and β_{1s} are not internal-conversion coefficients in the usual usage of the term but are internal-conversion *probabilities* in the sense that, given an internal conversion, they express the likelihood that it take place in the $5p$ or $1s$ shells; thus the sum of the β's for all shells is unity. The internal-conversion coefficients for the K, L, and M shells are known experimentally[4,5] to be 29, 12.7, and 4.3, respectively, so we can evaluate $\beta_{1s} = 0.62$. The fluorescence yield w_K for the $1s$ shell has the value[6,7] 0.86. The symbol A_{5p1s} represents the radiation probability of the last and faintest line of the K series in xenon relative to that of the total K series as unity. It appears to be experimentally unknown, so we attempt to calculate it by the use of atomic wave functions and thus arrive at an evaluation of β_{5p}.

For the $1s$-np series, the relative electric dipole transition probabilities may be estimated by means of the formula

$$(2)\qquad A_{1snp} = c\,|\langle 1s\,|\,r\,|\,np\rangle|^2 \lambda_{1snp}^{-3} \ ,$$

where, in view of the identity of the spin and angular factors, c is the same for all members of the series. To obtain reasonably accurate estimates of these transition probabilities, it is vital that the np radial wave functions be quite accurate in the neighborhood of the $1s$ shell. Calculations with screened coulomb functions and with an analytical wave function which approximated those expected in a Fermi-Thomas atom led to rather unreasonable answers because of their inadequacy in the $1s$ shell region. Fortunately, the fact that Hartree functions are available[8] for Cs^+, which is isoelectronic with xenon, makes possible a rather reliable estimate of the transition probabilities.

For convenience in tabulation, the radial functions (P_{nl}) given by Hartree are unnormalized, and normalization constants (N_{nl}) are given to five significant figures. To minimize the effects of errors of mechanical integration, the calculations have been carried out in a way which takes advantage of the close agreement of $\frac{1}{2}P_{2p}$, P_{3p}, P_{4p}, and P_{5p} in the region of small r. In essence, the mechanical integrations were carried out with small differences, and the work was arranged so that it was unnecessary to evaluate common factors. The final formula took the form

$$(3)\quad A_{1snp} = k\,\frac{1}{N_{np}\lambda_{np1s}^3}\left(1 - \sum_{i=1}^{n-2} \rho_i\right) ,$$

where k is a constant and ρ_i are ratios, small compared with 1, which are calculated from the differences between the radial p functions. Choosing k so that the four transition probabilities add up to unity, the following results were obtained:

Transition	Relative Probabilities (Calculated)
A_{1s2p}	0.8122
A_{1s3p}	0.1559
A_{1s4p}	0.0289
A_{1s5p}	0.0030

The changes in these relative probabilities in going to neutral xenon are expected to be small, although a truly quantitative estimate would require a rather involved calculation, since the readjustments of the entire electron clouds are involved. Qualitatively, one would expect the change to be such that the higher terms in the series A_{1snp} would become smaller on the following physical grounds: The addition of one extra negative charge to the nucleus will have only a slight direct effect on the $1s$ and np wave functions in the neighborhood of the $1s$ shell, since the nuclear charge is so great. On the other hand, the outer part of the $5p$ wave function, which is screened from the nucleus by about 37 units, moves out more markedly, with a consequent reduction in the magnitudes of the inner antinodes. This renormalization effect is not expected to be large for a change of nuclear charge of only one unit. On the basis of pure scaling considerations,[9] it is

[5] I. Bergström, *Arkiv Fysik* 5, 191 (1952).

[6] C. D. Broyles, D. A. Thomas, and S. K. Haynes, *Phys. Rev.* 89, 715 (1953).

[7] E. H. S. Burhop, *The Auger Effect and Other Radiationless Transitions*, p 48, Cambridge University Press, Cambridge, England, 1952.

[8] D. R. Hartree, *Proc. Roy. Soc.* (*London*) A143, 506 (1934).

[9] D. R. Hartree, *The Calculation of Atomic Structures*, p 116, Wiley, New York, 1957.

estimated that the effect would change the value of A_{1s5p} to 0.0029. Using Eq. 1, one then obtains

$$\beta_{5p} = 0.0045 \pm 0.0008 \ . \tag{4}$$

It would appear that the predominant part of the sum represented in Eq. 1 is due to internal conversion in the $5p$ shell.

The corresponding internal-conversion coefficient takes the value 0.21 ± 0.03 when expressed in conventional terms. An independent check would obviously be obtained by a separate, direct computation; such a computation is being considered by Green.

The use of the charge spectrum for determining outer-shell conversion coefficients in this manner is not likely to find wide applicability. The requirements that the element be in the form of a monatomic vapor and that a single isomeric transition be involved as a pure activity are so restrictive that the case of Xe^{131m} may be almost unique.

PHENOMENOLOGICAL NUCLEAR POTENTIALS FOR O^{17}

H. O. Cohn J. L. Fowler

The neutron differential elastic-scattering cross sections for oxygen and beryllium have been measured[1,2] as a function of angle at a number of energies between 0.7 and 2.0 Mev. Neutrons were produced by the $H^3(p,n)$ reaction in a gas cell by protons accelerated with the 5.5-Mv Van de Graaff machine. The neutron energy resolution was about 50 kev full width at $^1/_2$ maximum. Scattered neutrons were detected with a shielded recoil counter by a standard technique.[3,4] The scattering samples were BeO $4^1/_2$ in. long and $^5/_8$ or $^7/_8$ in. in diameter and beryllium samples of the same length and containing the same number of beryllium nuclei as in the BeO samples. Runs were made with a BeO sample, with a beryllium sample, and with no sample.

Some of the experimental results are given in Fig. 1. On the right-hand side is a curve of the total cross section of oxygen taken from the literature.[5] The resonance which shows up as a dip at 2.37 Mev indicates that the s-wave potential phase shift is about 90 deg at this energy. The arrows indicate the energy at which the differential cross-section curves on the left-hand side are measured. For the data on the left-hand side, the center-of-mass differential cross section, in barns, is plotted against the cosine of the center-of-mass angle as the abscissa. The data have been corrected for multiple scattering and for a slight change of

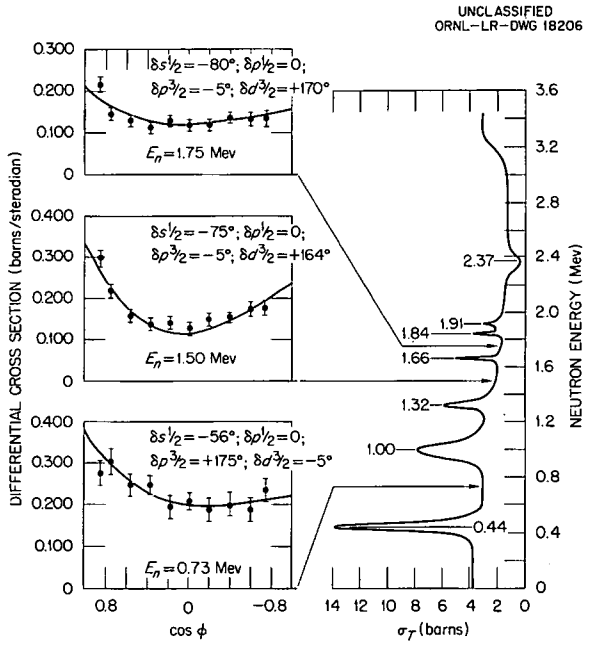

Fig. 1. Differential Cross Sections of Oxygen in the 0.7- to 2.0-Mev Range.

---

[1] J. L. Fowler and H. O. Cohn, *Bull. Am. Phys. Soc.* 2, 32 (1957).

[2] H. O. Cohn and J. L. Fowler, *Phys. Semiann. Prog. Rep. Sept. 10, 1956*, ORNL-2204, p 32.

[3] H. B. Willard, J. K. Bair, and J. D. Kington, *Phys. Rev.* 98, 669 (1955).

[4] J. L. Fowler and C. H. Johnson, *Phys. Rev.* 98, 728 (1955).

[5] C. K. Bockelman *et al.*, *Phys. Rev.* 84, 69 (1951).

counter efficiency with energy. The curves are theoretical fits to the data, and the phase shifts required are given beside each curve. A change of any phase shift by 5 deg gives an appreciably worse fit to the experimental data.

In Fig. 2 the differential cross section at the 1-Mev resonance is plotted against the cosine of the center-of-mass angle. The multiple scattering correction in this case was quite complicated, since the scattered neutrons have their energy reduced below the resonance energy. Since at some angles this correction amounted to about 30% and since various approximations to this correction differed by ⅓ of this amount, the errors on each point were increased statistically by ⅓ of the multiple scattering correction at the point. The theoretical curve through the data is calculated with an s-wave phase shift of −62 deg and a $d_{3/2}$ resonance averaged over 50 kev due to the neutron energy spread.

Figure 3 is a plot of the phase shifts given in the last figures vs neutron energy. For the $p_{3/2}$ and $d_{3/2}$ phase shifts the curves go through 90 or 270 deg at resonance energies with a slope given by the width of the resonance.[5] Within ±5 deg, the $p_{1/2}$ phase shift is zero up to 1.75 Mev, as Okasaki has observed[6] below 700 kev. The uncertainty of the s-wave phase shift, the sine of which is larger than that of the other phase shifts except near resonances, is determined primarily by that of the total cross section.

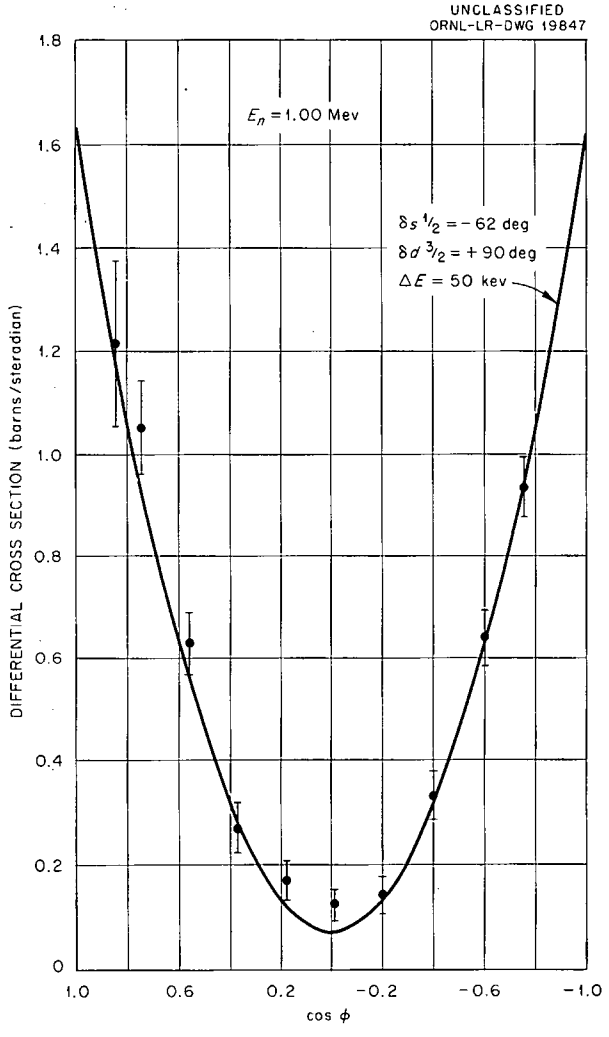

Fig. 2. Differential Scattering of Neutrons by Oxygen at the 1-Mev Resonance.

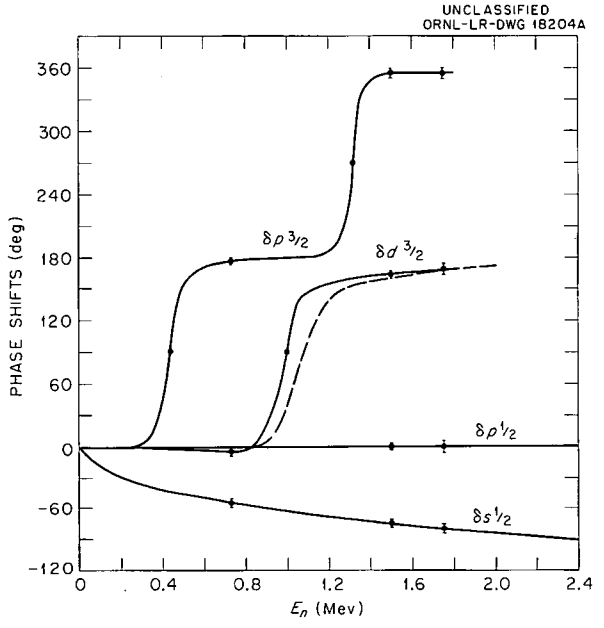

Fig. 3. Phase Shifts for Scattering of Neutrons by Oxygen.

It has been pointed out previously[1,7] that the s-wave neutron scattering phase shifts for zero-spin light nuclei can be calculated under the assumption that the effect of the nucleus on the neutron is that of a simple static potential. For O^{16} scattering this should be especially true, since in this case both the neutrons and the protons form closed shells. In Fig. 4 the s-wave

[6] A. Okasaki, *Phys. Rev.* **99**, 55 (1955).

[7] J. L. Fowler, *Phys. Semiann. Prog. Rep. Sept. 10, 1956*, ORNL-2204, p 10.

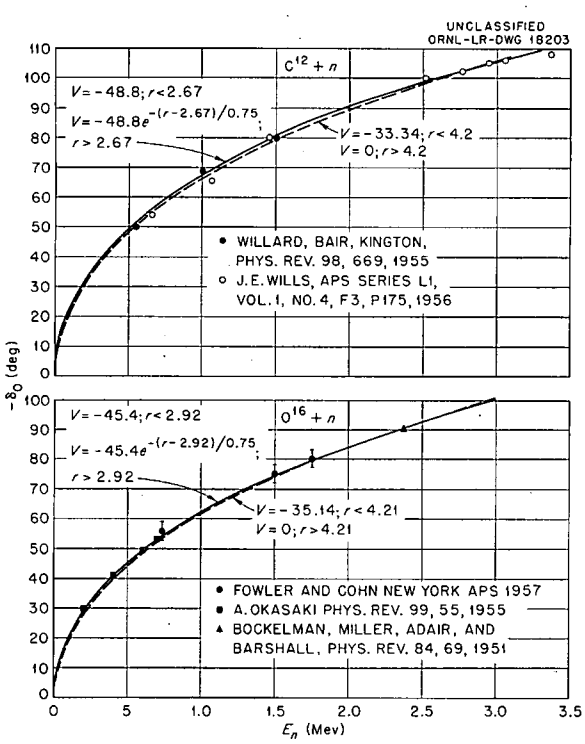

Fig. 4. The s-Wave Phase Shifts for Neutron Scattering from Carbon and Oxygen.

phase shifts for O^{16}, as well as those for C^{12}, have been replotted. Below 700 kev the oxygen points are from the data of Okasaki.[6] In the case of O^{17} there is a $j = \frac{1}{2}+$ single-particle level at −3.27 Mev below the $O^{16} + n$ unbound state.[8] If one requires that the average potential which describes the elastic-scattering data also gives the correct position of this $2s$ bound state, one finds for a square well only one set of parameters is possible. A well 35 Mev deep and 4.2×10^{-13} cm in radius fits the required conditions. For the case of carbon, with the corresponding bound state at −1.86 Mev, the well is 33.3 Mev deep with the same radius. Since it seemed unreasonable for oxygen and carbon to have the same radius, the case of a well with a diffuse boundary was investigated.[9] With an exponential boundary which decreases with a $1/e$ distance of 0.75×10^{-13} cm, as indicated above each curve, equally good fits to the data are obtained, and, furthermore, the central constant region of the potential wells varies as $A^{1/3}$. An exponential boundary was chosen, since the eigenvalue problem has been solved in this case by Green to give bound-state energies.[9]

Since the 1-Mev $d_{3/2}$ resonance of Fig. 1 is a single-particle level,[10] it should be possible to predict its energy position and the variation of the $d_{3/2}$ phase shifts with energy from the properties of the type of potentials used to calculate the s-wave phase shifts. It is necessary to introduce a spin-orbit potential-energy term, and for this purpose the Thomas form is used. With an exponential well which fits the $2s$ bound state and the s-wave phase shifts, and with the Thomas spin-orbit term increased by about the same factor found to be consistent with experimental data for much higher mass nuclei,[11,12] the dashed $d_{3/2}$ curve in Fig. 3 is obtained. The potential parameters used were as follows:

$$V = -44.2 \text{ Mev}, \qquad r < 2.76 \times 10^{-13} \text{ cm},$$

$$V = -44.2e^{-(r-2.76\times10^{-13})/1\times10^{-13}} - 1.05 \times \times 10^{-26} \frac{1}{r}\frac{\partial V}{\partial r}\frac{\vec{l}\cdot\vec{s}}{\hbar^2}, \qquad r > 2.76 \times 10^{-13} \text{ cm},$$

where

$$\frac{\vec{l}\cdot\vec{s}}{\hbar^2} = \frac{1}{2}\begin{Bmatrix} l \\ \text{or} \\ -(l+1) \end{Bmatrix} \text{ if } \begin{Bmatrix} j = l + \frac{1}{2} \\ \text{or} \\ j = l - \frac{1}{2} \end{Bmatrix}.$$

A very slight adjustment of the factor multiplying the Thomas term would shift the resonance to correspond to the 1-Mev level. With this potential the $d_{5/2}$ bound state occurs slightly below the $j = \frac{5}{2}+$ ground state of O^{17}, which presumably is the other member of the $1d$ doublet.[9] By detailed fitting of these higher angular-momentum states and phase shifts, it may be possible to establish in more detail the behavior of these phenomenological nuclear potentials.

[8] F. Ajzenberg and T. Lauritsen, *Revs. Mod. Phys.* 27, 77 (1955).

[9] A. E. S. Green and K. Lee, *Phys. Rev.* 99, 772 (1955).

[10] R. K. Adair, *Phys. Rev.* 92, 1491 (1953).

[11] A. E. S. Green, *Phys. Rev.* 104, 1617 (1956).

[12] A. A. Ross, H. Mark, and R. D. Lawson, *Phys. Rev.* 102, 1613 (1956).

COULOMB EXCITATION OF 2^+ STATES IN EVEN-EVEN ISOTOPES OF TIN AND ZIRCONIUM

P. H. Stelson F. K. McGowan

The location of the first excited state in several of the even-even tin isotopes is known from radioactive-decay work. These levels are at 1.30, 1.28, 1.18, and 1.14 Mev for Sn^{114}, Sn^{116}, Sn^{120}, and Sn^{122}, respectively. A composite gamma-ray peak with an average energy of 1.20 Mev was observed when a target of normal tin was bombarded by 9.0- and 10.0-Mev doubly ionized alpha particles accelerated by the 5.5-Mv electrostatic generator. This spectrum is shown in Fig. 1 for the 10-Mev alpha-particle energy. The variation in gamma-ray yield with alpha-particle energy was consistent with that expected for coulomb excitation, and the angular distribution of the gamma rays exhibited the strong anisotropy characteristic of coulomb excitation of 2^+ states. Having this evidence that coulomb excitation of tin was measurable, samples of enriched isotopes were ordered to obtain more detailed information. The targets of the enriched samples were prepared by sintering the metallic tin powders into thin foils ½ in. in diameter. These were mounted on 5-mil nickel target backings. The observed pulse-height spectra at an alpha-particle bombarding energy of 10.13 Mev for Sn^{116}, Sn^{118}, Sn^{120}, Sn^{122}, and Sn^{124} are shown in Figs. 2 and 3. In addition to the peak ascribed to coulomb excitation of the 2^+ state, the spectra show numerous other peaks. The origin of some of these is known; for example, the 340-kev peak results from the $O^{18}(\alpha,n)Ne^{21*}$ reaction, but the rest are not known. These are probably caused by small amounts of light-element impurities. In general, the observed gamma-ray energies are in agreement with those deduced from radioactive-decay work. The 2^+ states for Sn^{118} and Sn^{124} were not previously known.

A single gamma ray with an energy of 0.92 Mev was observed when a target of normal zirconium was bombarded with 9.0-Mev alpha particles (see Fig. 1). The 2^+ states of Zr^{92} and Zr^{94} are known to be at 0.92 Mev from other work.

Table 1 contains a summary of the information obtained on the gamma-ray energies, the gamma-ray yields, and the $B(E2)_{ex}$. Table 2 contains the half lives for the excited states and a comparison of the observed $B(E2)_d$ with that calculated for transitions between independent particle states $[B(E2)_{sp}]$. For the calculation of $B(E2)_{sp}$ it is assumed that the radius of the nucleus is $1.2 \times 10^{-13} A^{1/3}$ cm.

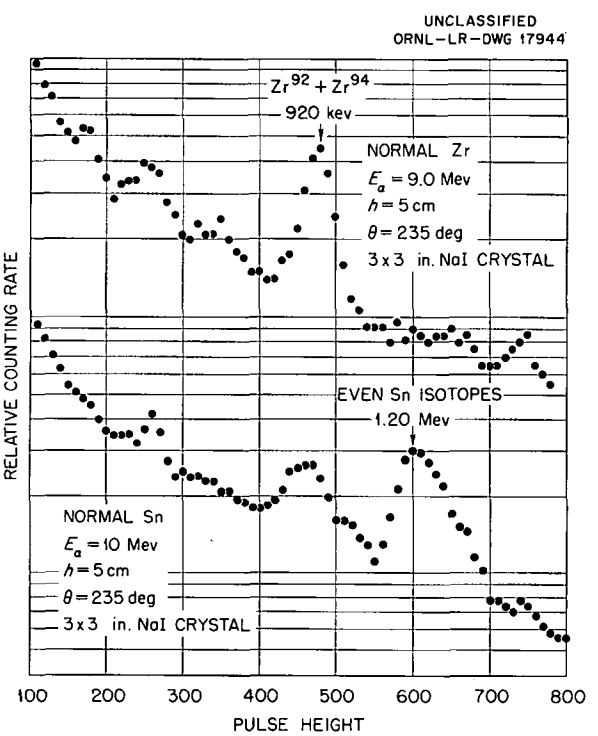

Fig. 1. Pulse-Height Spectra Resulting from Coulomb Excitation of the 2^+ States of Tin and Zirconium.

Table 1. Summary of Gamma-Ray Yields and Reduced $E2$ Transition Probabilities for Excitation of 2^+ States in the Tin and Zirconium Isotopes

Target	E_γ	E_α	I (gammas per microcoulomb)	Excitations per microcoulomb	$\int \frac{E_f g_2}{dE/d\rho x}$	$B(E2)_{ex} \times 10^{49}$ (cm^4)
Sn^{116}	1.268	9.13	3.36×10^4	3.54×10^4	2.03×10^3	1.82 ± 0.17
		10.13	8.58×10^4	9.07×10^4	5.72×10^3	1.65 ± 0.14
Sn^{118}	1.219	8.12	1.18×10^4	1.21×10^4	6.95×10^2	1.81 ± 0.26
		9.13	4.62×10^4	4.75×10^4	2.56×10^3	1.93 ± 0.14
		10.13	1.19×10^5	1.23×10^5	6.88×10^3	1.87 ± 0.10
Sn^{120}	1.155	8.12	2.10×10^4	2.08×10^4	9.85×10^2	2.21 ± 0.26
		9.13	6.84×10^4	6.82×10^4	3.39×10^3	2.09 ± 0.10
		10.13	1.59×10^5	1.59×10^5	8.72×10^3	1.90 ± 0.07
Sn^{122}	1.130	8.12	2.71×10^4	2.90×10^4	1.13×10^3	2.67 ± 0.35
		9.13	7.89×10^4	8.46×10^4	3.80×10^3	2.32 ± 0.22
		10.13	1.59×10^5	1.71×10^5	9.56×10^3	1.88 ± 0.14
Sn^{124}	1.128	8.12	2.33×10^4	2.44×10^4	1.15×10^3	2.21 ± 0.28
		9.13	6.13×10^4	6.43×10^4	3.85×10^3	1.74 ± 0.12
		10.13	1.62×10^5	1.71×10^5	9.66×10^3	1.84 ± 0.12
$Zr^{92,94}$	0.92	9.00	7.17×10^4	2.05×10^5	1.33×10^4	0.79 ± 0.08

Table 2. Summary of the Information on the 2^+ States of the Even-Even Isotopes of Tin

Columns 2 and 3 show a comparison of positions of 2^+ states located from coulomb excitation with those obtained from radioactive-decay studies; column 4 lists the best values for $B(E2)_{ex}$; column 5 gives the half lives for the excited states calculated from the observed $B(E2)_{ex}$; column 6 gives a comparison of the observed transition probabilities with those expected for transitions between independent particle states

Isotope	E_γ (Mev) Coulomb Excitation	E_{2^+} (Mev) Radioactive Decay	$B(E2)_{ex} \times 10^{49}$ (cm^4)	$T_{1/2}$ (sec)	$\frac{B(E2)_d}{B(E2)_{sp}}$
Sn^{114}		1.30			
Sn^{116}	1.268 ± 0.010	1.28	1.73 ± 0.13	5.0×10^{-13}	10.3
Sn^{118}	1.219 ± 0.010		1.87 ± 0.13	5.6×10^{-13}	10.9
Sn^{120}	1.155 ± 0.010	1.18	2.00 ± 0.11	6.9×10^{-13}	11.4
Sn^{122}	1.130 ± 0.010	1.14	2.03 ± 0.17	7.5×10^{-13}	11.3
Sn^{124}	1.128 ± 0.010		1.90 ± 0.13	8.5×10^{-13}	10.3
$Zr^{92,94}$	0.92 ± 0.01	0.92	0.79 ± 0.04	5.5×10^{-12}	6.3

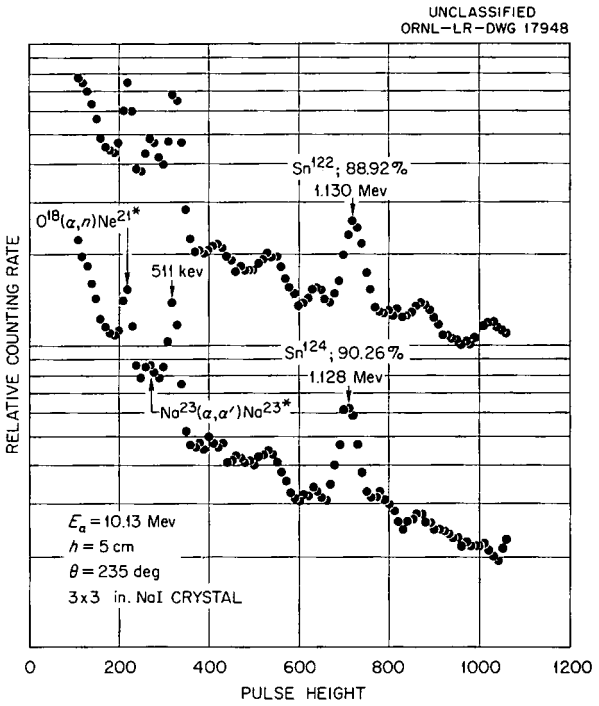

Fig. 2. Pulse-Height Spectra Resulting from Coulomb Excitation of Enriched Isotopes of Sn^{122} and Sn^{124}.

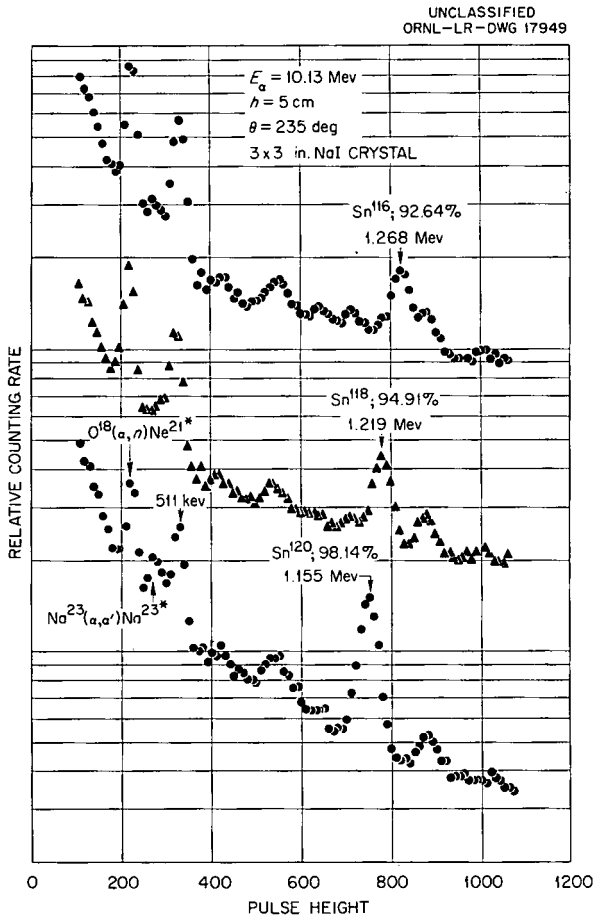

Fig. 3. Pulse-Height Spectra Resulting from Coulomb Excitation of Enriched Isotopes of Sn^{116}, Sn^{118}, and Sn^{120}.

THE REACTIONS $Si^{28}(p,p'\gamma)Si^{28}$, $P^{31}(p,\alpha\gamma)Si^{28}$, AND $P^{31}(p,p'\gamma)P^{31}$

J. K. Bair H. O. Cohn H. B. Willard

In previously reported[1-4] work on the reaction $Si^{28}(p,p'\gamma)Si^{28}$, mention was made of five very narrow, low-intensity resonances at 2.64, 3.88, 3.93, 3.97, and 4.93 Mev proton bombarding energy. These levels gave rise to, and were detected by, the 1.78-Mev gamma rays resulting from the de-excitation of the 1.78-Mev state in Si^{28} and were presumed to be the result of the inelastic scattering of protons on Si^{28}. It might, however, be possible that the gamma rays from these low-intensity levels were the result of the excitation of the same level in Si^{28}, but by an entirely different reaction, $P^{31}(p,\alpha\gamma)Si^{28}$. While the original silicon targets were made with reasonable care and with silicon from various sources, it was impossible to rule out the presence of a small amount of phosphorus impurity.

To check whether or not these weak levels were indeed present in the $P^{31}(p,\alpha\gamma)Si^{28}$ reaction, thin phosphorus targets were prepared, and the yield of the 1.78-Mev gamma ray was studied as a function of bombarding proton energy. Some 25 resonances for the production of this gamma ray were found in the range of 3 to 4 Mev proton bombarding energy; however, their intensities and energy locations were such as to exclude this reaction from being the cause of the weak levels seen in the previous work on silicon. We conclude, therefore, that the original assignment is correct.

In addition to the $P^{31}(p,\alpha\gamma_{1.78})Si^{28}$ reaction, a preliminary yield was obtained for the 1.26-Mev gamma rays resulting from the $P^{31}(p,p'\gamma_{1.26})P^{31}$ reaction. Again some 25 levels[5] were found in the range of 3 to 4 Mev proton bombarding energy. Evidence was also found for the excitation and decay of the second excited state at 2.234 Mev excitation energy[6] in P^{31}. Figure 1 shows the spectra of the gamma rays (as seen by a 3 × 3 in. NaI crystal at 0 deg with respect to the incoming proton beam) taken at 3.11 (lower curve) and 3.73 Mev (upper curve) bombarding proton energy. Also shown is the 2.62-Mev ThC″ calibration. At the higher proton energy, the 2.24-Mev gamma ray from the second excited state of P^{31} is clearly evident in addition to the 1.26-Mev gamma ray

[1] H. B. Willard *et al.*, *Phys. Semiann. Prog. Rep. March 20, 1955*, ORNL-1879, p 5.

[2] J. K. Bair *et al.*, *Phys. Semiann. Prog. Rep. Sept. 10, 1955*, ORNL-1975, p 15.

[3] H. O. Cohn *et al.*, *Phys. Rev.* **99**, 644A (1955).

[4] H. B. Willard *et al.*, *Bull. Am. Phys. Soc.* **1**, 264 (1956).

[5] J. W. Olness and H. W. Lewis, *Phys. Rev.* **99**, 654A (1955); D. M. Van Patter *et al.*, *Phys. Rev.* **103**, 656 (1956).

[6] D. M. Van Patter *et al.*, *Bull. Am. Phys. Soc.* **2**, 60 (1957).

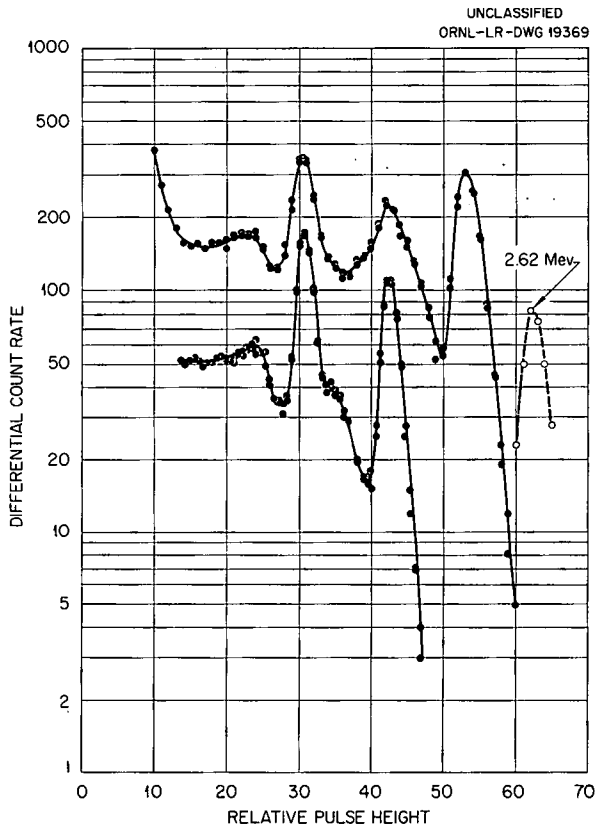

Fig. 1. Gamma-Ray Spectrum as Measured with a 3 × 3 in. NaI Scintillation Counter. The upper curve was measured at a bombarding energy of 3.73 Mev, whereas the lower curve was measured at 3.11 Mev. The dashed curve is the full energy peak of the ThC″ calibration gamma ray at 2.62 Mev.

from the first excited state of P^{31} and the 1.78-Mev gamma ray from the (p,α) reaction.

Figure 2 shows a thin-target yield curve in the vicinity of a strong resonance at 3.1 Mev. The data plotted are the readings of the peak channel corresponding to the 1.78-Mev resonance. Also shown (lower curve) is the background of 1.78-Mev radiation from the tantalum target backing obtained before the phosphorus was laid down; this background is from the ever-present surface impurity layer of silicon. Figure 3 shows the angular distribution of these gamma rays from the phosphorus (p,α) reaction at the peak of this resonance; these data were corrected for the presence of the silicon gamma rays by means of the known[2,3] silicon angular distribution. The solid curve is a plot of $1 + 0.32 \cos^2 \phi$.

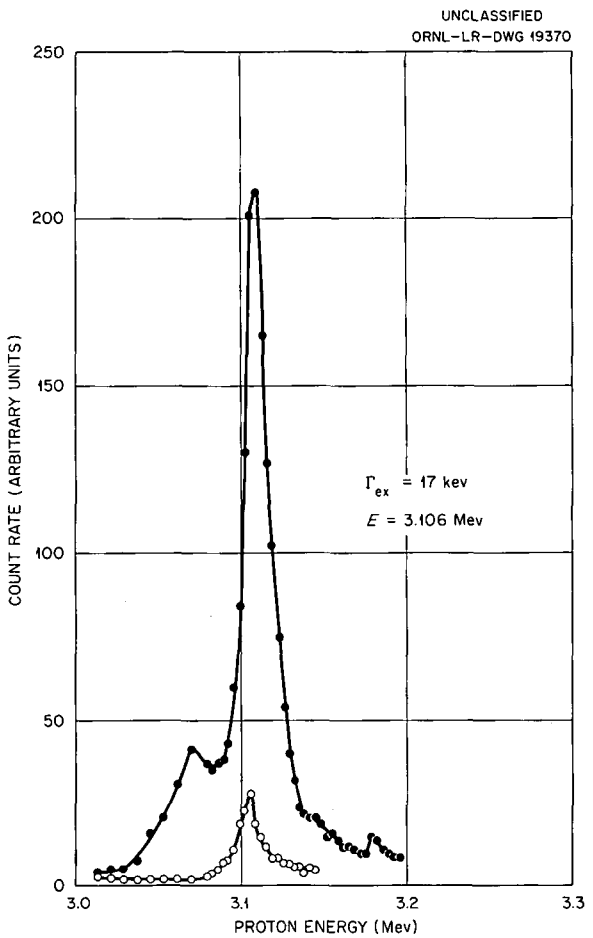

Fig. 2. Yield Curve of the 1.78-Mev Gamma Ray. The lower curve is the background from silicon contamination of the target backing.

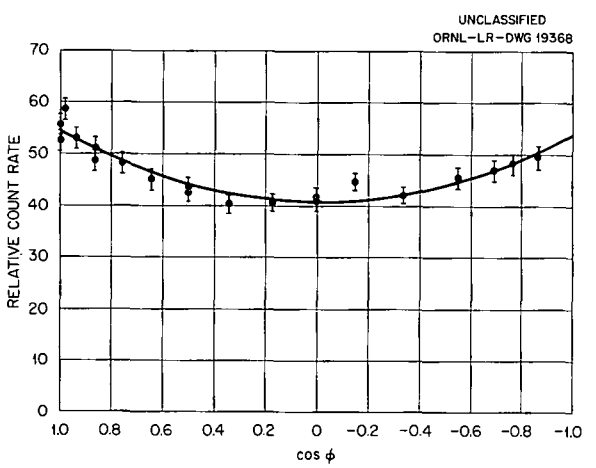

Fig. 3. Angular Distribution of the 1.78-Mev Gamma Rays at the Resonance Shown in Fig. 2. The solid curve is a plot of $1 + 0.32 \cos^2 \phi$.

CROSS SECTIONS FOR (p,n) REACTIONS IN INTERMEDIATE NUCLEI

C. H. Johnson A. Galonsky

The cross sections for (p,n) reactions in intermediate nuclei for proton energies well below the coulomb barrier offer a test of the statistical theory for the reactions. Figures 1 through 12 give the cross sections measured by the method previously described[1] for 12 nuclei from Cl^{37} to Nb^{93}. The cross sections for Ti^{49}, V^{51}, Mn^{55}, and As^{75} are those reported previously.[1] The targets, except for Nb^{93}, were nearly 20 kev thick for protons at the (p,n) threshold. Results for Nb^{93} were obtained by differentiating a thick-target yield.

In the statistical theory[2] the cross section is resolved into a sum of components for each l value for the incoming proton. Each term in the series is essentially the cross section for compound nucleus formation multiplied by the relative probability for neutron emission. For these intermediate nuclei, except for Cl^{37}, the coulomb

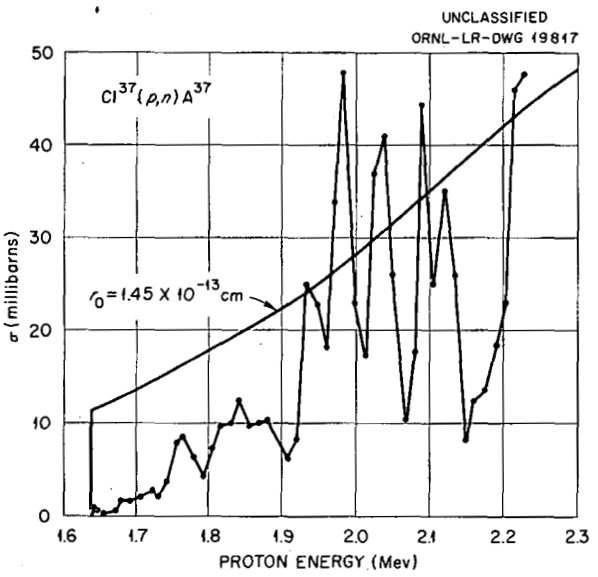

Fig. 1. Cross Section for the $Cl^{37}(p,n)A^{37}$ Reaction. The theoretical cross section for formation of the compound nucleus is given for $R = 1.45A^{1/3} \times 10^{-13}$ cm.

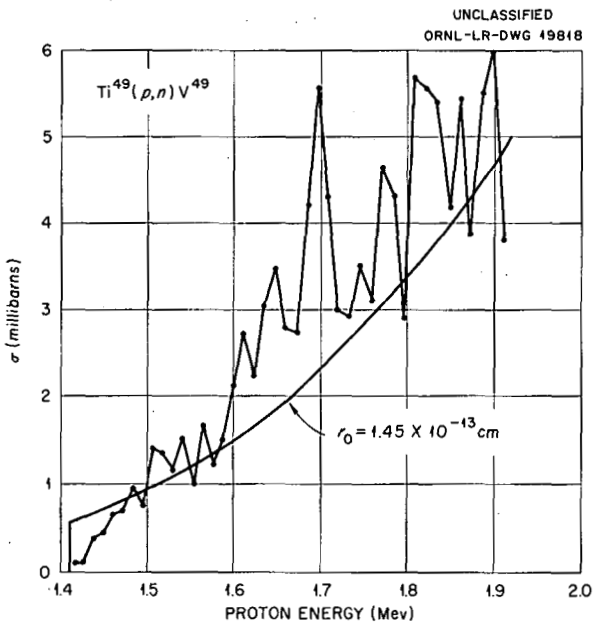

Fig. 2. Cross Section for the $Ti^{49}(p,n)V^{49}$ Reaction.

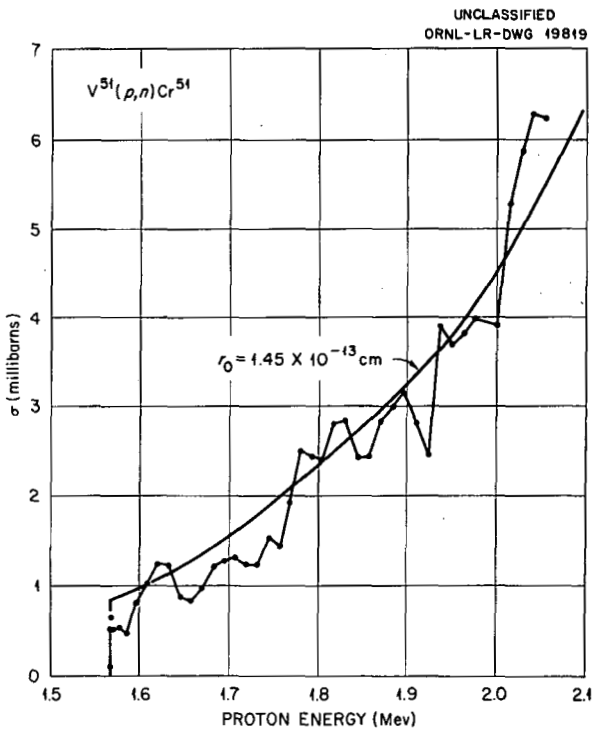

Fig. 3. Cross Section for the $V^{51}(p,n)Cr^{51}$ Reaction.

[1] C. H. Johnson, A. Galonsky, and J. Ulrich, *Phys. Semiann. Prog. Rep. Sept. 10, 1956*, ORNL-2204, p 28.

[2] W. Hauser and H. Feshbach, *Phys. Rev.* **87**, 366 (1952).

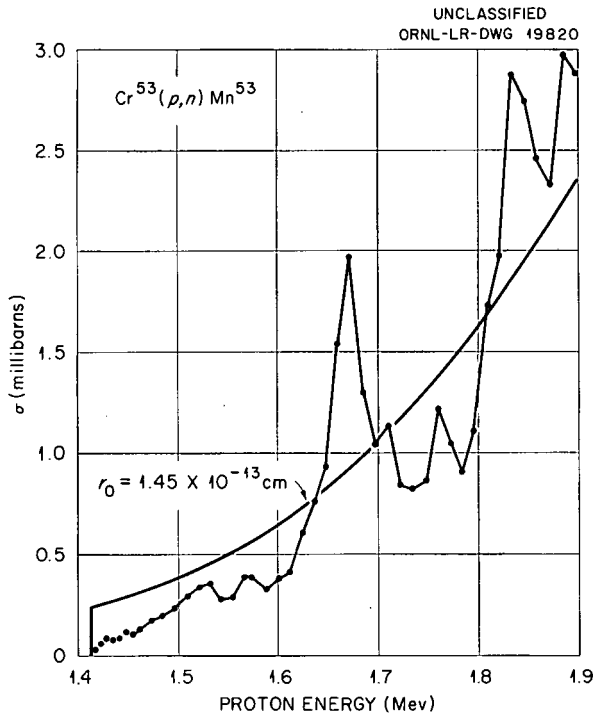

Fig. 4. Cross Section for the $Cr^{53}(p,n)Mn^{53}$ Reaction.

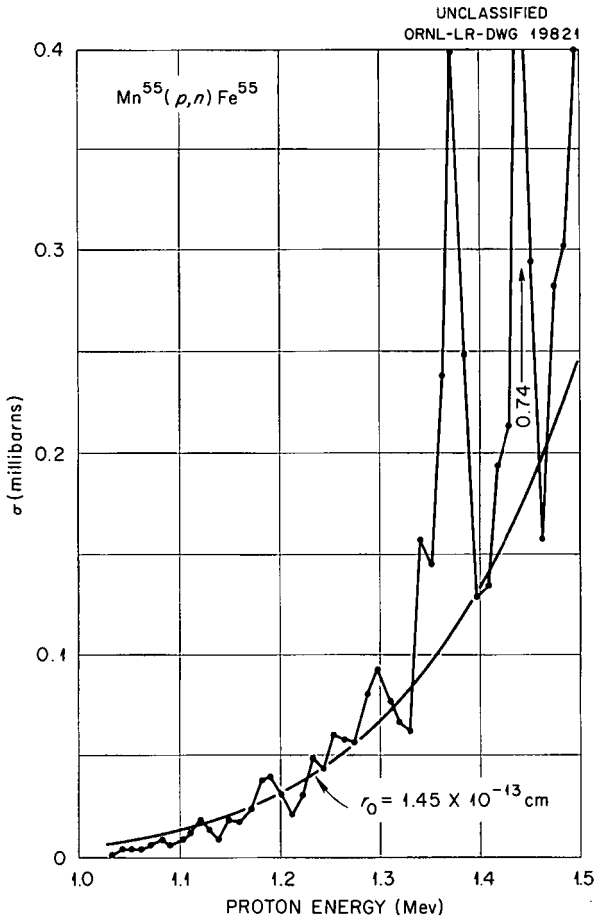

Fig. 5. Cross Section for the $Mn^{55}(p,n)Fe^{55}$ Reaction.

barrier effectively prohibits re-emission of a proton, so that neutrons compete only with gamma radiation. For energies about 0.3 to 0.5 Mev above the (p,n) threshold the probability for emission of s-, p-, and, in some cases, d-wave neutrons predominates over radiation. Hence, those terms in the expansion which lead to s-, p-, and d-wave neutrons reduce simply to the cross section for formation of the compound nucleus. These terms comprise most of the cross section. Terms involving neutrons of higher l values must come from terms which have higher proton l values and which contribute negligibly to the formation of the compound nucleus. Thus for energies about 0.3 to 0.5 Mev above the (p,n) threshold the cross section is approximately

$$\sigma = \pi \lambda\!\!\!^{-2} \sum_{l} (2l + 1)\, T_l(p) \ ,$$

where $\lambda\!\!\!^{-}$ is the wavelength, $l\hbar$ is the orbital angular momentum, and $T_l(p)$ is the penetration factor for the proton.

Penetration factors were found from the expression of Blatt and Weisskopf,[3] using the coulomb wave functions[4] and assuming a black nucleus with a square well 40 Mev deep. The results are not very sensitive to the well depth, varying mostly as the reciprocal of the square root of the depth. The results are sensitive to the radius of the well, changing by a factor of 2 for about a 13% change in radius. Curves of the

[3] J. M. Blatt and V. F. Weisskopf, *Theoretical Nuclear Physics*, p 360, Wiley, New York, 1952.

[4] I. Bloch *et al.*, *Revs. Mod. Phys.* **23**, 147 (1951); *Tables of Coulomb Wave Functions*, National Bureau of Standards Applied Mathematics Series 17, U.S. Government Printing Office, Washington, 1952.

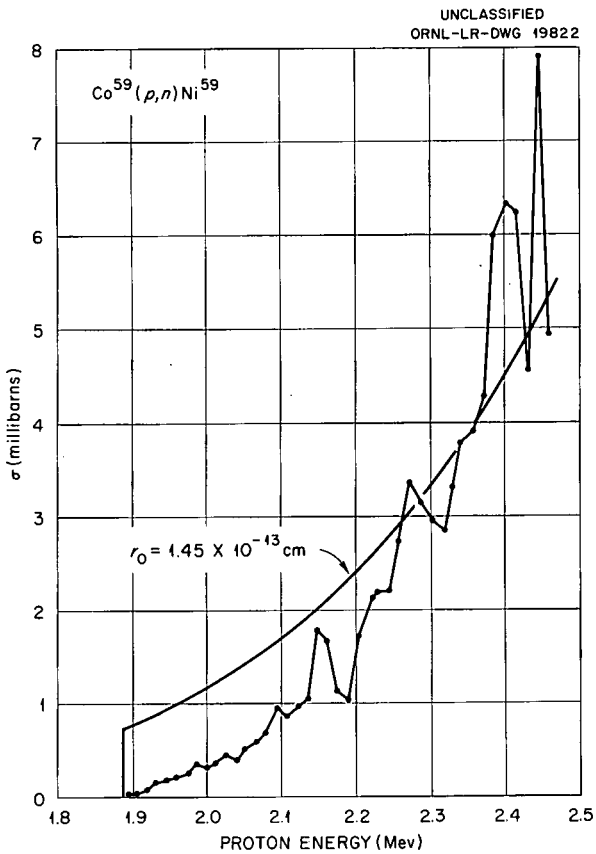

Fig. 6. Cross Section for the $Co^{59}(p,n)Ni^{59}$ Reaction.

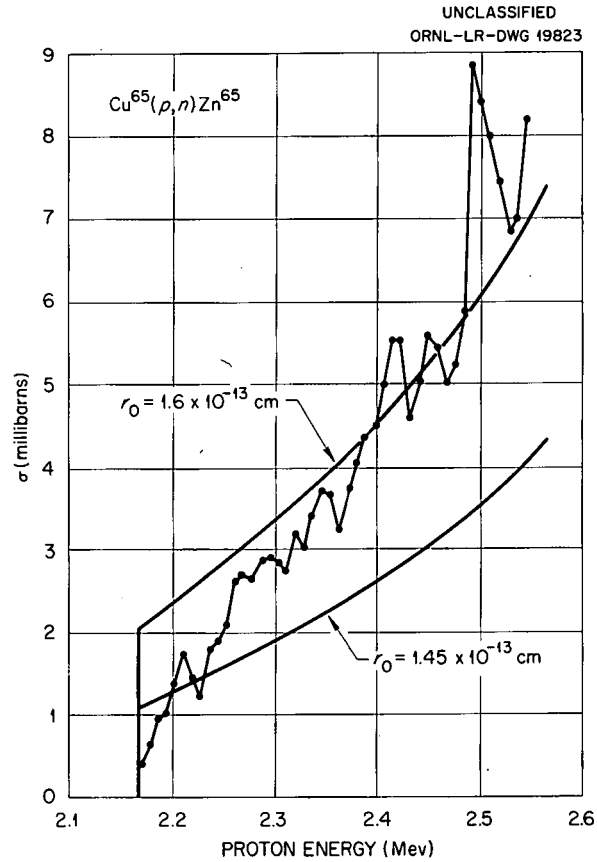

Fig. 7. Cross Section for the $Cu^{65}(p,n)Zn^{65}$ Reaction.

cross section for the formation of the compound nucleus are shown for all 12 nuclei for

$$R = r_0 A^{1/3} = 1.45 A^{1/3} \times 10^{-13} \text{ cm} .$$

For nuclei from Cu^{65} to Se^{82}, curves are also given for

$$R = r_0 A^{1/3} = 1.60 A^{1/3} \times 10^{-13} \text{ cm} .$$

Comparisons between theory and experiment show systematic agreement with the smaller radii for Ti^{49} through Co^{59} and Nb^{93} and with the larger radii for Cu^{65} through Se^{82}. Chlorine-37 is a special case, since re-emission of the proton is probable.

The theoretical yields are shown with a discontinuity at threshold. Thresholds for Se^{82} and Nb^{93} are not known. Deviations near threshold are in the expected direction. In the group from Ti^{49} to Co^{59}, for example, two nuclei, Cr^{53} and Co^{59}, show large deviations. These result from the fact that the $Cr^{53}(p,n)Mn^{53}$ and $Co^{59}(p,n)Ni^{59}$ reactions each require a spin change of two units, whereas the other three, Ti^{49}, V^{51}, and Mn^{55}, require a change of only zero or one unit. The greater spin change forces the neutron to be emitted with higher angular momentum, so that it cannot compete as well with gamma-ray emission. The next step in this investigation will be to make a more detailed comparison by use of reasonable ratios, Γ_γ/Γ_n, for the relative probability of emission for gamma rays and neutrons.

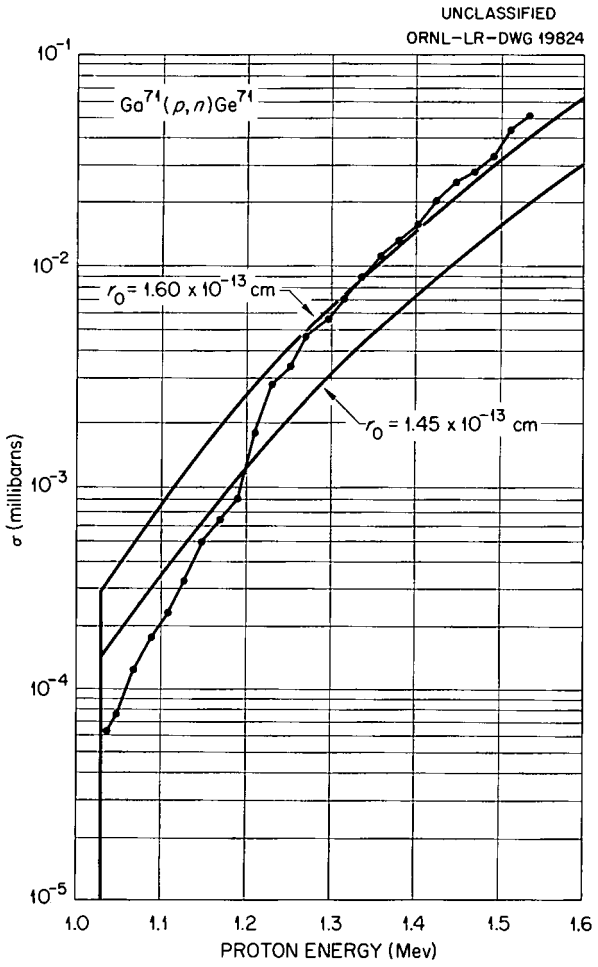

Fig. 8. Cross Section for the $Ga^{71}(p,n)Ge^{71}$ Reaction.

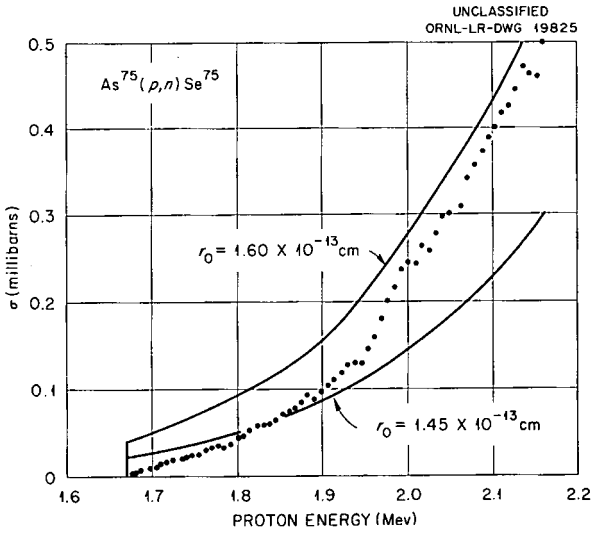

Fig. 9. Cross Section for the $As^{75}(p,n)Se^{75}$ Reaction.

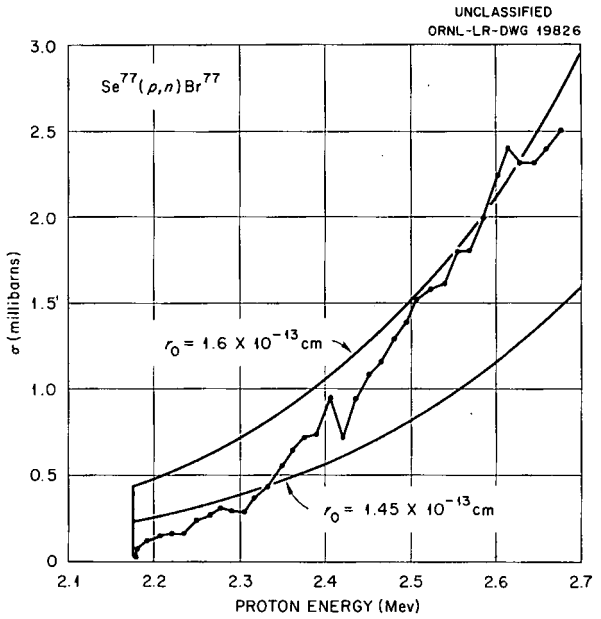

Fig. 10. Cross Section for the $Se^{77}(p,n)Br^{77}$ Reaction.

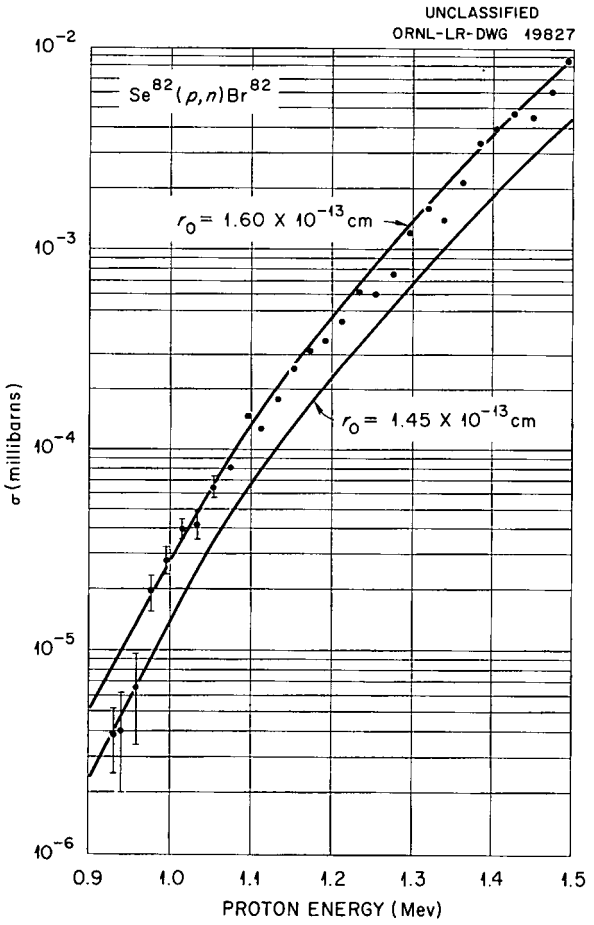

Fig. 11. Cross Section for the $Se^{82}(p,n)Br^{82}$ Reaction.

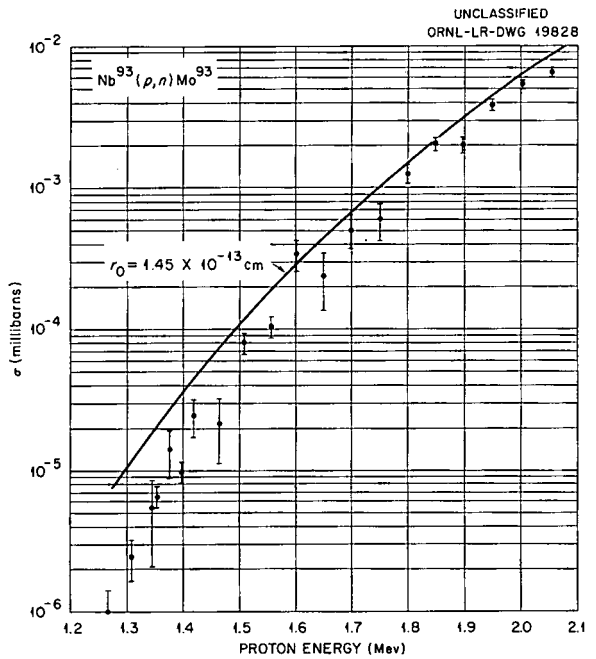

Fig. 12. Cross Section for the $Nb^{93}(p,n)Mo^{93}$ Reaction.

ENERGY LEVELS OF C^{13}

A. Galonsky C. D. Moak R. L. Traughber[1] C. M. Jones[2]

Doubly charged He^3 ions of 1.25 Mev from the 625-kv cascade accelerator have been used to produce the $B^{11}(He^3,p)C^{13}$ reaction.[3] The spectra of protons emitted at 45, 90, and 135 deg with respect to the He^3 beam have been analyzed in an NaI crystal spectrometer. They are shown in Figs. 1, 2, and 3, respectively. Besides the $B^{11}(He^3,p)C^{13}$ protons there are proton groups from the inevitable carbon on the target, and deuteron groups leading to the first two states of C^{12}. As illustrated in Fig. 1, the groups from the carbon contaminant were identified by comparing a spectrum from a fresh B^{11} target with one that had had several days of bombardment. The deuteron groups were distinguished from the protons by the differential energy loss observed in spectra for which an absorber was interposed between target and detector.

The energy response of the crystal was calibrated by means of the proton groups corresponding to the well-known states at 0, 3.097, 3.684, 3.844, and 6.864 Mev excitation in C^{13} and those from the

---

[1]Summer participant from Louisiana State University (1956), now at Stanford University.

[2]Summer participant from Georgia Institute of Technology (1956).

[3]The boron, purchased from the Atomic Energy Research Establishment, Harwell, England, was 99.3% B^{11}.

$C^{12}(He^3,p)N^{14}$ reaction. Energies thus determined for the other levels in C^{13} are indicated above the corresponding peak in each figure. At the top is a copy of the level energies listed by Ajzenberg and Lauritsen.[4]

Previously unobserved states, shown with good statistics in Fig. 4, are those at 5.49 ± 0.08 and 6.09 ± 0.08 Mev. Since this spectrum was seen through a 25-mg/cm^2 aluminum absorber, the deuteron group has shifted down in pulse height with respect to the proton groups. Both states must be quite narrow, because they have not been seen in the n-C^{12} total cross section or for the mirror nucleus, N^{13}, in the p-C^{12} interaction. Intermediate coupling calculations by Kurath[5] indicate a narrow $\frac{5}{2}^-$ state near 5 Mev.

[4] F. Ajzenberg and T. Lauritsen, *Revs. Mod. Phys.* **27**, 77 (1955).

[5] D. Kurath, *Phys. Rev.* **101**, 216 (1956).

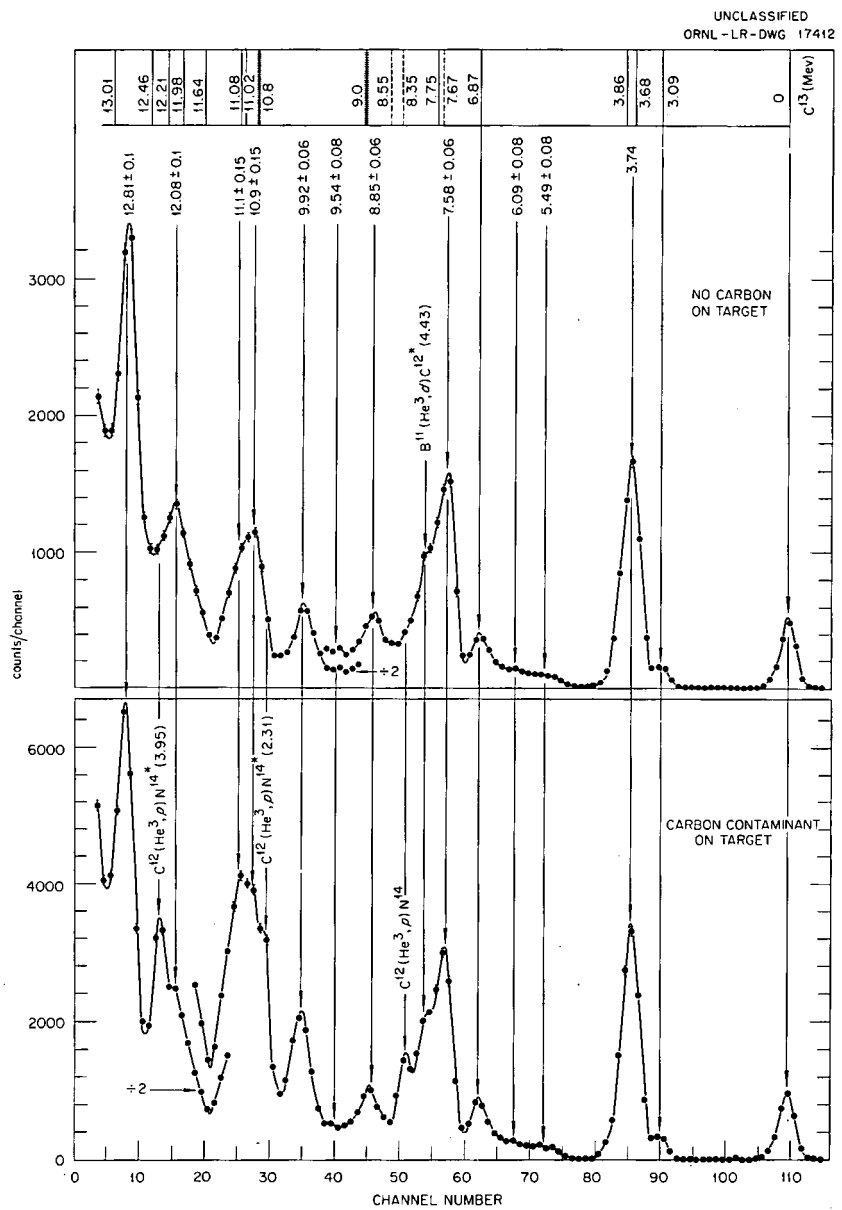

Fig. 1. Proton Spectrum in NaI at 45 deg from $B^{11} + He^3 \longrightarrow C^{13} + H^1$.

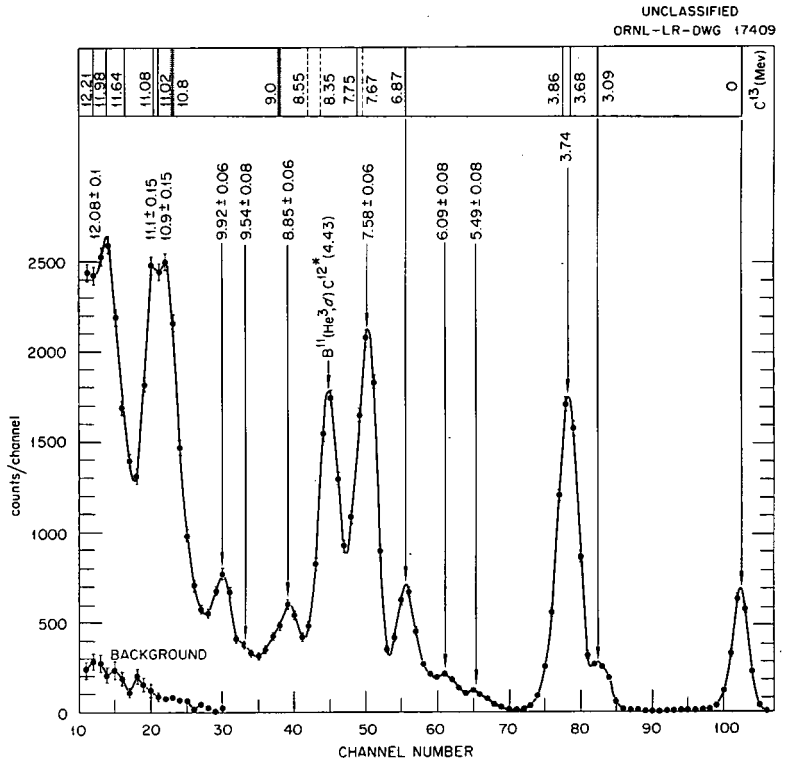

Fig. 2. Proton Spectrum in NaI at 90 deg from $B^{11} + He^3 \longrightarrow C^{13} + H^1$.

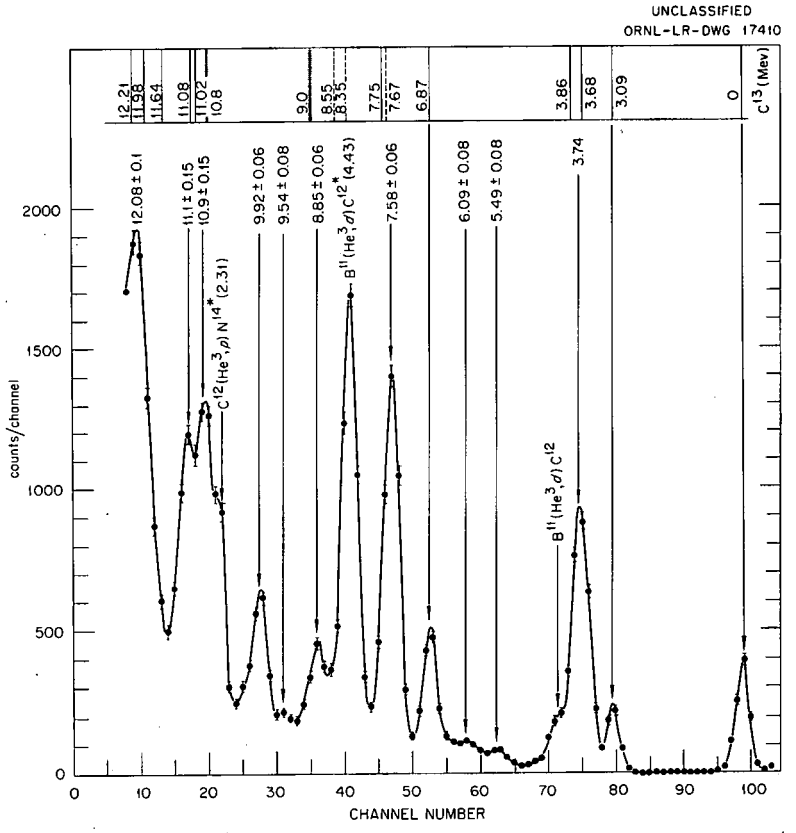

Fig. 3. Proton Spectrum in NaI at 135 deg from $B^{11} + He^3 \longrightarrow C^{13} + H^1$.

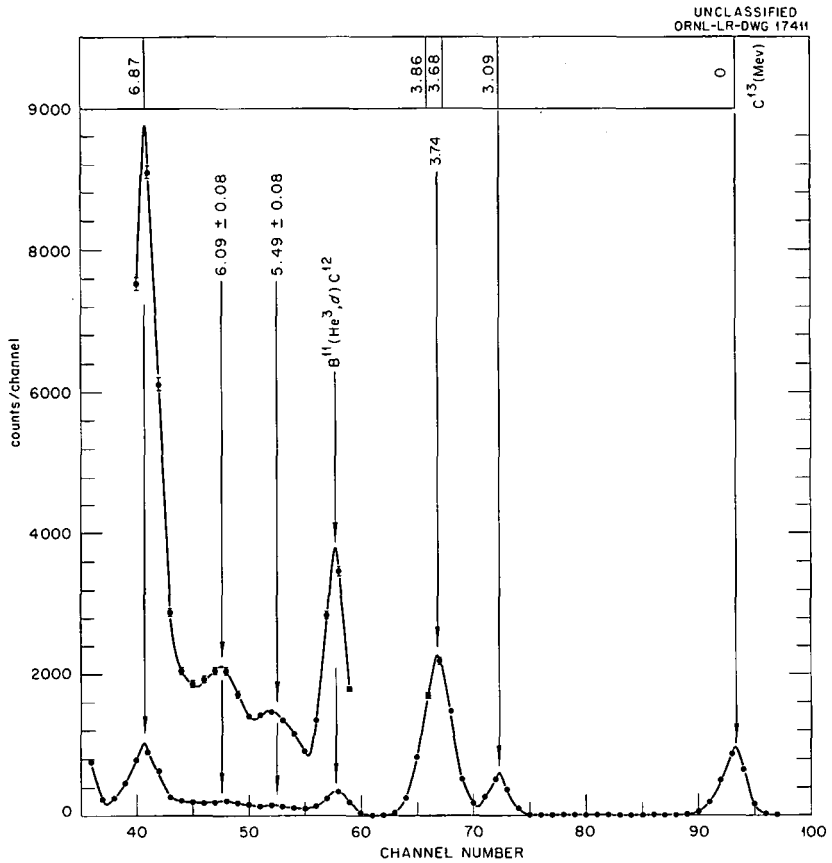

Fig. 4. Proton Spectrum in NaI at 135 deg from $B^{11} + He^3 \longrightarrow C^{13} + H^1$.

MILLIMICROSECOND NEUTRON TIME-OF-FLIGHT SPECTROMETRY

J. H. Neiler W. M. Good J. H. Gibbons

A pulsed Van de Graaff for producing bursts of ions of (5 to 10) $\times 10^{-9}$ sec duration at a repetition rate of 10^6/sec and at a peak current of about 400 μa has been undergoing development during the last 18 months. The instrument, together with timing circuits, is intended specifically for neutron time-of-flight studies, in two rather distinct applications. These are (1) for the measurement of neutron spectra, as in (d,n) reactions, inelastic scattering, fission, etc., and (2) for a new approach to the measurement of cross sections in the kilovolt region, whereby unmoderated neutrons from the Li(p,n) reaction are employed as the source from which neutrons of a specific energy are chosen by time-of-flight. In the latter application severe requirements are placed not only upon the steady performance of the Van de Graaff, and of the ion source especially, but also upon the stability of the multichannel pulse-height selector, which is the basis of the

multichannel time analyzer. A description of the difficulties encountered and the manner in which they are to be handled will be published in the coming months. However, a rather distressing amount of time has been required to reach a position so that as much as half the time available can go into measurements. This report, therefore, contains the very recent results obtained on the measurement of total neutron cross sections in the kilovolt region, together with some studies of (d,n) reactions.

For the kilovolt cross-section studies it has been possible, with the employment of strong focusing lenses, to focus the pulsed proton beam to a spot 2 or 3 mm in diameter on the lithium target. By virtue of this relatively small neutron source, total cross-section measurements can be made on separated isotopes. Figures 1, 2, and 3 show some of the results obtained for the separated isotopes of K^{39}, K^{41}, and Rb^{87}, respectively. The resolution of the spectrometer was 3% or less in energy. A representative area analysis made

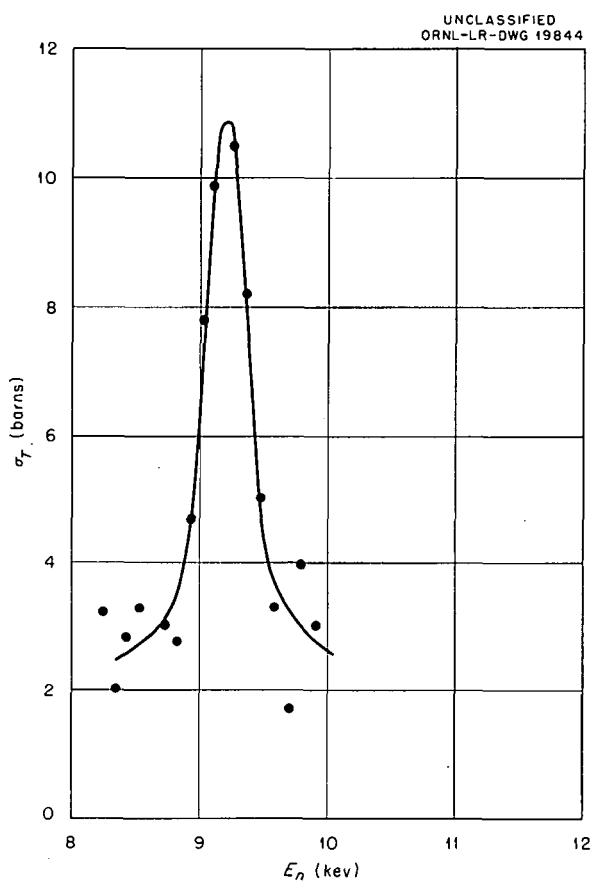

Fig. 1. Total Cross Section of K^{39} as a Function of Energy.

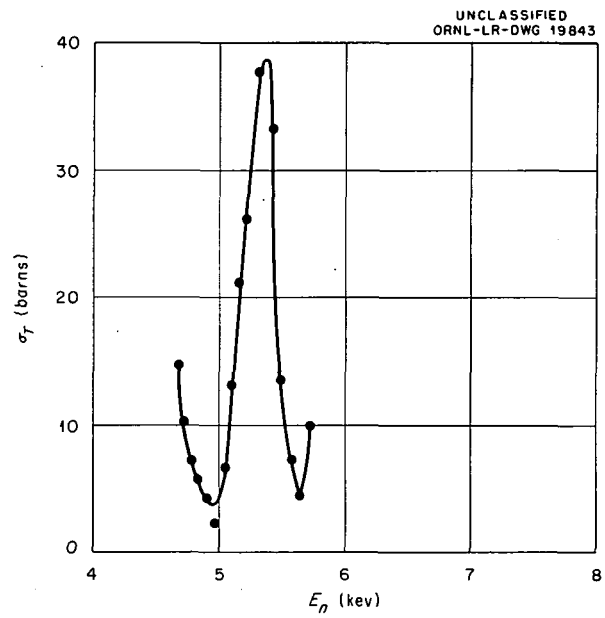

Fig. 2. Total Cross Section of K^{41} as a Function of Energy.

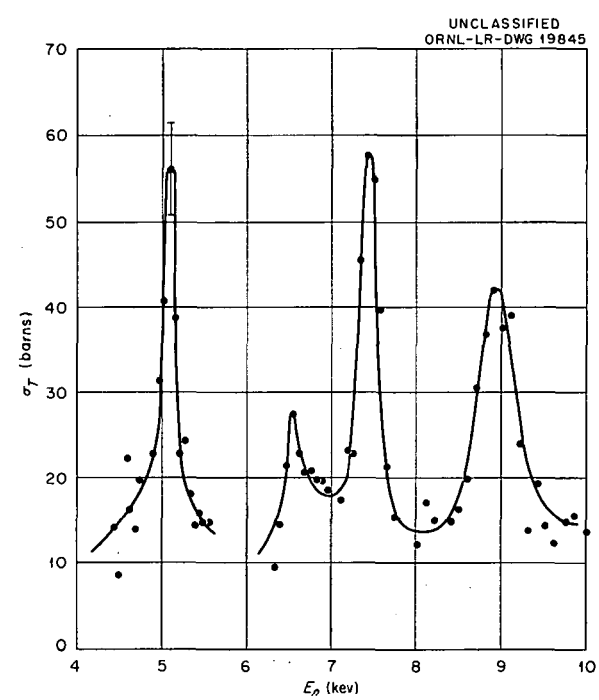

Fig. 3. Total Cross Section of Rb^{87} as a Function of Energy.

on K^{41} indicates a Γ of 50 ev. The results obtained for K^{39} and K^{41} serve to establish the energies of corresponding levels in K^{40} and K^{42}. In the case of Rb^{87}, the energies of the corresponding levels in Rb^{88} were established; the levels corresponding to 6.55 and 7.45 kev neutron bombarding energy on Rb^{87} have not previously been resolved. The level appearing at 8.95 kev appears broad and is no doubt being partially resolved, yielding roughly a width of 350 v. Other isotopes that have been run but which, for one reason or another, have to be re-examined are Y^{89}, Rb^{85}, Sr^{86}, and Sr^{88}.

Application of the time-of-flight equipment to higher neutron energies continues to be largely devoted to a study of (d,n) reactions on the light elements. Comparison of recent (d,n) neutron spectra with those obtained a year ago shows the progress that has been made with the technique.

The spectrum of $Be^9(d,n)B^{10}$ has been remeasured,[1] along with several other spectra, with the better resolution now obtainable and with the 3 × 3 in. plastifluor detector shielded by a 1-in. lead housing to reduce room background. For this work the terminal pulser oscillator frequency was increased to 2 Mc, giving, with the alternate pulse eliminator, a pulse repetition rate of 2 Mc. The best over-all resolution measured with this setup was ~4 mμsec on target gamma rays of about 500 kev; this was obtained at an average pulsed current of ~0.25 μa. The operating resolution throughout the life of the source was ~6 mμsec at a current of ~0.6 μa.

The spectrum of high-energy neutrons from $Be^9(d,n)$, using a flight path of 6.0 m, is given in Fig. 4. The peaks labeled η_0, η_1, η_2, η_3, and η_5 are neutron groups leading to the B^{10} ground state and to the 0.72-, 1.74-, 2.15-, and 3.58-Mev levels, respectively. The group labeled η_4 (?) has a Q value of 1.50 ± 0.15 Mev, corresponding to a B^{10} excitation of ~2.8 Mev. The existence of this level has been previously suggested[2] and reported[3] but has not been confirmed by more recent measurements.[4] We plan to continue the study of this group to ensure that it is due to a level in B^{10} and to determine Q more precisely.

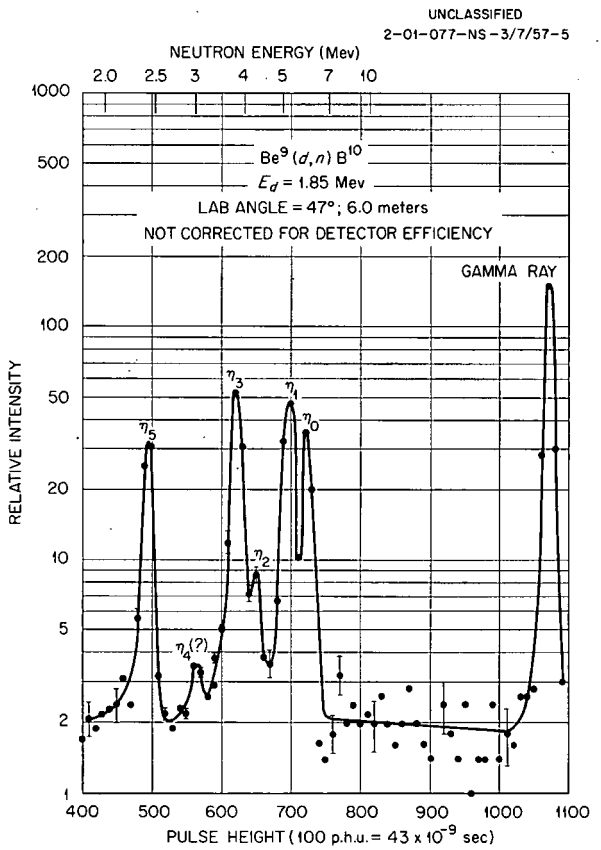

Fig. 4. Neutron Time-of-Flight Spectrum from $Be^9(d,n)B^{10}$.

In order to study the usefulness of this equipment for angular-distribution measurements, the distribution of group η_4 was measured at E_d = 1.85 Mev. It appears to be consistent with previously reported measurements[4] made on this level, but we have not yet attempted to fit it with stripping or compound-nucleus parameters.

A study of the reaction $B^{11}(d,n)C^{12}$ has been started. Figure 5 is the neutron spectrum obtained with a target enriched to 99% B^{11}. The groups labeled η_0, η_1, η_2, and η_3 correspond to the ground state and to the 4.43-, 7.65-, and 9.61-Mev levels in C^{12}. The peaks at lower neutron energies probably correspond to unresolved sets of levels at higher excitations in C^{12}. We plan to determine the angular distribution of this level if it can be properly resolved at the flight paths and resolutions presently obtainable.

[1] H. E. Banta *et al.*, *Phys. Semiann. Prog. Rep. March 10, 1956*, ORNL-2076, p 29–31.

[2] V. K. Rasmussen, W. F. Hornyak, and T. Lauritsen, *Phys. Rev.* **76**, 581 (1949).

[3] A. J. Dyer and J. R. Bird, *Austral. J. Phys.* **6**, 45 (1952).

[4] F. Ajzenberg and T. Lauritsen, *Revs. Mod. Phys.* **27**, 77 (1955).

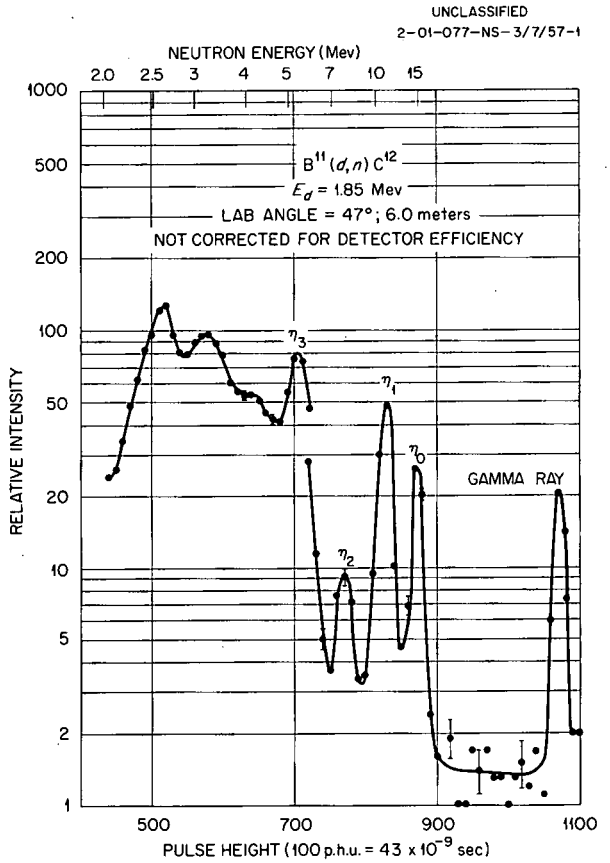

Fig. 5. Neutron Time-of-Flight Spectrum from $B^{11}(d,n)C^{12}$.

ELASTIC SCATTERING OF NEUTRONS BY C^{12}

H. B. Willard J. K. Bair H. O. Cohn

Previous angular-distribution measurements[1] in the energy region of 1.45 to 4.1 Mev were made by use of a scintillation detector. As a check on this method, and also to obtain greater statistical accuracy, it was felt worthwhile to repeat the measurements, using a gas recoil counter (propane). The geometry and details have already been described,[2] but in this case the neutron source was the $H^3(p,n)He^3$ reaction. Energy resolutions of 50 to 100 kev were used. Multiple scattering was less than 14%. The results were in good agreement with the earlier work;[1] accordingly, the two sets of data were averaged together. Table 1 shows the center-of-mass data corrected for multiple scattering.

[1] J. E. Wills, Jr., *Bull. Am. Phys. Soc.* 1, 175 (1956).

[2] H. B. Willard, J. K. Bair, and J. D. Kington, *Phys. Rev.* 98, 669 (1955).

Table 1. Center-of-Mass Differential Cross Section, $\sigma(\cos\phi)$, for the $C^{12}(n,n)C^{12}$ Reaction

Values are in millibarns/steradian

$\bar{E}_n$, Incident Neutron Energy (Mev)	Cos ϕ								
	0.78	0.59	0.39	0.19	−0.01	−0.20	−0.41	−0.60	−0.80
1.45	207 ± 6	181 ± 6	172 ± 6	154 ± 7	154 ± 8	152 ± 8	146 ± 8	146 ± 8	137 ± 13
2.02	155 ± 6	166 ± 6	147 ± 7	135 ± 7	129 ± 7	132 ± 7	120 ± 7	138 ± 8	150 ± 8
2.15	149 ± 13	122 ± 10	118 ± 11	105 ± 12	118 ± 10	138 ± 11	148 ± 11	159 ± 12	
2.28	158 ± 6	154 ± 6	114 ± 7	100 ± 7	111 ± 7	105 ± 7	111 ± 7	121 ± 8	147 ± 8
2.51	153 ± 6	136 ± 6	117 ± 6	100 ± 6	81 ± 6	91 ± 6	127 ± 7	147 ± 8	186 ± 8
2.76	196 ± 8	159 ± 9	114 ± 9	96 ± 10	74 ± 11	73 ± 11	113 ± 13	186 ± 14	258 ± 17
2.95	360 ± 15	224 ± 16	142 ± 16	59 ± 18	25 ± 20	45 ± 22	97 ± 26	292 ± 28	431 ± 30
3.05	117 ± 6	103 ± 6	85 ± 6	81 ± 6	82 ± 6	81 ± 6	91 ± 7	124 ± 8	163 ± 8
3.25	247 ± 10	161 ± 10	79 ± 11	53 ± 11	15 ± 12	32 ± 13	101 ± 14	197 ± 15	280 ± 18
3.51	337 ± 11	198 ± 13	98 ± 11	35 ± 13	5 ± 12	34 ± 13	90 ± 13	245 ± 18	352 ± 16
3.76	308 ± 11	163 ± 11	69 ± 11	59 ± 13	51 ± 13	74 ± 13	96 ± 14	197 ± 15	336 ± 17
4.10	99 ± 6	89 ± 6	54 ± 6	58 ± 6	58 ± 6	63 ± 7	79 ± 8	158 ± 9	193 ± 9

PRELIMINARY FAST-NEUTRON POLARIZATION MEASUREMENT

H. O. Cohn J. K. Bair H. B. Willard

A preliminary measurement of the polarization of fast neutrons was undertaken by using elastic neutron scattering from helium as a polarization analyzer. Helium can be used as a convenient analyzer in the Mev neutron range, because of the strong spin-orbit splitting of the $P_{3/2}$-$P_{1/2}$ inverted doublet. This results in large values of the polarization for scattering through 90 deg (in the center-of-mass system). It is greater than +0.50 between 0.5 and 1.5 Mev, is greater than −0.50 above 4 Mev, and is 0 near 2.4 Mev. The phase shifts required to calculate the amount of polarization are known.[1]

[1] J. D. Seagrave, *Phys. Rev.* **92**, 1222 (1953).

Neutrons, with an unknown degree of polarization, were produced through the $H^3(p,n)He^3$ reaction by 5.2-Mev protons accelerated with the 5.5-Mv Van de Graaff; 2.66-Mev neutrons were observed at 70 deg to the proton beam with a helium-filled cloud chamber. The volume-controlled expansion type of cloud chamber was 10 in. in diameter, 4 in. deep, and was filled with helium gas at 18 psi. Stereoscopic photographs were taken, although in the present analysis only one view was used. The chamber was expanded at ½-min intervals. Since the neutron beam was not pulsed, tracks of all ages appeared in the photographs. The number of helium recoil tracks to the right (R) and the number to the left (L) give the product

of the reaction polarization (R_R) and the analyzer polarization (P_A):

$$P_R P_A = \frac{L - R}{L + R},$$

where the sign of P is defined by the unit vector

$$\vec{n} = \frac{\vec{k}_{in} \times \vec{k}_{out}}{|k_{in}|\ |k_{out}|},$$

where k_{in} is the wave vector for the incident particle and k_{out} is the wave vector for the outgoing particle.

All tracks making an angle between 10 and 80 deg with, and to the right and left of, the line joining the target and the chamber were counted, subject to a restriction on the length of the tracks. Tracks longer than the maximum recoil track length permissible in the n-He collision at the observed angle were rejected. Tracks that were very short were also rejected, since they correspond to (1) tracks that are scattered at too steep an angle to the desired plane, (2) tracks that leave (or enter) the illuminated volume and hence are of unknown nature. This criterion does not eliminate tracks which are too long but which appear shorter due to reason 1 or 2. The number of these long tracks can be estimated, since they are mainly due to hydrogen recoils.

Accepting the angular spread of 10 to 80 deg, 234 tracks were observed to be recoiling to the right, and 211 to the left, giving a value of $P_R P_A = -0.052 \pm 0.048$. For the narrower angular spread of 30 to 60 deg, $R = 95$ and $L = 94$ for $P_R P_A = -0.005 \pm 0.073$. These values are in agreement with a small value for P_R or/and P_A. The energy and angles chosen correspond to $P_A = -0.09$ (calculated). This small value was purposely chosen to check for possible instrumental asymmetries in this preliminary measurement.

EXCITATION OF ISOMERIC STATES IN Pb AND As^{75} BY THE (n,n') REACTION

P. H. Stelson E. C. Campbell

Measurements of delayed nuclear effects resulting from fast-neutron bombardment of a sample have been made with the 5.5-Mv accelerator being used as a square-wave-modulated neutron source of variable frequency, together with a synchronized multichannel time analyzer. This apparatus has previously been described.[1] The fast neutrons were produced by bombardment of a thick beryllium metal target with 2.5-Mev alpha particles. An activity with a half life of 127 ± 10 μsec was observed when a sample of normal lead was irradiated. The decay curve is shown in Fig. 1. From an investigation of the decay of Bi^{206}, Alburger and Pryce[2] discovered an isomeric state in Pb^{206} with a half life of 145 ± 15 μsec. This state is at the 2.20-Mev excitation energy and is given the assignment 7^-. Its mode of decay is complex; none of the resulting gamma rays exceed an energy of 880 kev. An energy bias curve of the gamma rays detected by the anthracene crystal indicated that the 127-μsec activity was associated with gamma rays with energies up to but not exceeding 900 kev. It is concluded that we are exciting the isomer found by Alburger and Pryce. It is planned to obtain further confirmation by measurement of the threshold for excitation and by the use of radiogenic lead enriched to 88% in Pb^{206}.

A decay curve for the short-lived isomer in As^{75}, first reported by Schardt[3] from the study of the decay of Se^{75}, has been obtained and is shown in Fig. 2. The observed value of 18 ± 2 msec is in good agreement with Schardt's value of 18 ± 1.5 msec.

[1] E. H. Campbell and P. H. Stelson, *Phys. Semiann. Prog. Rep. March 10, 1956*, ORNL-2076, p 32.

[2] D. E. Alburger and M. H. L. Pryce, *Phys. Rev.* 95, 1482 (1954).

[3] A. W. Schardt, *Bull. Am. Phys. Soc.* 1, 85 (1956).

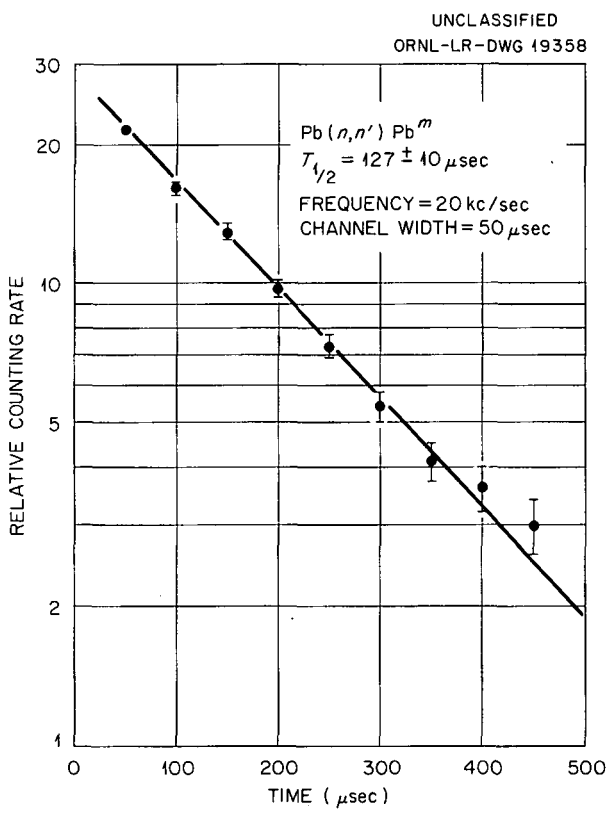

Fig. 1. Decay Curve for Isomeric State in Lead.

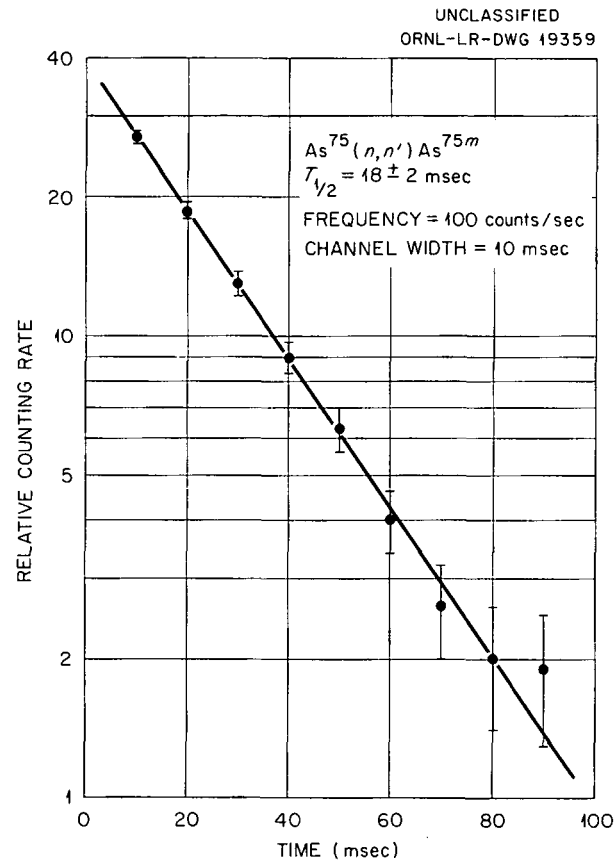

Fig. 2. Decay Curve for Isomeric State in As^{75}.

CROSS SECTION FOR THE $Be^9(n,\alpha)He^6$ REACTION

P. H. Stelson E. C. Campbell

The work on the $Be^9(n,\alpha)He^6$ cross section has been completed and has been submitted to *The Physical Review* with the following abstract: The cross section for the reaction $Be^9(n,\alpha)He^6$ has been measured for neutron energies of 0.7 (threshold) to 4.4 Mev. The cross section exhibits a smooth rise from less than 0.1 mb at the expected threshold to a broad maximum of 104 ± 7 mb at 3.0 Mev, followed by a gradual decrease to 70 mb at 4.4 Mev.

ACTIVATION CROSS SECTIONS WITH Sb-Be NEUTRONS

R. L. Macklin N. H. Lazar W. S. Lyon[1]

The neutron activation cross sections near 25 kev have been determined for about 50 nuclei. For irradiation, a spherical Sb-Be source was raised to the approximate center of a pair of aluminum hemicylindrical containers filled with the sample material. The weighed material, usually in the form of powdered element, oxide, or carbonate, was then transferred to a beaker, and the intensity of a particular gamma ray, following the normal beta decay, was determined with a 3 × 3 in. NaI(Tl) crystal and a multichannel analyzer. The gamma/beta branching ratio, either taken from the literature[2] or measured, was then used to obtain the activity of the sample. Corrections were made for self-absorption in the sample (usually less than 25%), and in many cases this correction was determined experimentally by mixing a known activity of the same radioactive nuclide, produced by a separate pile irradiation, into an amount of inert material equal in size to, and in the same geometry as, the Sb-Be irradiated sample.

The neutron flux was determined from a similar experiment with I^{127}, taking its cross section as 0.82 ± 0.06 barn.[3] The flux was determined several times during the period that activations were carried out, and the results obtained are plotted as a function of time in Fig. 1. The straight line corresponds to an exponential decay with a half life of 60 days, normalized to the first point, and the data deviate from it by less than ±1.3%.

The results of these measurements are given in Table 1 and plotted in Fig. 2. All the activities correspond to nuclei for which no alternate decay modes are known, except in the popular 54-min In^{115} often used as a standard. Table 1 and Fig. 2 also show the gamma ray measured and its yield per disintegration.

For several of the heavier elements, neutron widths, radiation widths, and level spacing for s-wave resonances have been determined. Using these data and the familiar Breit-Wigner single-level formula averaged over many resonances, one can predict the capture cross section at 25 kev for s-wave neutrons. The p-wave contribution to the cross section can also be predicted by taking the s-wave values of D per spin state and of Γ_γ, and estimating (Γ_n^0/D^*) by use of a "black-nucleus" model. The results are compared with the experimental values in Table 2. Within the experimental uncertainties (particularly of the parameters), the values agree. The nearly equal contribution of s- and p-wave capture near 25 kev is notable.

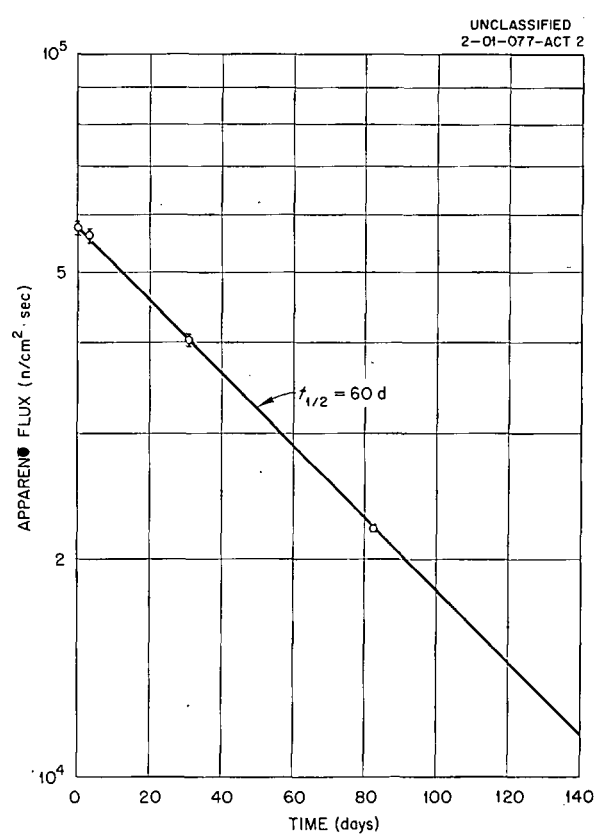

Fig. 1. Flux of Sb-Be Neutron Source as a Function of Time as Determined by Activation of I^{127} in $NaIO_3$ Standards.

[1] Analytical Chemistry Division.

[2] *Nuclear Science Abstracts*, Nuclear Data Group, National Research Council, Washington, D.C.

[3] R. L. Macklin, *Neutron Activation of Iodine Near 25 kev*, ORNL CF-56-1-40 (Jan. 6, 1956); *Bull. Am. Phys. Soc.* 1, 264 (1956).

Table 1. Activation Cross Sections with Sb-Be Neutrons

Measurements based on 820 ± 60 mb for I^{127}

Target Isotope	E_γ (Mev)	γ/d	σ (mb)*	Target Isotope	E_γ (Mev)	γ/d	σ (mb)*
Na^{23}	1.38	1.00	1.0 ± 0.2	Pd^{108}	0.088	0.0463*	540 ± 60
Mg^{26}	0.83	0.70	<14	Ag^{107}	0.61	0.0225*	930 ± 180
Al^{27}	1.78	1.00	1.4 ± 0.2	In^{115}	1.28	0.848	805 ± 80
Cl^{37}	2.1	0.47	1.1 ± 0.2	Sb^{121}	0.57	0.664	950 ± 100
K^{41}	1.52	0.20	<20	Sb^{123}	0.603	1.00	456 ± 46
Ti^{50}	0.32	0.95	5 ± 3	[I^{127}	0.455	0.172	820 ± 60]
V^{51}	1.45	1.00	50 ± 5	Ba^{138}	0.165	0.23*	11.4 ± 1.1
Mn^{55}	0.82	1.00	55 ± 6	La^{139}	1.60	0.882*	50 ± 7
Cu^{63}	0.511	0.38	116 ± 12	Ce^{140}	0.145	0.615	31 ± 4
Cu^{65}	1.04	0.10	46 ± 5	Ce^{142}	0.29	0.426*	425 ± 43
Ga^{71}	2.50	0.30	68 ± 13	Pr^{141}	1.59	0.041*	547 ± 55
Ge^{74}	0.274	0.112	54 ± 8	Sm^{152}	0.105	0.357	668 ± 100
As^{75}	0.55	0.446*	740 ± 70	Sm^{154}	0.25	0.037*	540 ± 70
Br^{81}	1.03	0.255*	550 ± 55	Gd^{158}	0.364	0.123*	710 ± 71
Rb^{85}	1.08	0.15	181 ± 35	Er^{170}	0.308 + 0.295	0.91**	298 ± 30
Rb^{87}	(1.85)	(0.23)	75 ± 15	Hf^{180}	0.482	0.85	441 ± 66
Zr^{94}	0.745	0.97	243 ± 36	W^{186}	0.686	0.288*	296 ± 44
Zr^{96}	0.660 (Nb^{97})	1.00	22 ± 4 (?)	Re^{185}		0.105*	2650 ± 500
Mo^{98}	0.14 + 0.18	0.72*	209 ± 21	Re^{187}	0.155	0.162*	970 ± 200
Mo^{100}	0.192	1.00	38 ± 8	Os^{190}	0.129	0.224	886 ± 130
	0.30 (Tc^{100})	1.00	45 ± 9	Au^{197}	0.411	0.95	1120 ± 110
Ru^{96}	0.216	0.92	321 ± 60	Hg^{202}	0.279	0.828	57 ± 13
Ru^{102}	0.498	0.90	386 ± 39	Th^{232}	0.310 (Pa^{233})		500 ± 100
Ru^{104}	0.73	1.00	211 ± 21	U^{238}	0.210 + 0.270 (Np^{239})		610 ± 61

*Our measurement.

**The authors express their thanks to M. E. Bunker for permission to use this value prior to publication.

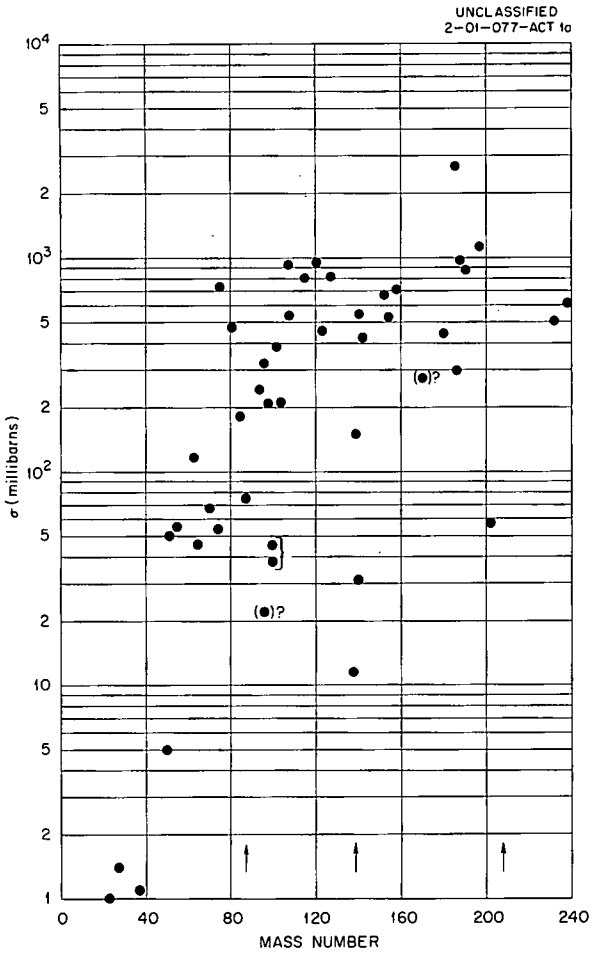

Fig. 2. Activation Cross Section vs Atomic Mass for Neutrons from Sb-Be Source [Relative to σ_{act} (I^{127}) = 0.82 ± 0.06 barn].

Table 2. The 25-kev (n,γ) Cross Sections

Target Isotope	$\sigma(n,\gamma)$ from Strength Functions (barns)			Measured $\sigma(n,\gamma)$ (barns)
	s	p	$s+p$	
Mo^{98}				0.21
Mo^{100}				0.038, 0.045
Mo (even)	0.07	0.13	0.20	
Ag^{107}	0.41	0.32	0.73	0.93
In^{115}	0.44	0.36	0.80	0.81, 0.80
Sb^{121}	0.42	0.35	0.77	0.95
Sb^{123}	0.28	0.30	0.58	0.46
I^{127}	0.56	0.36	0.92	0.82
Re^{185}				2.65
Re^{187}				0.97
$Re^{185,187}$	0.76	0.49	1.25	
Au^{197}	0.30	0.37	0.67	1.10, 1.15
Th^{232}	0.21	0.33	0.54	0.5
U^{238}	0.22	0.32	0.54	0.61

PROBABILITY OF THERMALIZATION OF FISSION NEUTRONS IN SMALL H_2O-U^{235} SUBCRITICAL SYSTEMS

E. C. Campbell P. H. Stelson

Measurements of the decay constants of subcritical H_2O-U^{235} solutions excited by a square-wave-modulated neutron source have been described in previous reports.[1] In the interpretation of these experiments by means of diffusion theory, the decay constant of the thermal-neutron flux (fundamental mode) can be expressed in terms of certain parameters, all of which are known accurately from experiment with the exception of $\bar{P}(B^2)$, which is defined as the probability that a fission neutron will be thermalized inside the system of buckling B^2. The experimentally determined decay constant is then used to evaluate

[1] E. C. Campbell and P. H. Stelson, *Phys. Semiann. Prog. Rep. March 10, 1956*, ORNL-2076, p 37; *Phys. Semiann. Prog. Rep. Sept. 10, 1956*, ORNL-2204, p 34.

$\bar{P}(B^2)$. The decay constant λ is given by the following expression:

$$(1)\quad \lambda = v\Sigma_a + DB^2 + v\Sigma_{25}[1 - \eta\bar{P}(B^2)] ,$$

where v is the thermal-neutron velocity, D is the diffusion coefficient of thermal neutrons in the solution, Σ_a and Σ_{25} are the macroscopic thermal absorption cross sections of moderator and of U^{235}, respectively, and η is the number of *prompt* neutrons emitted per neutron absorbed in U^{235}. The assumption is made that the slowing-down time of fission neutrons is small compared with the characteristic decay time of the system. The physical meaning of the four separate terms in Eq. 1 are, in order, as follows: probability per unit time for absorption of thermal neutrons in moderator, leakage of thermal neutrons, thermal-neutron absorption in U^{235}, thermalization of fission-produced neutrons.

The value of $\bar{P}(B^2)$ determined by this method for two different concentrations of U^{235}, namely 26.5 g/liter and 53.0 g/liter, is shown in Fig. 1. Included in the figure for purposes of comparison are (*a*) the Fourier transform of a diffusion kernel $(1 + 21.2B^2)^{-1}$, which appears to be a good fit for $B < 0.4$ cm^{-1}, and (*b*) the curve $q(k, 1.44\,\text{ev})$ calculated[2] by means of the B_3 approximation for a source of fission neutrons slowing down in water to indium resonance energy. Neither theoretical curve fits very well over the whole range of B. One would expect that if curve *b* were recalculated to thermal energy, the fit would be somewhat better, particularly for small systems (large B). It is difficult to evaluate the errors of the experimental points; these become progressively larger as the size of the system becomes smaller. In general the decay-constant measurements are considered to be accurate to about 1%, but since the evaluation of $\bar{P}$ involves the small difference of large quantities in the case of the smallest system (3-in.-dia, 3-in.-high cylinder), the result may be in error by as much as a factor of 2. For the larger systems the error should not exceed a few per cent.

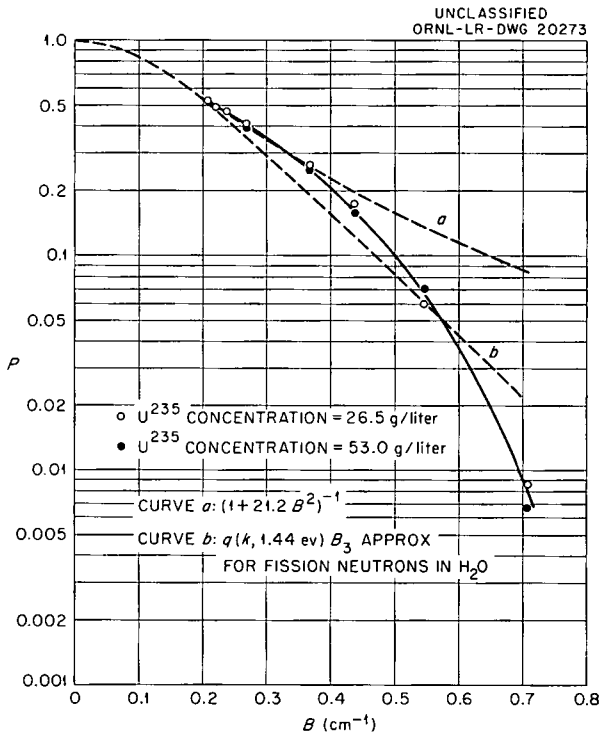

Fig. 1. Probability for Thermalization of Fission Neutrons Derived from Decay Measurements of Subcritical H_2O-U^{235} Systems.

[2] J. E. Wilkins, R. L. Hellens, and P. E. Zweifel, *Proceedings of the International Conference on the Peaceful Uses of Atomic Energy*, vol 5, p 62, United Nations, New York, 1955.

ORIENTATION OF ACTINIDE-GROUP NUCLEI

L. D. Roberts J. W. T. Dabbs G. W. Parker

FISSION OF ALIGNED NUCLEI

In the past three semiannual reports, work has been described on the alpha-particle emission from aligned U^{233} and Np^{237}. The nuclei were aligned through the nuclear electric quadrupole coupling in the UO_2^{++} or NpO_2^{++} ions, and the salts used were $UO_2Rb(NO_3)_3$ or $NpO_2Rb(NO_3)_3$. Further, a nuclear orientation effect has been observed through a measurement of the specific heat associated with this quadrupole coupling in the salt $U^{235}O_2F_2$.

A natural extension of this work is the observation of the fission of oriented U^{235} or U^{233} nuclei. The latter isotope is especially suitable for this experiment, in that one can make a simultaneous measurement of the alpha-particle and fission-fragment angular distributions. By using our earlier measurements of the temperature dependence of the alpha angular distribution as a standard, the observation of the alpha distribution in this case would constitute a thermometer and, furthermore, would provide an unequivocal demonstration and measure of the nuclear alignment.

To perform this fission experiment, a set of metal Dewar vessels for containing liquid nitrogen and helium was installed at neutron beam hole 52 at the south face of the ORNL Graphite Reactor. The apparatus[1] used for observing anisotropic alpha emission was then placed in the liquid-helium flask, with a $U^{233}O_2^{++}$-coated $UO_2Rb(NO_3)_3$ crystal located in the neutron beam. As before, the crystal could be rotated about an axis perpendicular to the crystalline *c* axis. The rotation axis was parallel to the thermal-neutron beam. Thus it was possible to count alpha particles and fission fragments emerging from the crystal, either parallel or perpendicular to the *c* axis.

As a counting material, we studied ZnS and CsI and found that the ZnS gave a better resolution of the alpha particles from the fission fragments. To minimize alpha-radiation damage to the counting screen, a shutter was installed to protect this screen between experiments. A neutron-beam monitor and also an effective beam shutter were installed.

An experiment was performed by, first, counting alpha particles at 0 and 90 deg to the *c* axis with the neutron beam off and at a low amplifier pulse-height setting. Then the pulse-height setting was raised to a point at which the alpha count was essentially shut off and the neutron beam was opened. Here the fission-fragment count was taken again at 0 and 90 deg. In all cases the neutron beam was monitored, and the fission-fragment intensity per unit neutron beam intensity was calculated. The above cycle was performed at 77 and at 1.32°K. At 77°K it was found that the intensity ratio $W(0°)/W(90°)$ was the same within statistics for the alpha particles and fission fragments. However, at 1.32°K these values were found to diverge. Here, for the alpha particles, the ratio had the expected value based on previous alpha experiments. This demonstrated that the U^{233} nuclei had the expected degree of nuclear alignment. The anisotropy observed for the fission of these aligned nuclei was, however, some five times smaller than the alpha-intensity ratio change. These results are illustrated in Fig. 1.

Bohr has presented a qualitative theoretical discussion[2] of fission which may provide a basis

[1] L. D. Roberts, J. W. T. Dabbs, and G. W. Parker, *Phys. Semiann. Prog. Rep. March 10, 1956*, ORNL-2076, Fig. 1, p 3.

[2] A. Bohr, *Proceedings of the International Conference on the Peaceful Uses of Atomic Energy*, vol 2, p 151, United Nations, New York, 1955.

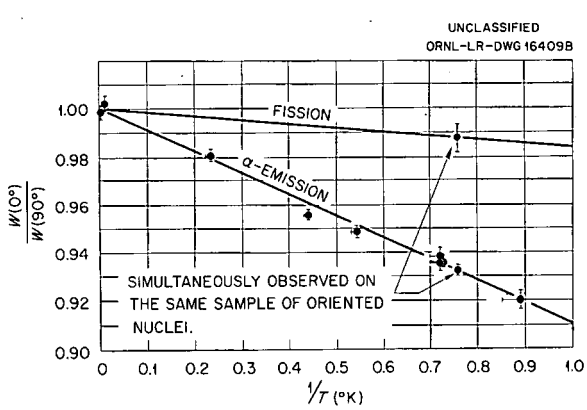

Fig. 1. Observed Anisotropies of Thermal Fission and of Alpha-Particle Emission from Oriented U^{233} Nuclei in $U^{233}O_2Rb(NO_3)_3$.

for the interpretation of results of the above type. The nucleus U^{233} has $I = 5/2$ and is thought to have positive parity.[3] Bohr suggests that the compound nucleus formed upon the capture of a neutron has a long life compared with a rotation period; that is, it is in a state of good angular momentum. For *s*-wave capture with compound-state angular momentum $J = 2$, one would expect that the angular momentum of the lowest state results from pure core rotation, while for $J = 3$ the ground state should involve a coupling of an excited nuclear state with possible core rotation. Bohr then assumes that when fission occurs it will be along the major nuclear axis. Thus for an aligned nuclear spin system, the state of pure core rotation, $J = 2$, should lead to a high degree of anisotropy in the direction observed (Fig. 1), whereas the anisotropy might be expected to be less for the $J = 3$ compound states, where the nucleon-core coupling would lead to a more complex – less well-defined – core motion.

The above discussion neglects the effects on the fragment angular distribution arising from the manner in which compound-state angular momentum is carried away by the fragments, and, since these ideas have not yet been formulated mathematically, no definite comparison with our result is possible. This comparison is further complicated by the fact that the compound state for thermal fission of U^{233} has not been determined. In spite of this, the observed fission anisotropy is strikingly small compared with that for the alpha particles. Further experiments will be necessary in order to gain an understanding of this. These measurements probably should be the observation of the fission-fragment anisotropy at fission resonances where the angular momentum is well defined, and, further, this compound-state angular momentum should be determined through the use of nuclear polarization or other techniques.

$NpO_2Rb(NO_3)_3$ MAGNETIC SUSCEPTIBILITY

In connection with the effort to study alpha emission from aligned Np^{237} nuclei at temperatures below 1°K, as well as in attempted specific-heat measurements on $U^{235}O_2Rb(NO_3)_3$, some experiments[4] indicated the possibility of an internal heating at liquid-helium temperatures in the uranyl rubidium nitrate. If this heating effect came from a recrystallization of the salt, this phase change might introduce a serious uncertainty in our alpha-particle–nuclear-alignment results. To check this we have made two measurements of the magnetic susceptibility of a single crystal parallel to the crystalline *c* axis. The measurements were made between 1 and 4.2°K, using an apparatus previously described.[5] The crystal was cooled to this temperature range and the parallel susceptibility measured. The sample was then allowed to return to 300°K over a period of several days. Then the sample was again cooled and the susceptibility measurement repeated. Since the perpendicular susceptibility is several hundred times smaller than the parallel susceptibility, this measurement would be a sensitive detector of any recrystallization occurring in this temperature cycle. In the two experiments the observed susceptibilities reproduced within 0.1%, indicating that no appreciable recrystallization occurred. The average Weiss constant for the two experiments was of the order of only a few millidegrees, and we assume it to be zero.

Within this assumption of a zero Weiss constant, these measurements lead to a $g_{\parallel} = 3.40 \pm 0.02$ for the pure single crystal $NpO_2Rb(NO_3)_3$. This may be compared with the microwave value[6] of 3.405 for a very dilute solid solution of the neptunyl salt in $UO_2Rb(NO_3)_3$.

We have formerly reported the results[4] of a measurement of the powder susceptibility of $NpO_2Rb(NO_3)_3$. In the interpretation of these results we assumed the existence of a small Weiss constant $\Delta \sim -0.04$°K and calculated the value of this constant which gave the best fit of $\chi = C/(T + \Delta)$ to our results. On the basis of the above more recent single-crystal measurements, it seems more reasonable to take a value of $\Delta \sim -0.004$°K, corresponding simply to the shape correction. A recalculation of the powder susceptibility results then gives

$$g_{\parallel}^2 + 2g_{\perp}^2 = 11.41 \pm 0.1 \ .$$

This may be compared with the microwave result of 11.68 ± 0.06. This agreement is possibly fortuitous, in that the susceptibility measurements are on pure salt, while the microwave result is for a very dilute salt.

[3] S. G. Nilsson, private communication.

[4] L. D. Roberts, J. W. T. Dabbs, and G. W. Parker, *Phys. Semiann. Prog. Rep. Sept. 10, 1956*, ORNL-2204, p 60.

[5] R. A. Erickson, L. D. Roberts, and J. W. T. Dabbs, *Rev. Sci. Instr.* 25, 1178 (1954).

[6] P. M. Llewellyn, thesis, Clarendon Laboratory, 1955.

DISSOCIATION CROSS SECTION OF H_2^+

C. F. Barnett

The cross section for dissociation of the diatomic hydrogen ion has been determined in the energy range of 500 kev to 2.25 Mev in target gases of hydrogen, helium, nitrogen, and argon. At energies less than 500 kev the measurements become difficult due to the competing process of charge exchange. The apparatus used was essentially the same as that used for the charge-exchange experiments.[1] The principal differences are that the first gas cell was eliminated, and an additional detector was installed to measure the deflected charge beam.

An H_2^+ beam was incident on the differentially pumped gas cell, in which the pressure was sufficiently low to prevent multiple collisions. Emerging from the gas cell was a mixture of H^0, H^+, and H_2^+. Using the set of electrostatic deflection plates, the beam was analyzed into its various components. The axial detector was used as a secondary electron detector to measure both the neutral component and the total charge component of the beam. The other detector was used both as a secondary electron detector and as a Faraday cup to measure the individual charged beams.

The total beam available for dissociation was found by summing the emergent H_2^+ with the number of reactions occurring, which were determined by a charge or particle balance between H^0 and H^+. Using such a balance the per cent of the reactions going by simple dissociation (i.e., $H_2^+ \rightarrow H^0 + H^+$) or by an ionizing dissociation (i.e., $H_2^+ \longrightarrow 2H^+ + e$) can be determined. From these measurements the cross section is calculated from the following relation:

$$\frac{\text{total number of reactions}}{\text{total } H_2^+} = 1 - e^{n\sigma_d x} ,$$

where n is the target-gas density, x is the particle path length in the gas, and σ_d is the dissociation cross section.

During a dissociating collision, momentum is imparted to the energetic particles, resulting in small-angle scattering. To estimate the magnitude of this scattering, the exit pinhole of the gas cell was enlarged. The measured cross section was independent of the defining geometry, indicating that the scattering is small.

In Fig. 1 are shown the dissociation cross sections as a function of the particle velocity or energy. For hydrogen and helium the cross sections behave in a manner similar to the electron loss cross sections, in that they have essentially a $1/v$ dependence. For the heavier gases of nitrogen and argon the cross sections decrease only 15 to 20% over the velocity range studied. Shown in Fig. 2 are the percentages of the total reactions going as simple dissociation for target gases of hydrogen and nitrogen. The mode of dissociation is independent of particle velocity and is dependent on the target atom.

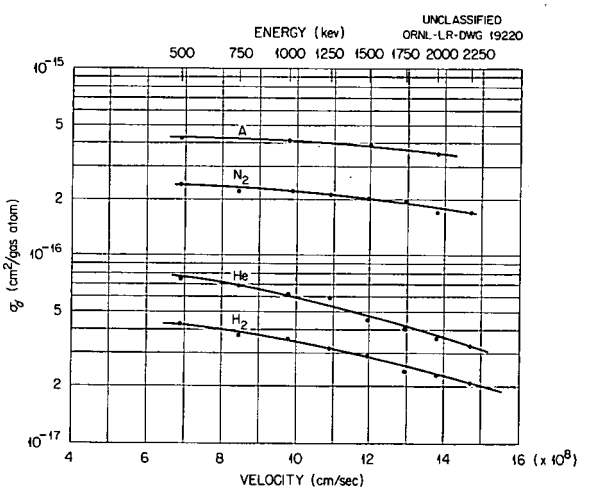

Fig. 1. Dissociation Cross Section per Atom of Gas Traversed as a Function of Particle Velocity or Energy. H_2^+ in hydrogen, helium, nitrogen, and argon gases.

[1] C. F. Barnett, H. K. Reynolds, and R. G. Reinhardt, *Phys. Semiann. Prog. Rep. Sept. 10, 1956*, ORNL-2204, p 39.

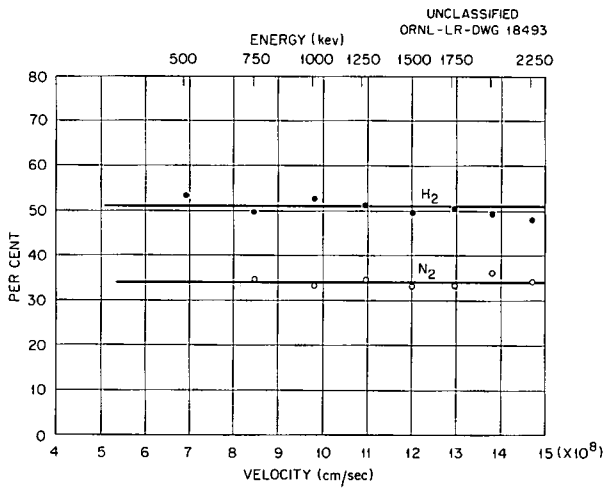

Fig. 2. Per Cent of Dissociation by the Reaction $H_2^+ + M \longrightarrow H^+ + H^0 + M$.

CHARGE SPECTRUM FOLLOWING THE RADIOACTIVE DECAY OF Kr^{79}

A. H. Snell F. Pleasonton

A preliminary determination of the distribution of charges on the product atom following the decay of $Kr^{79} \longrightarrow Br^{79}$ (34.5-hr) is shown in Fig. 1. The rather complex decay scheme of this transition is shown[1] in Fig. 2. It will be noted that electron capture plays the major role in the decay process, followed by a complex of gamma rays in 28% of all cases. Of these gamma rays, the four most highly converted are indicated by specifying their energies.

The charge spectrum shown in Fig. 1 is marked by a very flat maximum, in contrast with the sharp peaks found in the decays of $A^{37} \longrightarrow Cl^{37}$ (pure *K* capture)[2] and $Xe^{131m_2} \longrightarrow Xe^{131}$ (internal conversion of a single gamma ray).[3] It is thought that this flatness may be caused by vacancy cascades which are initiated by internal conversion of one or more of the gamma rays and which overlap, in time, earlier ones started by an electron capture. It will probably be impossible to give any detailed explanation of the spectral shape, but it seemed to be of interest to compare the results of such a complex decay mechanism with those of the pure types studied previously. A charge state of 12 is the highest we have sought so far and is not yet established as the highest which may exist. This may be compared with a maximum charge of 10 observed in the case of $Kr^{85} \longrightarrow Rb^{85}$ beta decay, one charge of which is the result of beta-minus emission.

It should be noted that the relative intensities of the neutral and negatively charged atoms shown in Fig. 2 are estimated by combining the branching ratio of the beta-plus emission with the charge distribution found following the beta-minus decay[4]

[1] *Nuclear Level Schemes*, TID-5300 (June 1955).

[2] A. H. Snell and F. Pleasonton, *Phys. Rev.* 100, 1396 (1955).

[3] A. H. Snell and F. Pleasonton, *Phys. Rev.* 102, 1419 (1956).

[4] A. H. Snell and F. Pleasonton, *Bull. Am. Phys. Soc.* 1, 263 (1956).

of isoelectronic $Kr^{85} \longrightarrow Rb^{85}$. Any contribution of neutral atoms from fluorescence yield alone is presently neglected. The combined spectrum of measured and estimated intensities gives an average charge of +4.7 ± 0.5.

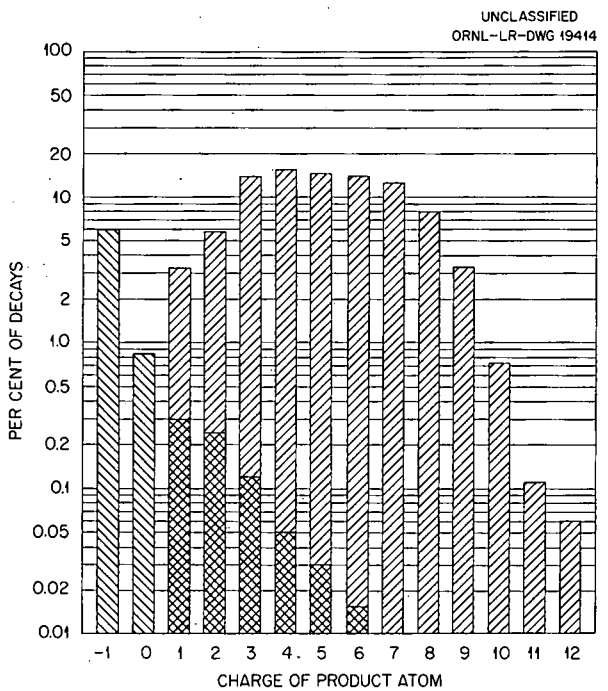

Fig. 1. Charge Spectrum Following the Decay of $Kr^{79} \longrightarrow Br^{79}$ (34.5 hr). The positive charge states as measured are equated to 92.3% of all decays. The negative and neutral states are estimated by combining the 7.7% β^+ branches with the spectrum following β^- emission in $Kr^{85} \longrightarrow Rb^{85}$. The crosshatched portions of the positively charged states represent the tail of the expected β^+ contribution.

We hope in the near future to adapt our apparatus for the detection of the negative ions.

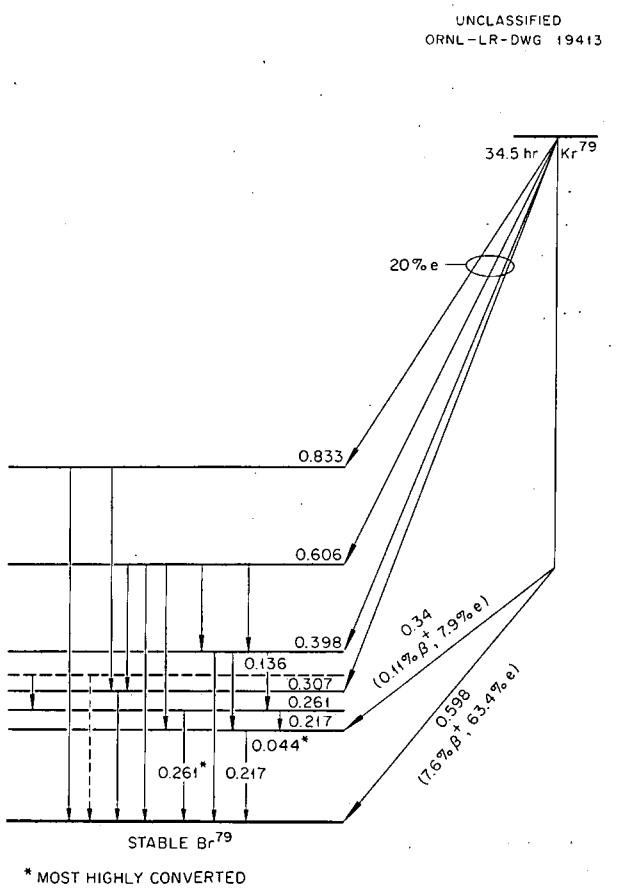

Fig. 2. Decay Scheme of $Kr^{79} \longrightarrow Br^{79}$ (34.5 hr). All gamma rays are indicated, but only the four most highly converted ones have the energy specified.

MOLECULAR BREAKUP FOLLOWING RADIOACTIVE DECAY OF C^{14} IN CO_2

A. H. Snell F. Pleasonton

Carbon-14 dioxide was generated from $BaCO_3$, isotopically enriched to 38.6% C^{14}, and was introduced into our apparatus[1] at an indicated pressure of about 1.5×10^{-5} mm Hg. It was then subjected to magnetic analysis to determine the relative abundances of positively charged ions following the radioactive decay of the constituent C^{14} atom.

Preliminary results yield the following distribution:

e/m	Ion	Relative Intensity
1/46	NO_2^+	81.4 ± 1.6
1/30	NO^+	8.4 ± 0.4
1/16	O^+	5.9 ± 0.6
1/14	N^+	3.6 ± 0.4
2/46	NO_2^{++}	0.4 ± 0.06
1/32	O_2^+	0.2 ± 0.4
2/30	NO^{++}	0.06 ± 0.04
2/14	N^{++}	0.02 ± 0.01
2/16	O^{++}	0.01 (upper limit)

As in the case of the breakup following the radioactive decay of tritium in the HT molecule,[2] there is a strong tendency for the molecule to remain bound as a singly charged ion, in spite of the nuclear recoil from the beta emission (7 ev for a free C^{14} atom). In the case of $C^{14}O_2$, both singly and doubly charged positive ions are observed. The NO_2^{++} ions can be attributed to the shake-off of an electron due to the nuclear charge change which takes place concurrently with the beta emission. The occurrence of NO^{++} and N^{++} may be accompanied by O^- ions, which are not observable in the present experimental arrangement. Since, however, the ratios of the intensities of the doubly charged ions to those of the singly charged ions of corresponding masses are the same within counting statistics, it is possible that they all reflect the nuclear charge-change shake-off demonstrated by the presence of NO_2^{++} ions.

We anticipate further work along these lines by looking at the dissociation following the decay of the radioactive constituent atom in the molecules CH_3I^{131}, CH_3T, and $C^{14}H_4$.

[1] The spectrometer has been described in detail by A. H. Snell and F. Pleasonton, *Phys. Semiann. Prog. Rep. March 10, 1956*, ORNL-2076, p 39.

[2] A. H. Snell, F. Pleasonton, and H. E. Leming, *Phys. Semiann. Prog. Rep. Sept. 10, 1956*, ORNL-2204, p 42.

ANTIFERROMAGNETIC STRUCTURES OF ANHYDROUS $[(1-x)Fe,xCo]Cl_2$ COMPOUNDS

M. K. Wilkinson J. W. Cable E. O. Wollan W. C. Koehler

Previous neutron diffraction measurements[1] have been used to determine the antiferromagnetic structures which exist at low temperatures in anhydrous $FeCl_2$ and $CoCl_2$. Both these compounds crystallize in the rhombohedral or pseudo-hexagonal structure characteristic of $CdCl_2$, so that they are actually hexagonal layer structures in which the layers of metal atoms are separated by two layers of chlorine atoms. The neutron data show that below the Néel transitions the atomic magnetic moments within a metal layer have parallel coupling and that the moments in adjacent layers are aligned antiparallel. There is one important difference in the magnetic structures for the two compounds: the axis of magnetization is not the same. In $CoCl_2$ the moments are within the layers, whereas in $FeCl_2$ the moments are oriented parallel to the *c* axis of the hexagonal unit cell. Since these two materials have almost identical crystal structures and Néel temperatures (24°K for $FeCl_2$ and 25°K for $CoCl_2$), it is interesting that the direction of alignment of the atomic magnetic moments is quite different. In an attempt to obtain information which might be useful in understanding the different moment directions of these compounds, neutron diffraction measurements have been obtained for solid solutions in which the ratio of Fe to Co was varied.

The samples were prepared by vacuum fusion of the proper proportions of pure $FeCl_2$ and $CoCl_2$ which were obtained from the hydrates by dehydration in HCl at about 300°C. The fused material was then ground as gently as possible to obtain sufficient quantities of 100-mesh powder. Both x-ray diffraction and neutron diffraction showed that the proper crystallographic structures were obtained without excessive stacking faults, and the x-ray measurements showed the existence of pure solid solutions with the lattice constants[2] given in Table 1.

Neutron diffraction patterns have been obtained for all five samples at a series of temperatures down to 4.2°K, and all showed superstructure lines at the lowest temperatures. By studying the temperature variation of the magnetic intensities, the Néel temperatures listed in Table 1 were obtained. These values were obtained from temperature measurements, using a calibrated copper-constantan thermocouple, and are probably accurate to about 2 deg. The scattered magnetic intensities were found to follow a Brillouin-type curve below

[1] M. K. Wilkinson and J. W. Cable, *Phys. Semiann. Prog. Rep. March 10, 1956*, ORNL-2076, p 44.

[2] We wish to express our appreciation to D. E. Lavalle of the Analytical Chemistry Division for preparing these samples, and to H. Yakel and R. M. Steele of the Metallurgy Division for the x-ray analyses.

Table 1. Lattice Constants and Approximate Néel Temperatures of $[(1-x)Fe,xCo]Cl_2$ Compounds

Compound	Lattice Constants (Hexagonal Cell)		
	$a_0 \times 10^{-8}$ (cm)	$c_0 \times 10^{-8}$ (cm)	Approximate T_N (°K)
$FeCl_2$	3.6027	17.536	25
$Fe_{3/4}Co_{1/4}Cl_2$	3.5893	17.506	24
$Fe_{1/2}Co_{1/2}Cl_2$	3.5767	17.464	21
$Fe_{1/4}Co_{3/4}Cl_2$	3.5655	17.425	23
$CoCl_2$	3.5533	17.359	24

T_N and did not appear to have any anomalous behavior.

Figure 1 represents the difference between diffraction patterns taken at 4.2 and 43°K for each of the five compounds, in which the data have been normalized so that the patterns can be compared directly. The diffraction peaks which are shown are therefore representative only of the coherent magnetic scattering present at 4.2°K, which was not present at 43°K. Similarly, the negative backgrounds are caused by the paramagnetic diffuse scattering which was present at 43°K and which disappeared below T_N. All these patterns indicate magnetic structures in which the moments are aligned parallel within a layer, with the moments in adjacent layers aligned antiparallel. The top and bottom patterns for $FeCl_2$ and $CoCl_2$ show the difference in the magnetic-moment directions in these compounds. In $FeCl_2$ the (003) magnetic reflection is absent, which requires that the atomic moments be oriented parallel to the c axis. In $CoCl_2$ the (003) reflection is large, while the (101) reflection is much smaller than that in $FeCl_2$. Specifically, for the moments to be aligned within the layers, the intensity ratio $I_{(101)}/I_{(003)}$ should be about 7%. The observed ratio is closer to 10%, and there is evidence that this difference is due to preferred orientation in the powdered sample. The diffraction patterns from the mixed samples show that as $CoCl_2$ is added to $FeCl_2$, there is a regular increase in the (003) intensity, while the (101) intensity shows a regular decrease. This variation indicates that there is not a specific concentration at which the orientation changes from along the c axis to within the layers, but that for mixed samples there must be a component of the moments in each direction.

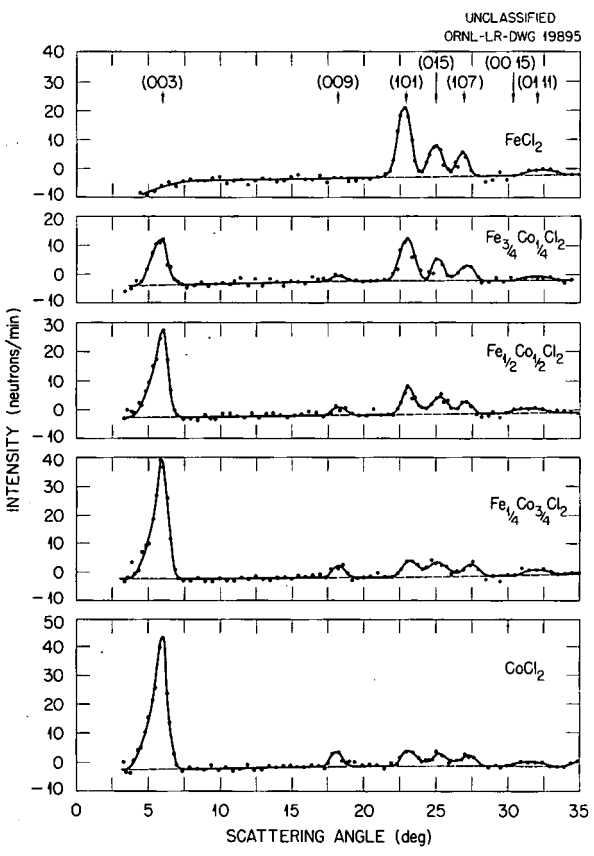

Fig. 1. Diffraction Patterns Representing the Difference in Data Obtained at 4.2 and at 43°K for a Series of $[(1-x)Fe, x\,Co]Cl_2$ Compounds.

For the pure $FeCl_2$ and $CoCl_2$ samples, analysis of the change in diffuse scattering between 295°K and 4.2°K, together with a study of the coherent magnetic reflections (including effects of preferred orientation), suggests that both the Fe^{++} and Co^{++} ions in the ordered magnetic lattice have "spin only" values of the atomic magnetic moments. Therefore in preliminary calculations which have been made in order to interpret the data on the $[(1-x)Fe,xCo]Cl_2$ compounds, no orbital contributions to the moments of either ion in the solid solutions have been assumed. If this assumption is correct, the results indicate that in the mixed samples the magnetic moments of both ions have the same axis of magnetization and that this axis changes regularly with sample concentration. The intensities are not consistent with a model in which the Co moments remain in the layers while the Fe moments remain parallel to the c axis. The absolute values of the angles between the axes of magnetization and the c axis of the unit cell in these magnetic structures are presently in doubt, because corrections have not been made for preferred orientation in the samples.

MAGNETIC ORDERING IN HOLMIUM SESQUIOXIDE

W. C. Koehler E. O. Wollan M. K. Wilkinson J. W. Cable

INTRODUCTION

In previous semiannual reports, results of neutron diffraction studies of magnetic ordering in Er_2O_3 (ref 1) and of paramagnetic scattering by Ho_2O_3 (ref 2) have been described. In the work on Ho_2O_3 some preliminary measurements at low temperatures were made which indicated that Ho_2O_3 becomes magnetically ordered in the liquid-helium temperature region, although it was necessary to apply an external magnetic field in order to obtain strong coherent magnetic reflections. An extensive study of the magnetic-scattering properties of polycrystalline Ho_2O_3 as a function of temperature and of externally applied field has now been completed. In this report the rather complex series of data so obtained is described, and some qualitative aspects of its interpretation are outlined.

EXPERIMENTAL PROCEDURE

Neutron diffraction patterns of polycrystalline Ho_2O_3 were taken with moderate resolution by means of Soller slits at temperatures ranging from 4.2 to 1.25°K and in applied fields up to 16.3 kilooersteds. The data so obtained were compared with a standard diffraction pattern taken at 77°K. The standard 77°K diffraction pattern was subtracted from each of the low-temperature patterns to give a series of difference patterns that display essentially only the magnetic-scattering effects which develop at the lower temperatures. A number of the stronger reflections were studied in greater detail by following their peak intensities as a function of field and temperature.

CRYSTALLOGRAPHIC AND MAGNETIC PROPERTIES

The high-temperature magnetic and nuclear scattering data for Ho_2O_3 have already been described.[2] For completeness, a brief review of the crystallographic and magnetic properties of Ho_2O_3 which are pertinent to the report is given.

The sesquioxides of the heavy rare-earth metals crystallize in the cubic Tl_2O_3 structure. The body-centered cubic unit cell contains 16 molecules, and the 32 metal ions occupy two sets of nonequivalent special positions of the space group $T_h^7 = Ia3$. One set of 24 metal ions has a single parameter u which, although not directly determined for Ho_2O_3, has been reported as $u = -0.030$ for the isomorphous mineral bixbyite.[3] If one ignores this parameter, the metal ions are on face-centered cubic positions, and the structure may conveniently be viewed as one intermediate between the fluorite and the zinc blende structures.

In the fluorite structure each cation is surrounded by eight anions at the corners of a cube. If two of these are removed in the proper manner the Ho_2O_3 structure results. Corresponding to the two sets of metal positions there are two types of oxygen ion neighborhoods in the structure: for the metal ions without parameter the two oxygen vacancies lie at opposite ends of a body diagonal; for the metal ions with parameter the vacancies occur at opposite ends of a face diagonal. In each case the orientations of the lines of vacancies vary according to the symmetry requirements of the space group.

The high-temperature magnetic susceptibilities of rare-earth salts in general indicate strongly that in the rare ions the magnetic moments arise from $4f$ electrons arranged in accordance with Hund's Rule. In Ho^{+++} the ground state has maximum spin ($S = 2$) and maximum orbital angular momentum ($L = 6$), and these are coupled by the spin-orbit interaction so that the maximum J ($J = 8$) lies lowest. To this ground state corresponds an effective magnetic moment of 10.6 Bohr magnetons.

For many of the rare-earth ions the Hund's Rule ground state may be split by crystalline-field interactions. The details of this splitting will depend, among other things, upon the ion in question and upon the symmetry of the crystalline electric field in which it is found. A particularly detailed analysis of paramagnetic resonance data for rare-earth ethylsulfates has been given by

[1] W. C. Koehler *et al.*, *Phys. Semiann. Prog. Rep. Sept. 10, 1956*, ORNL-2204, p 44.

[2] W. C. Koehler *et al.*, *Phys. Semiann. Prog. Rep. March 10, 1956*, ORNL-2076, p 48.

[3] L. Pauling and M. D. Shappell, *Z. Krist.* 75, 128 (1930).

Elliot and Stevens,[4] and, for the cases studied, over-all splittings of the ground level of about 100 wave numbers were derived. Although the theory developed for the rare-earth ethylsulfates is probably not directly applicable to the oxides, it may be expected that crystalline-field splittings of the same order of magnitude will be present. The situation in the oxide is further complicated by the fact that the environment of the Ho^{+++} ions is not the same for all ions, and the different crystalline-field symmetries may lead to different splittings. It should also be noted that for one or both sets of Ho^{+++} ions, a ground state corresponding to $J_Z = 0$ is possible, since Ho^{+++} has an even number of $4f$ electrons.

In addition to possible crystalline-field interactions, the oxides are sufficiently magnetically concentrated that dipole-dipole interactions and exchange interactions among the Ho^{+++} ions may be expected to be significant, particularly at temperatures in the liquid-helium range.

EXPERIMENTAL RESULTS

In the following paragraphs a brief description of the rather complex series of magnetic-scattering effects observed in Ho_2O_3 is given and illustrated. The results obtained in zero field are taken up first, and a series of difference patterns obtained at several temperatures is shown in Fig. 1. The indices shown refer to the chemical unit cell of Ho_2O_3 (a_0 = 10.606 Å). Each of these patterns exhibits a broad diffuse maximum centered near the (111) position, and the maximum is seen to increase with decreasing temperature. The general characteristics of these data are suggestive of short-range antiferromagnetic ordering. At temperatures below about 2.0°K there is a slight but distinct change in the shape of the diffuse maximum which may be indicative of the onset of a long-range ordering transition. If this be the case, the temperature dependence of the data from 2.0°K down would indicate that only a fraction of the moments can be participating in the ordering, and from the absolute intensities the moments must be much less than the maximum of 10 Bohr magnetons.

Alternatively, the slight evidence of coherence may be due to the effects of a small residual field

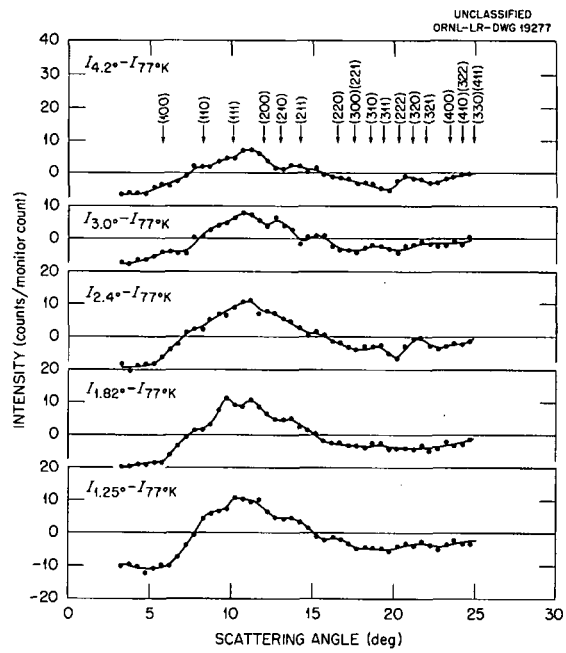

Fig. 1. Zero-Field Difference Patterns of Ho_2O_3.

in the magnet gap, although precautions were taken during the experiments to demagnetize the magnet for zero-field runs. As will be seen below, the effect of the magnetic field is greatest at the lower temperatures. In either case the zero-field data imply that a completely ordered state has not set in, even at 1.25°K.

In contrast with the zero-field data of Ho_2O_3, it is interesting to examine the data previously reported[1] for Er_2O_3, which are illustrated in Fig. 2. At 4.2°K the difference-pattern characteristics of short-range antiferromagnetic ordering are also observed, but at lower temperatures the broad maximum is replaced by the series of sharp coherent reflections shown, and the transition temperature is at about 4.0°K.

With the application of a magnetic field to the Ho_2O_3 sample, one observes the development of sharp coherent magnetic reflections which appear at positions characteristic of antiferromagnetic ordering. The distribution of magnetic intensity among the several reflections depends upon the field strength and upon the temperature. In Fig. 3, results of the application of the field to the sample at 4.2°K are shown. One notes a dimunition of the background scattering level with increasing field

[4] K. W. H. Stevens, *Proc. Phys. Soc. (London)* **A65**, 209 (1952); R. J. Elliott and K. W. H. Stevens, *Proc. Roy. Soc. (London)* **A215**, 437 (1952); **A218**, 553 (1953); **A219**, 387 (1953).

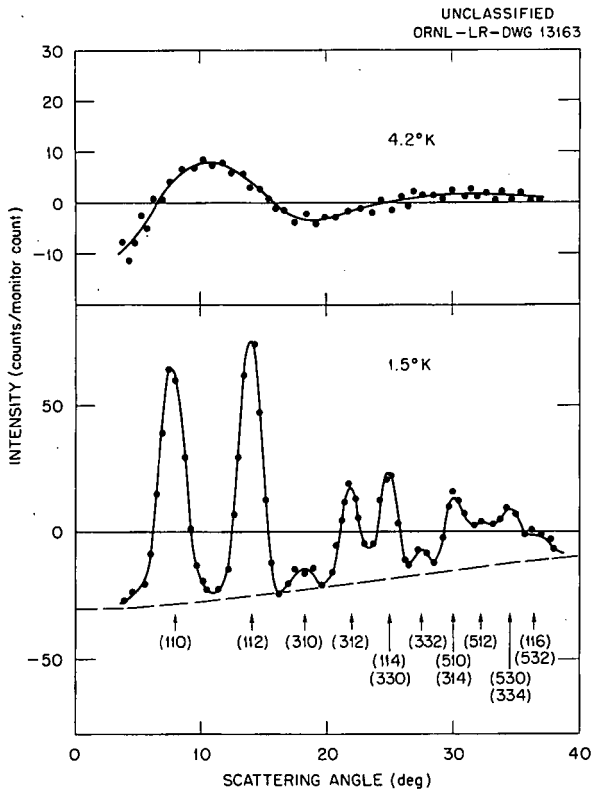

Fig. 2. Zero-Field Difference Patterns of Er_2O_3.

and a simultaneous increase of coherent intensity at the (110), (112), (310), and (312) positions. The last two reflections are only apparent with the maximum field. It is also apparent that a residual broad diffuse peak remains, even in the strongest field, but is much more striking for the intermediate fields. The reflections which are observed have the property that two of the indices are odd and one is even, and one will note that it is just this type of reflection which was observed for Er_2O_3.

At 1.25°K a more complex behavior is observed, as illustrated in Fig. 4. For a field of just 520 oersteds one notes a distinct (112) reflection and possibly also a (110) superimposed upon the diffuse maximum. As the magnitude of the field increases, reflections of all types grow in. Of particular interest are the (100) and (210) reflections which grow in to maximum intensity at about 5.0 kilooersteds, after which they begin to diminish in intensity. At 16.3 kilooersteds the strong reflections are again those of the type (110), (112), etc., but in addition one finds reflections of moderate intensity which have all indices even. One notes also that the (111) reflection is strongest, although always very weak, at about 2.66 kilooersteds. One may also observe that the diffuse

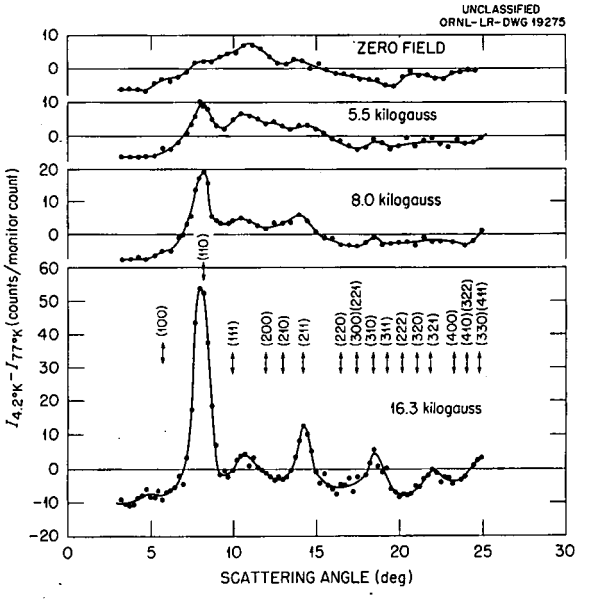

Fig. 3. Field Effect on Ho_2O_3 at 4.2°K.

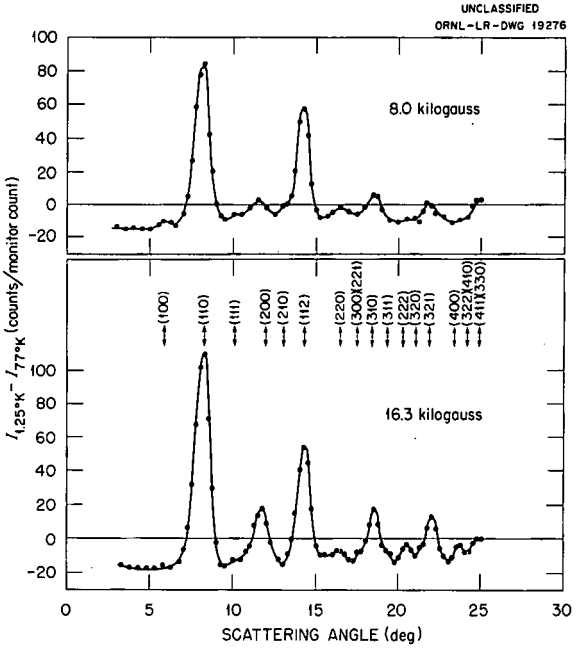

Fig. 4. Field Effect on Ho_2O_3 at 1.25°K.

peak is nearly completely gone at 1.25°K and 16.3 kilooersteds.

The results described above, together with additional data, are shown in Fig. 5 for the (110) reflection and in Fig. 6 for the (112). For the (110) reflection the intensity increases uniformly as a function of temperature for a fixed field. The curvature in strong fields is probably not real, since the peak intensity data displayed here are uncorrected for background changes. When such corrections are made, it is apparent that the (110) intensity is far from saturation. At the lowest temperature and highest field the (110) is just about half as strong as it can possibly be. Curves obtained for the (112) reflection show an inflection in the high-field region which is real, and may indicate changes in moment direction as a function of applied field. For example, the ratio of intensities of the (110) to the (112) is very sensitive to the moment direction. In weak fields this ratio is about unity, whereas in strong fields the (110) is the stronger. In Fig. 7 the region of observation of the (210) reflection is illustrated. As shown here the (210) is not observed for any field value at temperatures above about 1.5°K, and it disappears for fields in excess of about 8.0 kilooersteds.

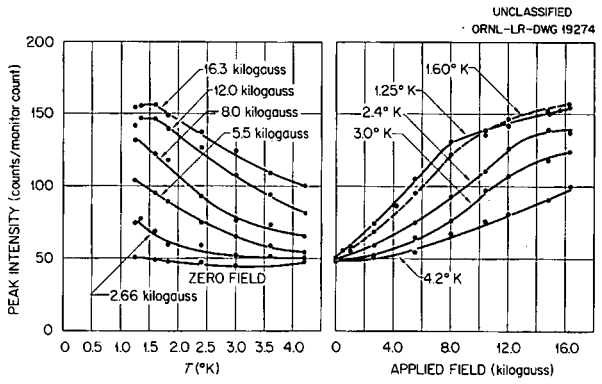

Fig. 5. Temperature and Field Dependence of (110) Magnetic Reflection of Ho_2O_3.

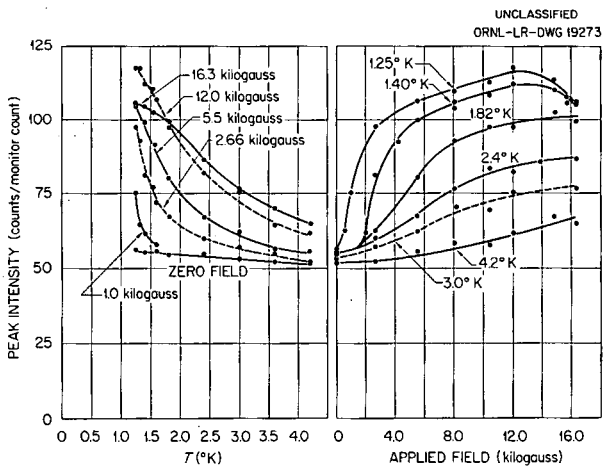

Fig. 6. Temperature and Field Dependence of (112) Magnetic Reflection of Ho_2O_3.

DISCUSSION

As mentioned above, one may expect crystalline-field interactions in Ho^{+++} of the order of 100 wave numbers. One may also make crude estimates of the strength of other possible interactions. If

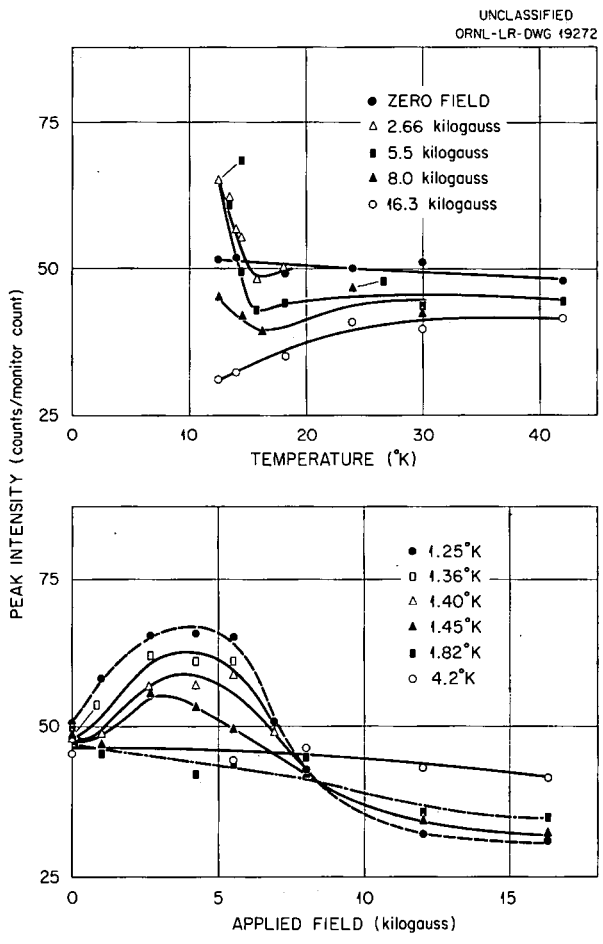

Fig. 7. Temperature and Field Dependence of (210) Magnetic Reflection of Ho_2O_3.

one estimates the mutual interaction energy of two dipoles of 10 Bohr magnetons magnitude that are separated by the nearest-neighbor distance in Ho_2O_3, an energy corresponding to a temperature of 3°K results. The interaction of an applied external field of 16.3 kilooersteds on a holmium ion may be approximately expressed as 1°K per Bohr magneton of moment. If one takes as an estimate of the exchange interaction the observed transition temperature of Er_2O_3, which is of the order of a few degrees, then there are a number of possible interactions, all of the same order of magnitude.

Of rather great interest is the role of the magnetic field on the scattering properties of the material. It seems apparent that there exists some type of short-range correlation between the holmium ion moments in the absence of a field, but that as a magnetic field of increasing strength is applied, long-range order sets in. It is difficult to conceive of a mechanism by which an external field applied parallel to the scattering vector can induce long-range order in such a system, although the possibility that there exist small domains in zero field should, perhaps, not be excluded. Qualitatively, a mechanism does exist whereby a Zeeman effect on levels close to the ground level, but lying above it, can produce states of large J_Z lying lowest, and then ions in these states may be ordered. It is interesting in this connection to recall that the intensity of the (110) reflection at 16.3 kilooersteds and 1.25°K is nearly half as large as it can possibly be, and there is some indication that it would continue to increase in intensity if higher fields were available. Obviously this cannot continue indefinitely, for at sufficiently high fields the system will approach paramagnetic saturation.

The complex growth and disappearance of some of the reflections and the changing intensity ratios of others may reflect the competition of several interactions and may also be related in a subtle way to differences in the level splittings of the two types of ions.

The assistance of H. R. Child in collecting and processing the data is gratefully acknowledged. The authors wish also to express their appreciation to F. H. Spedding for making the Ho_2O_3 available.

MAGNETIC ORDERING IN MANGANESE SESQUIOXIDE

J. W. Cable M. K. Wilkinson E. O. Wollan W. C. Koehler

The antiferromagnetic ordering of magnetic ions in the body-centered cubic bixbyite structure has been described for the Er_2O_3 system in a previous report.[1] The isomorphous system Mn_2O_3 offers the opportunity of extending the investigation of this type of lattice into the 3*d* transition-metal series. Magnetic data for Mn_2O_3 have not been reported below 90°K; however, measurements in the paramagnetic region show that the susceptibility follows the Curie-Weiss law $[\chi_M = C_M/(T - \theta)]$, with a large negative Weiss constant. Measurements in the 293 to 580°K region[2] yield the expression $\chi_M = 6.72/(T + 181)$ and $\mu_B = 3.66$ Bohr magnetons, while the 90 to 294°K data[3] give $\chi_M = 6.52/(T + 226)$ and $\mu_B = 3.58$ Bohr magnetons. Heat-capacity data[4] have recently been obtained in the temperature range 51 to 298°K. There is a sharp λ-type anomaly at 79°K, at which temperature the heat capacity rises by a factor of 2 above the extrapolation from higher temperatures. In view of these magnetic and thermal properties, it seemed quite likely that antiferromagnetic ordering would occur in Mn_2O_3, with a Neél temperature of ~80°K. Accordingly, a neutron diffraction study of the system has been carried out.

The Mn_2O_3 was prepared by ignition of $MnCO_3$ in an oxygen atmosphere at a temperature of 750°C for a period of 3 hr. The product, a black powder, was shown by x-ray analysis to contain only a slight impurity. The α-Mn_2O_3 structure (bixbyite

[1] W. C. Koehler *et al.*, *Phys. Semiann. Prog. Rep. Sept. 10, 1956*, ORNL-2204, p 44.

[2] S. S. Bhatnagar *et al.*, *J. Chem. Soc.* 1433 (1939).

[3] W. H. Albrecht, *Z. anorg. Chem.* **259**, 291 (1949).

[4] E. G. King, *J. Am. Chem. Soc.* **76**, 3289 (1954).

type) was confirmed for the sample, with a_0 = 9.414 Å.

Neutron diffraction patterns were taken at several temperatures from room temperature to liquid-helium temperatures. The room-temperature pattern is typical of a paramagnetic substance with coherent nuclear reflections superimposed on a background which decreases with increasing counter angle. Below 88°K, additional coherent scattering is observed due to the onset of antiferromagnetic ordering, and these peaks continue to increase in intensity as the temperature is lowered. A temperature difference pattern (4.2 to 298°K) which depicts only the magnetic scattering is shown in Fig. 1. The negative background represents the paramagnetic scattering at 298°K and corresponds to an effective spin of 1.81. This is in fair agreement with the spin value, $S = 2$, for the Mn^{+++} ion if one considers that complete magnetic order has not been attained at 4.2°K. This is best shown in Fig. 2, in which the intensities of the first three magnetic reflections are plotted as a function of temperature. Both the (100) and the (111) appear to be saturated at the

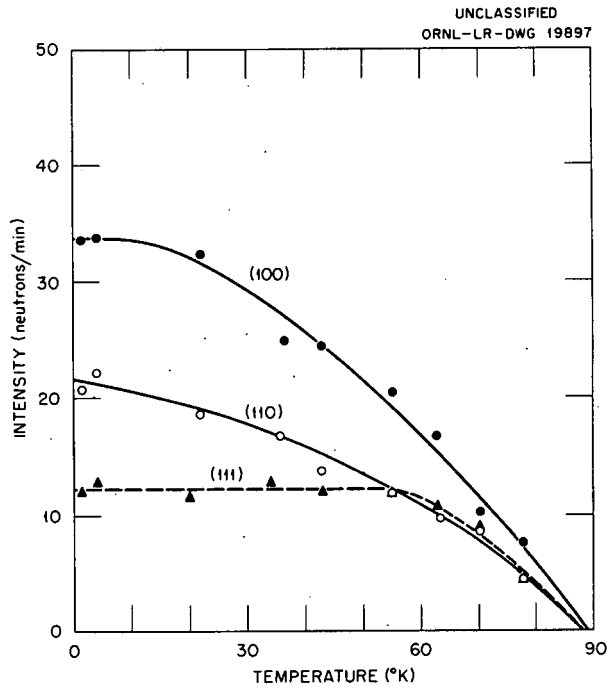

Fig. 2. Temperature Dependence of Magnetic Reflections in Mn_2O_3.

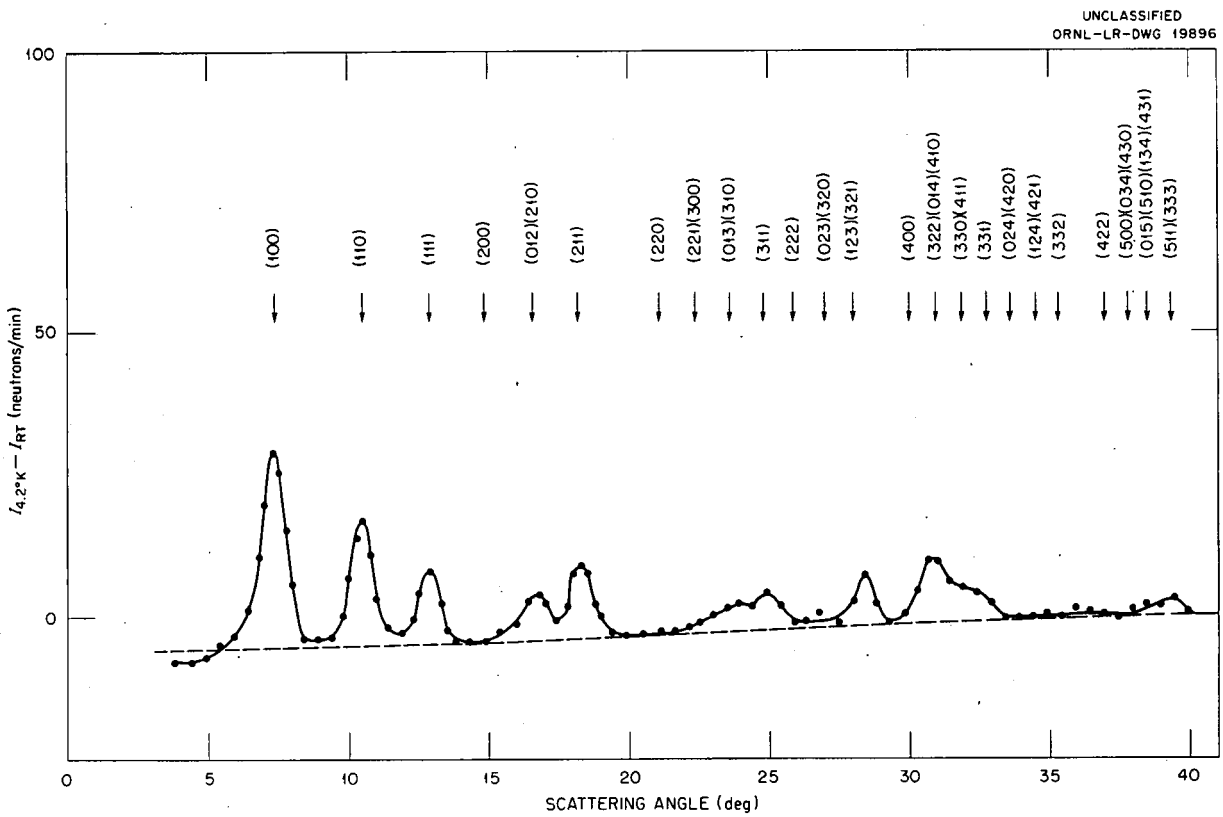

Fig. 1. Temperature Difference Pattern of Mn_2O_3.

lowest temperatures, but this is not true of the (110). Preliminary calculations on the coherent magnetic data indicate approximately 90% saturation at 4.2°K. Such calculations are necessarily approximate, since a unique structure determination has not yet been made.

Some insight into the magnetic structure of this system can be gained by utilization of the four sublattice models, as described in a previous report.[1] The metal ions in the bixbyite structure are very nearly on face-centered cubic positions. This lattice can conveniently be subdivided into four simple cubic sublattices. A convenient classification of simple cubic sublattice structure types has been previously described[1,5] and will be incorporated here without further explanation. According to this description, type *A* sublattices contribute only to reflections with one odd and two even indices, type *B* to those with all indices even, type *C* to those with two odd and one even, and type *G* to those with all indices odd. Thus a reasonable explanation of the (100) (210) (300) (221) ... series of reflections in the temperature difference pattern would be the presence of an *A*-type sublattice. Similarly, the series (110) (211) (310) (321) (411) (330) ... can be attributed to a *C*-type sublattice, and the series (111) (311) (331) (333) (511) ... to a *G*-type sublattice. The absence of reflections with all indices even excludes the *B*-type sublattice. The data then require that the fourth sublattice be of a type which contributes intensity both to reflections with all odd indices and to those with one even and two odd indices. This can be seen from the temperature dependence of the (100), (110), and (111) reflections (Fig. 2). In this figure the (100) intensity follows the normal Brillouin-type dependence. The (110), however, does not reach saturation, and the (111) saturates at a higher temperature than normal. Both anomalies could be explained if the fourth sublattice were disposed in such a way as to add intensity to the (110) reflection and cancel intensity of the (111) reflection. Thus a plausible description of the system is that it consists of one *A*, one *C*, one *G*, and one *E* type of sublattice.

It should be pointed out that a determination of sublattice types present does not constitute a structure determination for the system. There are numerous ways in which the sublattices can be added together. Furthermore, the sublattice model is not unique, and other more complicated models could well be required for this complex magnetic system. Calculations are being continued in an attempt to find an acceptable structure.

[5] E. O. Wollan and W. C. Koehler, *Phys. Rev.* 100, 545 (1955).

LOW-INTENSITY BACKGROUND MEASUREMENTS

P. R. Bell R. C. Davis G. G. Kelley

Counting of weak sources with scintillation spectrometers is limited by the natural background. A study of the nature of this background is being made in order to understand this limitation.

The background in NaI(Tl) crystals has previously been examined with small crystals, but the counting rates at high energy were inconveniently small. A large crystal weighing about 100 lb has been used, and pulses to 350 Mev gamma-ray equivalent energy have been examined.

The phosphor used was a $9\frac{3}{4}$-in.-dia by 11-in.-high single crystal of NaI(Tl). Three 5-in. photomultipliers were used. The detectors could be surrounded in successive layers by $\frac{3}{16}$ in. of boron carbide plastic, $2\frac{3}{4}$ in. of Pb and $1\frac{1}{2}$ in. of solution phosphor as an anticoincidence mantle. This equipment is mounted in a truck, along with a multichannel analyzer and other necessary electronic equipment. The truck is equipped with a 110-v 60-cycle generator.

Figure 1 shows the background spectrum at the Laboratory at an elevation of 800 ft above sea level. Figure 1*a* shows the background with the anticoincidence mantle not operating and with no shield around the crystal, except for 4 in. of lead on the floor of the truck. The low-energy peak in the spectrum is produced by the 1.46-Mev gamma ray of K^{40}, and the peak at 2.62 Mev is that from

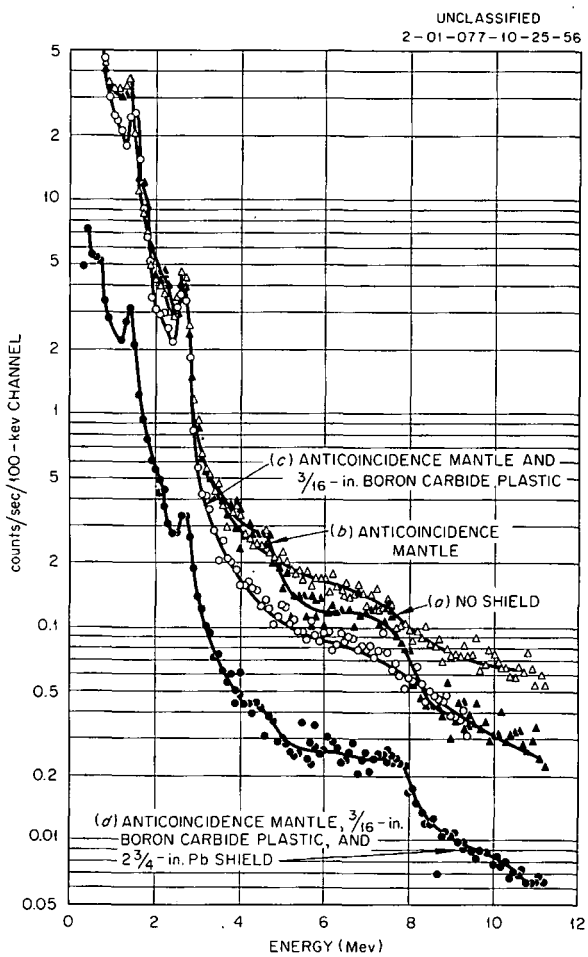

Fig. 1. Background Counts in $9\frac{3}{4}$-in. NaI(Tl) Crystal East of Building 4500. (*a*), (*b*), and (*c*) have 40 × 40 × 4 in. lead floor shield; (*d*) has 20 × 20 × 2 in. lead floor shield.

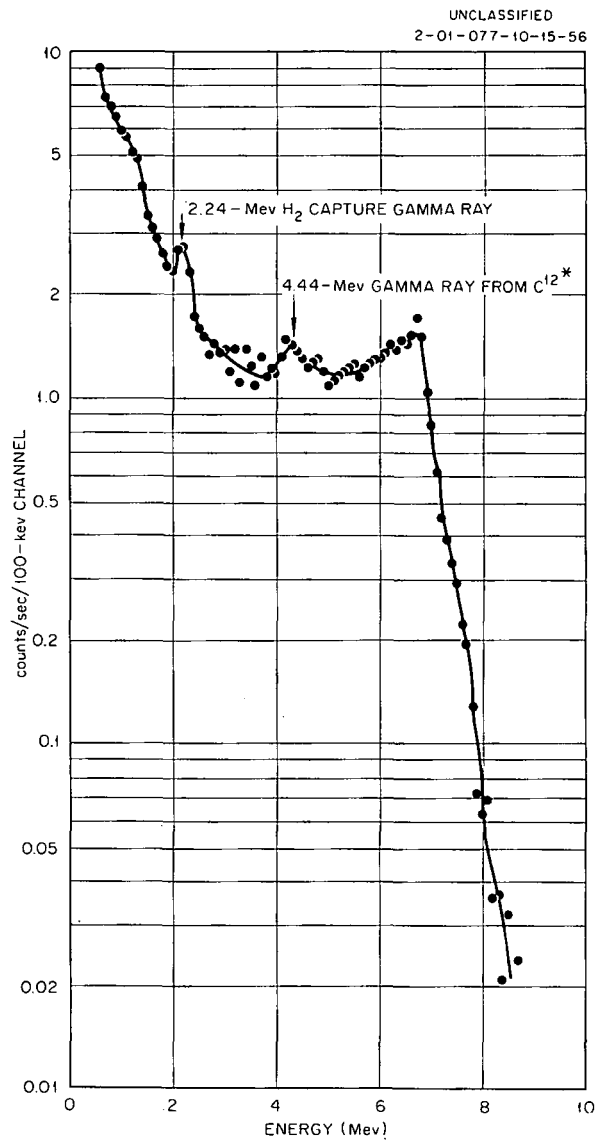

Fig. 2. Po-Be Source on $9\frac{3}{4}$-in. NaI(Tl) Crystal. Anticoincidence mantle and 2-in. lead shield.

ThC″. These gamma rays originate principally in the soil around the truck.

When the anticoincidence mantle is used, Fig. 1*b* results. Spectra 1*a* and 1*b* are nearly identical up to 5 Mev, where a noticeable difference begins. This difference becomes very large above 20 to 30 Mev equivalent energy.

The addition of a $\frac{3}{16}$-in.-thick boron carbide plastic shield very close to the phosphor to remove any thermal neutrons produced the effect shown in Fig. 1*c*. This shield has a noticeable effect from 3 to 8 Mev. This is just the region of the prominent response of NaI to neutrons. Figure 2 is the spectrum, produced by a Po-Be neutron source on this crystal, which supports this view. The source was shielded by 2 in. of lead to reduce the intense 4.44-Mev gamma rays from C^{12*} that were emitted by the source. The background spectrum was still further reduced by a $2\frac{3}{4}$-in.-thick lead shield around the phosphor and the boron carbide shield (Fig. 1*d*). Both shields were inside the anticoincidence mantle so that they might reduce incoming gamma rays without being a source of secondary radiations produced in them by the charged components of the cosmic-ray stream. A tenfold reduction of radioactivity gamma rays is evident. In the region 5 to 8 Mev the reduction factor is ~5.

The upper curve of Fig. 3 shows the background at much higher energy, without lead or anticoincidence mantle. The next lower curve shows the

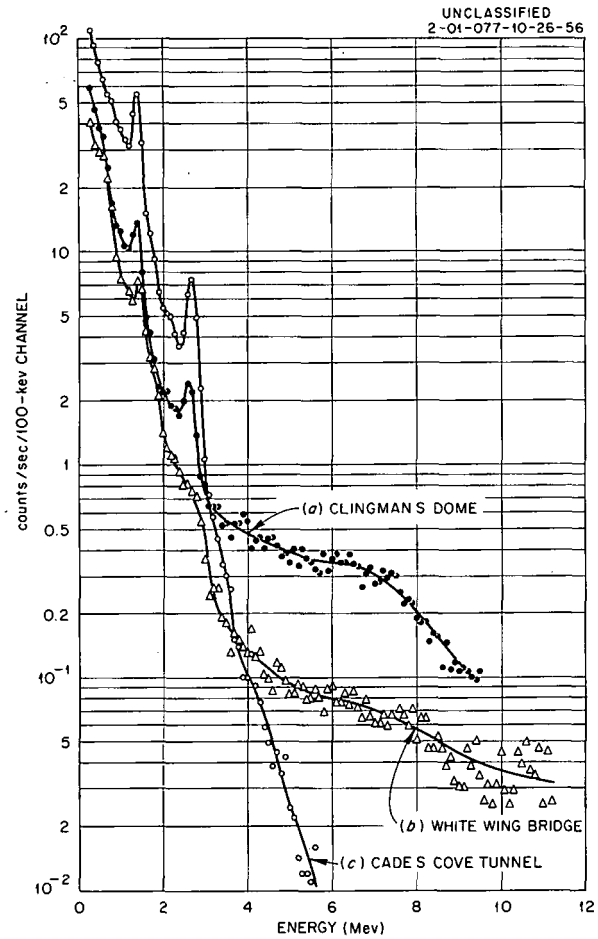

Fig. 3. High-Energy Background in $9\frac{3}{4}$-in.-dia NaI(Tl) Crystal at Laboratory. Elevation, 800 ft.

background with lead and without anticoincidence mantle and shows that the lead shielding effect declines considerably in the region of the broad peak at about 128 Mev gamma-ray equivalent energy. This peak is produced by μ mesons which penetrate the crystal. Above the region of this peak the lead again shows more shielding effect.

The lowest curve of Fig. 3 shows the background with both lead and anticoincidence mantle. The low shielding effect of the lead from ~4 Mev upward leads us to believe that many of these pulses are produced by fast neutrons of energies up to at least 350 Mev for the larger pulses.

Runs were made at an elevation of 6400 ft above sea level (Clingmans Dome), and a considerable increase in counting rate in the region 3 to 8 Mev was found (Fig. 4*a*). The increase from 6 to 8 Mev was about 2.3 times, while the increase of the mesonic component, as measured by the peak at ~128 Mev, was only a factor of 1.36. This greater increase in the 3- to 8-Mev region would be expected if the response was caused directly or indirectly by neutrons, since they are known to increase with altitude more rapidly than mesons. A run made in a tunnel under ~50 ft of rock gave the result shown in Fig. 4*c*. A great reduction of the counting rate above 3 Mev is evident.

Figure 4*b* shows the reduction of the radioactivity portion of the spectrum obtained when the counter is over a body of water on a bridge.

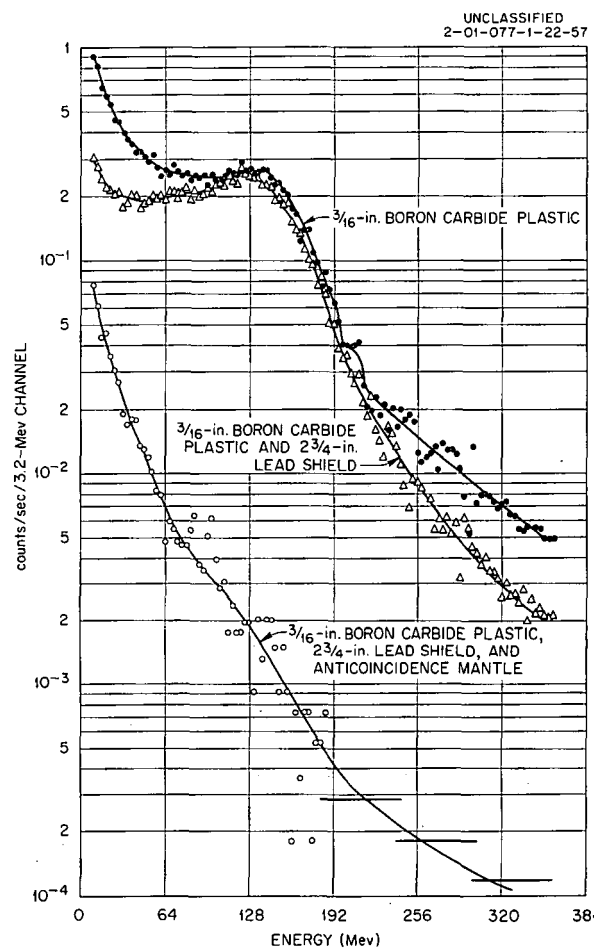

Fig. 4. Background in $9\frac{3}{4}$-in. NaI(Tl) Crystal with 4-in. Lead Shield and $\frac{3}{16}$-in. Boron Carbide Under Crystal and with Anticoincidence Mantle Operating.

An examination of the fluctuations of the counting rate with anticoincidence in operation in the region 6.5 to 8.4 Mev at a fixed location is being made. Figure 5 is a section of the record. Considerable fluctuations are noted in the "above 6.5 Mev" record that are not found in the "above 8.4 Mev" record. The source of the variations is not yet known.

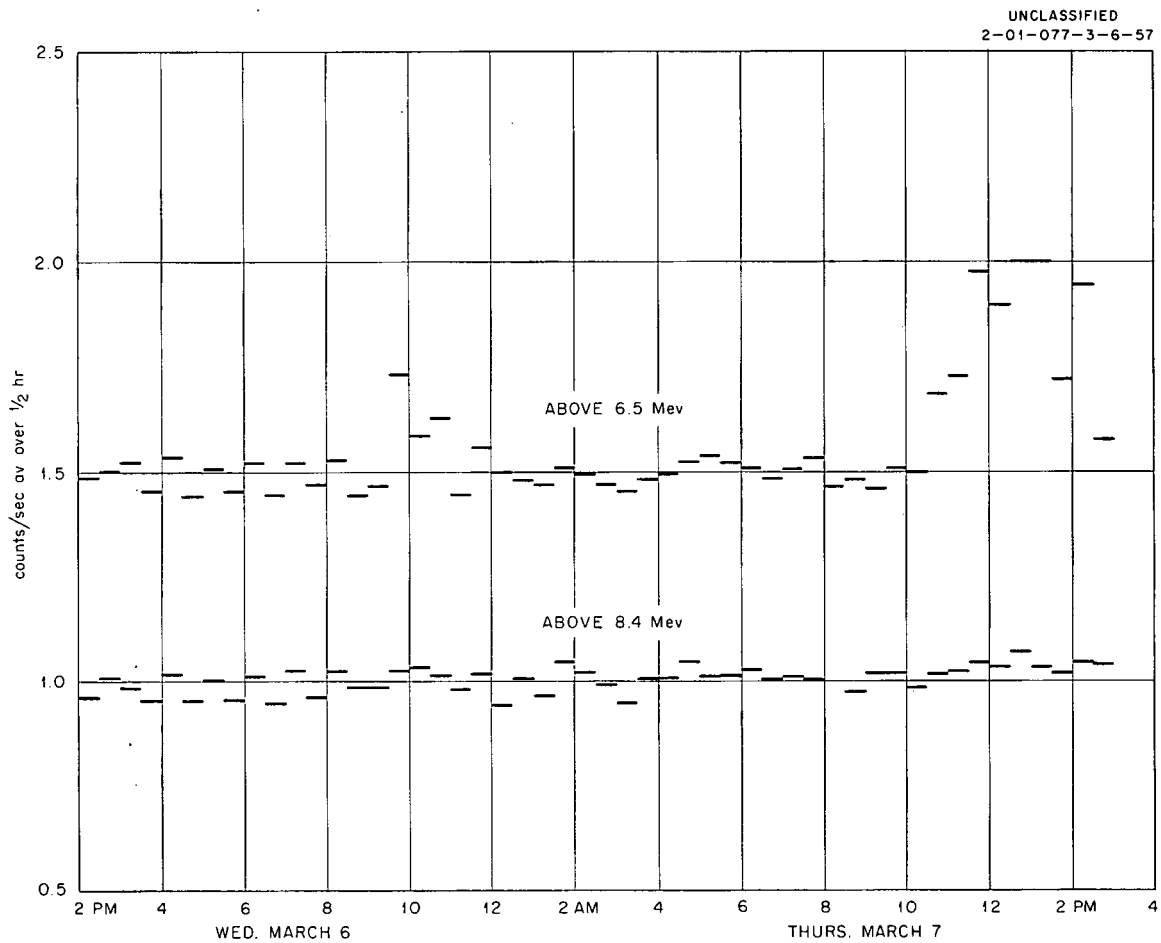

Fig. 5. Background in 9¾-in. NaI(Tl) Crystal. With 2¾-in. lead shield, 3/16-in. boron carbide, and anticoincidence mantle.

THE A-8 LINEAR AMPLIFIER

G. G. Kelley

The following changes have been made in the A-8 linear amplifier[1] since it was reported previously:

1. The over-all gain was found to be unnecessarily large and was reduced to 7000 in the main amplifier.

2. The 403B-6197 combination was found to be inadequate for driving a long 100-ohm cable. These tubes may be replaced by a 404A and a 417A, respectively, to provide the necessary performance.

3. Several improvements were made in the pulse-height selector.

The revised diagram is shown in Fig. 1.

[1] G. G. Kelley, *Phys. Semiann. Prog. Rep. Sept. 10, 1956*, ORNL-2204, p 49.

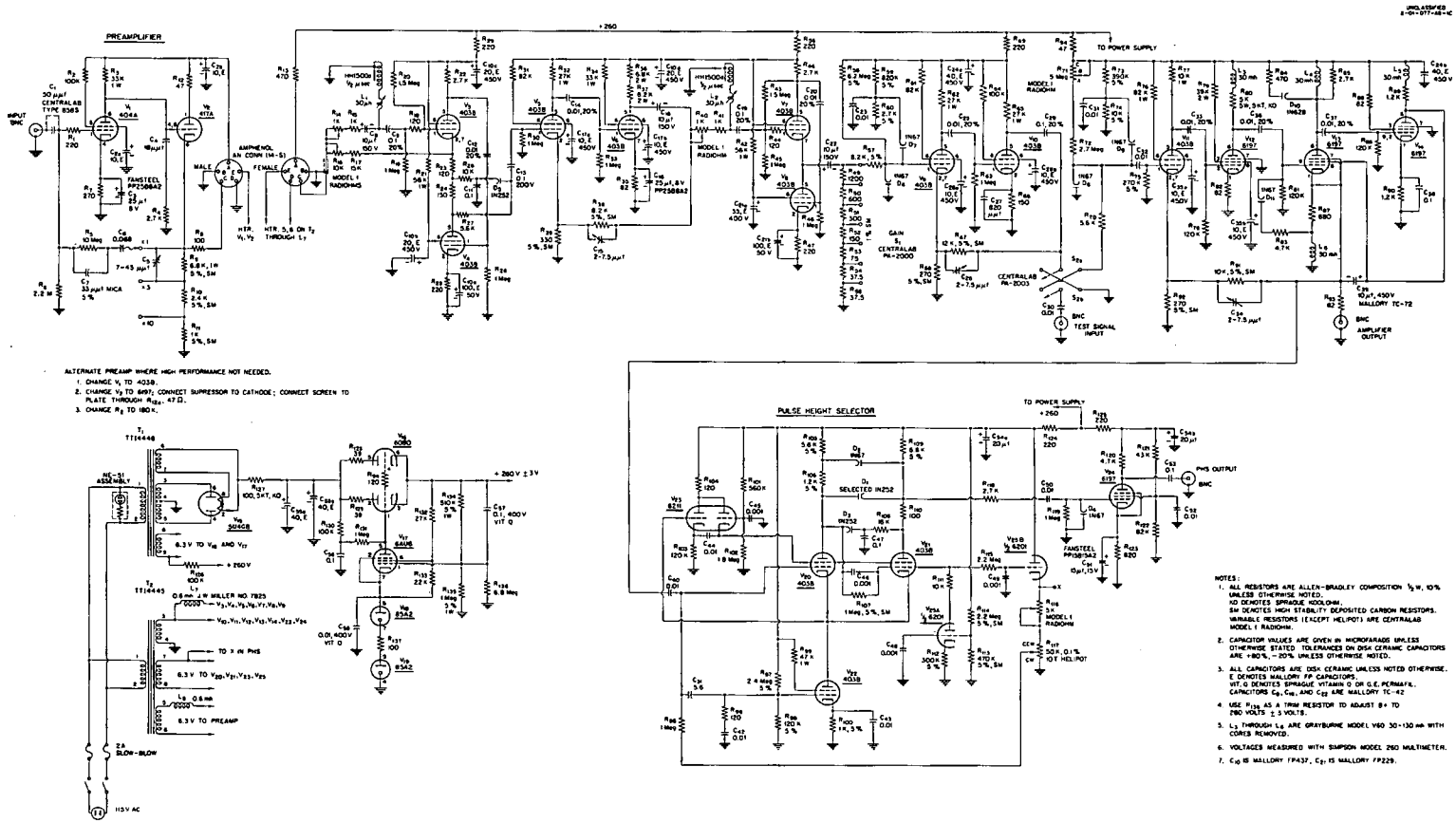

Fig. 1. Revised Diagram of A-8 Amplifier.

CONFERENCE ON NEUTRON PHYSICS BY TIME-OF-FLIGHT

Organized by W. M. Good, J. A. Harvey, and A. H. Snell

A conference on neutron physics by time-of-flight was sponsored by the Physics Division on November 1–2 at Gatlinburg. The conference was attended by more than 100 scientists, representing the national laboratories and some universities in the United States and the government laboratories of Canada and England.

The conference covered a wide range of topics in neutron nuclear physics. Thorough discussion was given to the measurements and the interpretation of total cross sections in the energy range from a few electron volts to 1 or 2 Mev. Results giving the progress in the study of elastic and inelastic neutron scattering were shown and discussed. Recent developments in the techniques for studying fission and the results from them were presented.

The meeting was organized into short papers giving new results, and featured speakers included Bretscher, Lane, Hughes, Wigner, Wheeler, and Bollinger. A comprehensive report of the complete conference has been prepared and will be published shortly.[1]

[1] *Conference on Neutron Physics by Time-of-Flight*, ORNL-2309 (in press).